# HIF-1 activated by PIM1 assembles a pathological transcription complex and regulon that drives JAK2V617F MPN disease

David Kealy[1,2‡], Ruth Ellerington[1,2‡], Suraj Bansal[3,4], Andy G.X. Zeng[3,4], Jessie J.F. Medeiros[3,4], Katie A. West[1,2], Nicole-Mae Blacknell[1,2], Catherine A. Hawley[1,2], Jakub Lukaszonek[1,2], Richard T. Gawne[2,6], Hwei Minn Khoo[7], Gillian Caalim[1,2], Bryce Drylie[1,2,5], Jenny Chatzigerou[1,2], Bianca Lima Ferreira[1,2], Adele K Fielding[1,2], Guanlin Wang[7,8,9,10], David G. Kent[1,2], Bethan Psaila[7,11], Adam C. Wilkinson[7], Andrew N. Holding[2,6], Ian S. Hitchcock[1,2], Andrew S. Mason[2,6], Vikas Gupta[3], John E. Dick[3,4] and Katherine S. Bridge[1,2]*

1 Centre for Blood Research, University of York; York, United Kingdom

2 York Biomedical Research Institute, University of York; York, United Kingdom

3 Princess Margaret Cancer Centre, University Health Network; Toronto, Canada

4 University of Toronto; Toronto, Canada

5 Barts Cancer Institute, Queen Mary University of London; London, UK

6 Jack Birch Unit for Molecular Carcinogenesis, University of York; York, UK

7 Hull York Medical School,

7 Medical Research Council Weatherall Institute of Molecular Medicine (MRC WIMM) and NIHR Biomedical Research Centre Haematology Theme; University of Oxford; Oxford, UK

8 MRC WIMM Centre for Computational Biology, University of Oxford; Oxford, United Kingdom

9 Shanghai Key Laboratory of Metabolic Remodeling and Health, Institute of Metabolism and Integrative Biology; Fudan University, Shanghai, China

10 Qizhi Institute, Shanghai, China

11 Oxford University Hospitals NHS Trust; Oxford, UK

‡ These authors contributed equally

*Correspondence to katherine.bridge@york.ac.uk

## Abstract

Hypoxia-inducible factors (HIFs) are master transcriptional regulators, central to cellular survival under limited oxygen (hypoxia) and frequently activated within malignancy. Malignant context affects the role of HIFs within oncogenesis; however, the mechanisms that regulate these context-disparities are not well understood. We therefore sought to determine whether HIF-1 function is determined by modality of activation, applying the JAK2V617F (JVF) model of myeloproliferative neoplasms (MPNs), in which HIF-1 is active in normal oxygen conditions (normoxia). First, we identify that HIF-1 is stabilised in normoxic JVF cells downstream of STAT1/5 signalling and upregulation of PIM1. PIM1 inhibition eradicates HIF-1 from normoxic JVF cells. We identify a novel phosphorylation couplet (T498/S500) within the oxygen dependent degradation (ODD) domain of HIF-1 in JVF cells that inhibits normoxic proteasomal degradation. Applying a single-input dual-omics output chromatin interactome methodology (DOCIA), we define distinct transcription cofactors and genomic redistribution of HIF-1, and differential expression of JVF-HIF-1 genes in primary haematopoietic stem/progenitor cells. In a cohort of 172 JVF-MPN patients, we observe significant association of the JVF-HIF-1 regulon (but strikingly, not canonical HIF-1 genes) with disease severity, progression, and patient survival. Finally, we identify a core set of JVF-HIF-1 targets significantly associated with spontaneous transformation of MPNs to AML. Our findings identify that HIF-1 activation by PIM1 substantially alters its function, and that this reprogramming drives MPN disease progression, restoring the potential for targeted therapies that delineate HIF-1 activity co-opted by malignancy from essential roles within physiological oxygen homeostasis.

## Introduction

Hypoxia-inducible factors (HIFs) are the major transcriptional regulators of cellular oxygen homeostasis. By coordinating both cellular and systemic responses to limited oxygen (hypoxia), the HIF regulon functions to conserve intracellular molecular oxygen and enhance delivery of exogenous oxygen to a hypoxic cell. Whilst critical to the physiological response to hypoxic exposure of normal cells, the portfolio of genes regulated by HIF provide a competitive advantage to cancer cells within hypoxic microenvironments such as those within solid tumours or in the bone marrow, or in malignant cells that activate HIF function by oncogenic signalling in normal oxygen (normoxic) conditions.

Under normal oxygen conditions, prolyl hydroxylase domain proteins (PHDs) hydroxylate two highly conserved proline residues on HIF-1α (Pro402 and Pro564), resulting in its recognition by the von Hippel-Lindau (VHL) E3 ligase complex, ubiquitination, and degradation by the proteasome [1]. During hypoxia, limited oxygen inhibits PHD activity, and stabilised HIF-1α protein translocates to the nucleus; the resulting heterodimerisation with the constitutively expressed HIF-1β/ARNT [2] forms an active transcription complex that binds to hypoxia-response elements (HREs) within target gene promoters [3]. The ensuing recruitment of transcription coactivators - most notably CBP/p300- forms an active transcription complex, initiating the activation of a wide array of genes involved in the response to hypoxia.

In both solid and haematological malignancies, HIFs are overexpressed as a result of two major factors: by hypoxic conditions - such as tumour or bone marrow microenvironments- and by genetic mutations, including those within *VHL*, *p53*, *Bcl2*, *Myc*, *Ras* and *JAK* [1]. Whilst overexpression of the two predominant HIF isoforms (HIF-1, HIF-2) is widely observed, HIF-2 is demonstrated as almost exclusively oncogenic, whereas HIF-1 can confer either oncogenic or tumour suppressive functions [2,3]. This is particularly evident in myeloid neoplasia; in mouse models, inhibition of HIF-1 has been demonstrated as efficacious for treatment of MPNs [4], whereas activation of HIF-1 was recently shown as efficacious for treatment of acute myeloid leukaemia (AML) [5]. In agreement with these contradictory results, high levels of HIF-1α have paradoxically been associated with both the best and worst patient disease outcomes in AML [4,5] whilst beyond leukaemia, pan-cancer analysis demonstrates that only 1.8% of HIF-1/-2 target genes are conserved across 6 cancer cell lines in response to hypoxia [3]. The underpinning mechanisms that orchestrate the multiplicity of HIF-1 within malignancy remain to be well characterised.

Contextual ‘reprogramming’ of transcriptional regulators as contributors to pathogenesis has previously been reported in various haematological malignancies. EVI1 activation in AML by

chromosome 3q26/MECOM rearrangements has been demonstrated to activate the transcriptional repressors CTBP1 and 2 in a fashion indispensable to leukaemic transformation [6]. Furthermore, similar to HIF-1, the transcription factor WT1 (an essential regulator of genes involved in healthy haematopoiesis) appears capable of behaving as both an oncogene and tumour suppressor in AML depending on disease context, behaving as an oncogene when aberrantly expressed, and a tumour suppressor gene when mutated [7].

HIF itself has also been shown to be 'reprogrammed' indirectly in malignant disease. In APL, the oncogenic fusion protein PML-RARα cooperates with HIF-1α to activate a pro-leukemogenic program of HIF gene signature upregulation independent of HIF mutation [8]. Furthermore, the renal tissue specificity of clear cell renal carcinoma has been shown to be mediated by the recruitment of HIF-2α to the lineage transcription factor PAX8 as triggered by VHL protein loss [9].

To reconcile the evident context-specificity of HIF-1 activity within malignant haematopoiesis, we sought to determine whether the mechanism of HIF-1 activation determines its function. The JAK2V617F (JVF) point mutation is highly prevalent within philadelphia chromosome negative MPNs and is carried by >95% of patients with polycythaemia vera (PV), 50-60% of patients with essential thrombocythemia (ET) and primary myelofibrosis (PMF) [10–13] . Additionally, it was previously shown that levels of HIF-1α are raised in JVF-mutant MPNs; treatment of these cells with the JAK inhibitor Ruxolitinib (Rux) caused HIF-1 levels to return to normal [4].

Herein, we provide evidence that the mutational context and subsequent method of HIF-1 activation directs its function: PIM1-mediated stabilisation of HIF-1α downstream of JVF signalling significantly alters the formation and function of HIF-1 transcription complexes compared to hypoxic activation, enacting a JVF-specific HIF1 regulon that is significantly associated with disease progression and survival of JVF MPN patients.

## Results

### HIF-1α is stabilised in JAK2V617F cells downstream of disproportionately activated STAT1/STAT5 signalling and increased PIM1 kinase expression.

We first sought to determine whether stabilisation of HIF-1α protein, previously reported in the *jak2v617f*-transduced 32D murine cell line [4], was detectable across other JVF mutant cell line models. Immunoblot analysis of the murine pro-B cell line hMPL BaF3 [14,15], the human leukaemic megakaryocytic cell line UT7/TPO [15,16], the human JVF mutation heterozygous transformed essential thrombocytopenia megakaryoblastic line SET2 [17,18] and the human erythroleukaemic erythroblastic JVF mutation homozygous line HEL [19] all

demonstrated elevated HIF-1α levels at 20% $O_2$ (normoxia) compared to corresponding wildtype JAK2 cell lines (Fig. 1A). We next employed the *ex vivo* PVA expansion culture system for murine HSCs to interrogate these findings further [6], as we previously demonstrated that the purity of HSC expansion cultures is enhanced by hypoxic conditions [7]. Flow cytometric analysis of HSCs expanded under normoxia (20% $O_2$), physioxia (5% $O_2$) and hypoxia (1% $O_2$) demonstrated correlative levels of HIF-1α with oxygen concentrations in WT HSCs (Fig. 1B). Upon treatment with the HIF-1α-specific inhibitor GN44028 [20,21], the percentage of LT-HSCs (CD201+ CD150+ LSK) in these populations significantly reduced across all oxygenation conditions, with a concomitant increase in percentage of lineage committed cells (Fig. 1C and Fig. S1), demonstrating that HIF-1 is active and necessary for HSCs across oxygen conditions to establish and expand in this system. We next analysed freshly isolated lineage depleted cells from JVF homozygous, heterozygous and wildtype C57/BL6 mouse bone marrow [22], which identified that the JVF-mutation stabilised HIF-1α correspondingly to allelic burden in primary HSCs (4h hypoxia; HIF-1α levels in LSKs remained below the limits of detection under normoxia) (Fig. 1D and Fig. S2A-B). Western blot analysis of HIF-1α protein extracted from lineage depleted bone marrow lysate further confirmed these findings (Fig. S2C).

We next undertook *ex vivo* expansion culture of JVF homozygous, heterozygous and wildtype long-term HSCs. First, we discovered that expansion of LT-HSCs from homozygous JVF mice was not supported by the PVA expansion culture conditions; HSCs could be maintained for <7 days but not expanded. We hypothesise this may be due to supraphysiological levels of TPO within the culture media in concert with homozygous JAK2V617F mutation resulting in an ultimately lethal hyperstimulation of the MPL/JAK2 axis in these HSCs, although this is yet to be fully interrogated. Heterozygous JVF HSCs did expand in these conditions, and we observed significant differences in lineage committal decisions, with a reduction in the proportion of Lin- Sca1+ cKit+ (LSK) HSPCs and a corresponding increase in the proportion of progenitors ($Lin^-$ $Sca1^-$ $cKit^+$; Prog) (Fig. S3A-B). This is in keeping with the immunophenotypes observed from fresh bone marrow from these mice, indicating that this expansion system supports the maintenance of the physiological phenotypes of this model [8]. Expansion cultures performed under a dose-range of GN44028 (HIF-1 inhibitor) demonstrated inhibition of the proportion of LSKs within the cultures regardless of phenotype, although disease-beneficial effects on the expanded progenitor population were observed in JVF heterozygous HSC cultures. These findings mirror the effects of the antibiotic Echinomycin (also an inhibitor of HIFs) which inhibited proliferation of 32D cells indiscriminately of JVF-mutation status and increased the colony-formation capacity of healthy CD34+ peripheral blood mononuclear cells (PBMCs) [4]. Taken together,

these data demonstrate a central role of HIF-1 within both normal and JVF-mediated malignant haematopoiesis, thereby compelling the delineation of HIF-1 function in each of these settings for potential therapeutic approaches for JVF-MPN disease.

We therefore sought to define the mechanism and modality of HIF activation within the JVF context. Previous findings implicated reactive oxygen species (ROS) as stabilising HIF-1α downstream of TPO/JVF signalling [23,24], however we did not observe destabilisation of HIF-1α in our panel of JVF cell lines after application of the ROS scavenger N-acetyl-l-cysteine (NAC) (Fig.1E and Fig.S4A-B). ERK1/2 kinase activity is known to be elevated downstream of JVF signalling [13] and to mediate phosphorylation of HIF-1 [25]; however application of the specific ERK1/2 kinase-activity inhibitor SCH874 to UT7/TPO JVF cells also failed to reduce elevated levels of HIF-1α protein (Fig. S5). Given that phosphorylation of HIF-1α has been extensively demonstrated to critically modulate both the interactome of HIF-1 and its function [26–31] we reasoned that aberrant kinase activation downstream of JVF could be responsible for HIF-1α stabilisation. We therefore applied an unbiased, high-throughput phospho-flow cytometry approach (Fig. S6) [32] to fully characterise the signalling cascades downstream of JVF mutation compared to TPO/MPL-mediated wildtype JAK2 signalling in matched isogenic UT-7/TPO cells. These analyses demonstrated not only a global amplification of JAK2 signalling in JVF mutant cells but identified disproportionate activation of specific downstream kinase cascades (Fig. 1F[I]). We applied parts of a whole analysis, wherein MFI values for each phospho-peptide are calculated as a fraction of total phospho-peptide MFI, and identified that STAT1 and STAT5 showed disproportionately increased activation downstream of JVF, collectively representing a third (34.3%) of the total downstream signalling output in JVF cells compared to a quarter (24.9%) in TPO-stimulated WT JAK2 cells (Fig. 1F[II]). We did not observe any change in contribution of STAT3, whereas relative ERK activation was reduced in JVF cells, which corroborated our earlier findings whereby inhibition of ERK did not reduce HIF-1 protein levels (Fig. S5).

Unlike STAT3, STAT1/5 are not known to be direct protein-protein interactors of HIFs [9,10]. We therefore interrogated STAT1/5 target genes for known kinase regulators of HIF-1α [33–36], identifying 1078 common gene targets between STAT1 and STAT5 (Fig. 1G). Of these common targets, 17 kinases were identified and of these, 1 was a known kinase of HIF: the CAMK serine/threonine kinase PIM1. PIM1 is known to contribute to the pathogenesis of haematological malignancies [11] and has previously been described as phosphorylating HIF-1α at Thr455 in prostate cancer [12], stabilising HIF-1α in an oxygen-independent manner. PIM1 has also shown to be upregulated in murine HSPCs harbouring the JVF mutation [13], implicating PIM1 as a possible candidate mediating HIF-1α aberrant stabilisation.

To pursue this theory, we analysed pre-existing publicly available HSPC bulk RNAseq datasets from heterozygous JVF mice [14] and observed raised levels of PIM1 transcript in the LSK and megakaryocyte erythroid progenitor (MEP) cell population compared to wildtype counterparts (Fig. 1H and Fig. S7). This finding was confirmed via RT-qPCR in both whole and lineage depleted bone marrow from homozygous JVF mice where significantly higher PIM1 transcript expression compared to wildtype was observed (Fig. 1I). To confirm these findings in patients, we re-analysed myelofibrosis (MF) MPN patient scRNAseq data [15] for patients harbouring the JVF mutation, and found that not only were total levels of PIM1 transcript elevated in these patients, but that overexpression was localised to the disease-driving expanded megakaryocyte progenitor (MkP) population (Fig. 1J). Taken together, these findings demonstrate that disproportionate activation of STAT1/5 occurring downstream of JVF upregulates PIM1 and subsequent HIF-1α stabilisation in MPN disease driving HSPCs.

### PIM1 inhibition confirms JAK2V617F-induced PIM1 stabilises HIF-1α without modifying JVF signalling.

To confirm PIM1-mediated HIF-1α stabilisation, we dosed both JVF and wildtype UT7/TPO and BaF3 hMPL cells with increasing concentrations of the PIM1-specific inhibitors TCS PIM1 and SMI-4a and the pan-PIM inhibitor PIM447. We observed dose-dependent decreases in HIF-1α stabilisation by immunoblot with all PIM inhibitors (Fig. 2A(I) and Fig. S8-9), thus suggesting that PIM, and more specifically PIM1, is necessary for JVF-mediated HIF-1α stabilisation. Of the specific PIM1 inhibitors tested, SMI-4a did not alter levels of PIM1 protein, and thus was chosen for PIM1 inhibition investigations going forward. To contrast the effect of PIM1 inhibition with JAK inhibition on HIF-1α levels, we next applied either SMI-4a or Rux to JVF and WT UT7/TPO cells, either starved overnight or starved then stimulated with TPO and cultured under normoxic (20% $O_2$) or hypoxic (1% $O_2$) conditions and analysed downstream signalling cascades by phospho-flow. In keeping with western blot data, SMI-4a reduced HIF-1α levels in JVF cells in both normoxia and hypoxia, however we observed no effect on HIF-1α levels in WT cells stimulated with TPO in either oxygen condition (Fig. 2A[II]). These findings demonstrate that inhibition of PIM1 can confer specificity to HIF-1 inhibition downstream of JVF signalling, whilst not affecting physiological activation of HIF-1 by hypoxia or TPO.

The JAK inhibitor Ruxolitinib (Rux) is currently the most common drug treatment given in JVF-positive cases of myeloproliferative neoplasia [37–40]. However, JAK inhibition disrupts many crucial signalling pathways within the cell, and therapeutically causes a number of poorly tolerated side effects [41]. Additionally, whilst Rux-treatment caused downregulation

of HIF-1α levels in JVF cells regardless of oxygen concentrations, our data demonstrated a paradoxical increase in HIF-1α levels in WT JAK hypoxic cells treated with Rux (Fig. 2A[II]). To investigate if PIM1 inhibition could create a more targeted downstream therapeutic approach, we treated SET2 and HEL myeloproliferative patient-derived cancer cell lines with either Rux or SMI-4a (Fig. 2B[I]). Rux-treatment significantly downregulated signalling across all pathways analysed, whereas SMI-4a selectively affected levels of HIF-1α. Broader analysis of signalling in JVF mutant UT7/TPO cells demonstrated inhibition of both TPO signalling in JAK2 WT cells and oncogenic JVF signalling, whereas SMI-4a treatment did not deregulate these pathways (Fig. 2B[II] and Fig. S10).

To further investigate whether PIM1 inhibition of HIF-1α could confer disease-specific effects on JVF HSPCs, we conducted *ex vivo* expansion of long-term HSCs from wildtype and JVF heterozygous mice in the PVA culture system (Fig. 2C and Fig. S11-13). Expansion cultures performed under a dose-range of PIM1 (SMI-1a) inhibition demonstrated that PIM1 inhibition rescued the JVF heterozygous LSK/Prog phenotype, returning the LSK/Prog ratios observed in wildtype expansion cultures. This was in contrast to HIF-1 inhibition, which indiscriminately inhibited the proportion of LSKs within the cultures, regardless of phenotype (Fig. S3A-B). Taken together, these data demonstrate that HIF-1α is stabilised in JVF cells as a result of PIM1 kinase activity, and that inhibition of PIM1 can rescue aberrant HIF-1α activation whilst not altering physiological JAK or HIF-1 activity.

### HIF-1α is stabilised via phosphorylation of Thr498/Ser500 in JAK2V617F cells.

PIM1 kinase has previously been shown to phosphorylate HIF-1α at the Thr455 site in prostate cancer cells, inhibiting canonical hydroxylation-mediated degradation in normoxia [42]. We therefore performed phospho-proteomic mass spectrometry analysis of UT7/TPO JVF, and wildtype cells exposed to hypoxia, enriched for HIF-1α via immunoprecipitation and enriched for phosphorylated proteins by $TiO_2$. Phosphorylation of HIF-1α in wildtype cells was detected at the canonical hypoxia/ERK sites (Ser641/643), whereas in the matched isogenic JVF cell line under the same hypoxic conditions, an additional phosphorylation couplet was detected at Thr498/Ser500 (Fig. 3A(I)-[II]). Interestingly, no phosphorylation at the Thr455 site was detected in any condition, further suggesting that the mechanism of PIM1-mediated HIF-1α stabilisation downstream of JVF is distinct from that observed in prostate cancer cells. Whilst the Thr498 site is not well conserved, the Ser500 site is well conserved evolutionarily among mammals and a variety of other non-mammalian species, underscoring the importance of the Ser500 site as a regulatory site (Fig. 3B).

Whilst distinct from the Thr455 site in prostate cancer, the location of Thr498/Ser500 within the ODD and their proximity to the P402/564 hydroxylation sites (Fig. 3C) suggested that the

mechanism of PIM1-mediated HIF-1α stabilisation through inhibition of canonical oxygen-mediated degradation may be similar. WT/JVF mutant UT7/TPO cells were therefore treated with the proteasome inhibitor MG-132 in combination with SMI-4a (Fig. 3D) to assess the role of proteasomal degradation in PIM1-mediated stabilisation of HIF-1α in the presence of the JVF mutation. Combined treatment with MG-132 and SMI-4a was sufficient to re-stabilise HIF-1α levels, demonstrating that PIM1-mediated stabilisation of HIF-1α downstream of JVF signalling occurs via inhibition of canonical normoxic proteasomal degradation.

### HIF-1α assembles a non-canonical transcription complex in JAK2V617F cells.

Having identified that HIF-1α stabilised in JVF cells is phosphorylated at non-canonical sites, we next sought to determine whether this altered the transcriptional activity of HIF-1. HIF-1α phosphorylation is known to alter its interaction with co-regulatory proteins (in recent years, newly identified HIF transcription cofactors including TRIM28 and PAX8, identified in breast [43] and renal cancer [9], respectively, identify the existence of cancer context-specific regulators of HIF transcription activity.); we therefore wanted not only to capture the genomic loci and target genes of HIF-1 in JVF cells, but also the transcription co-regulators as potential targetable disease-specific regulators. We therefore developed a dual-output chromatin-interactome assay (**DOCIA**), which integrates the principles of ChIPseq and qPLEX-RIME (quantitative multiplexed Rapid Immunoprecipitation Mass spectrometry of Endogenous proteins), to quantitatively analyse both the genomic DNA and protein interactors of HIF-1α from a single input sample (Fig. 4A[I]). WT/JVF hMPL BaF3 cells were cultured at normoxia (20%) or hypoxia (1%, 6h) and chromatin immunoprecipitation against HIF-1α was performed. First, we observed that despite equal input chromatin loading on to ChIP beads, we observed significantly higher HIF-1α protein levels (MS) at the chromatin in JVF cells compared to WT cells (Fig. 4A[II]) despite presumed equal input of HIF-1α protein between WT and JVF conditions (Fig. S14 illustrates expected levels of HIF-1α post 6hrs hypoxic treatment in JVF and wildtype BaF3 hMPL cells). Unexpectedly, this was coupled with a significant reduction in chromatin associated with HIF-1α in JVF cells (NGS) compared to WT. This was particularly evident in the VF_Nx conditions: normalised abundance of HIF-1α protein (MS) was comparable to WT_Hx, whereas the mean genomic DNA peak intensity (NGS) was significantly reduced.

Analysis of the protein interactors of HIF-1α at the chromatin in WT_Hx cells identified known co-regulator interactors including HIF-1β/ARNT, Hsp90 and Ncoa5 (Supplementary Tables S1-S2) [9]. Common cofactors associating with HIF-1α across all conditions included HIF-1β/ARNT, Ncoa5, Epg5, polyubiquitin-B, centrosomal protein Cep63 and Gapdh. 94

proteins were found to be significantly enriched with HIF-1α relative to isotype control across the conditions, of which 43 were common to all four conditions and 24 to those conditions with stabilised/active HIF-1a (WT_Hx, VF_Nx, VF_Hx) (Fig. 4B and Supplementary Table S2). Strikingly, we detected 19 binding partners that are uniquely associated with HIF-1α in cells harbouring the JVF mutation, whereas we did not detect any wildtype-specific factors. Exposure of a given genotype to hypoxia also did not significantly alter the associated factors, with only 3 proteins detected only in hypoxic mutant cells (VF_Hx/+WT_Hx): these included two ribosomal components (Fbl, Rps3a) and the DNA damage repair protein Rad23.

To quantitatively determine the differences in HIF-1α cofactors between JVF and wildtype cells next, samples were first normalised against HIF-1α abundance to control for the variability of HIF-1α detected across samples (Fig. 4A[II], Supplementary Table S1), and relative enrichment compared to WT_Hx was subsequently calculated (Fig. 4C). This illuminated key patterns of protein association unique to JVF cells, such as an increased association with cofactor TDP-43 and decreased association with protein markers of degradation such as ubiquitin and VHL, further lending evidence to our hypothesis that HIF-1αs JVF stabilisation is due to an inhibition of hydroxylation and subsequent VHL-mediated ubiquitination. Protein intensity relative to HIF-1α for each of the identified cofactors were ranked for each condition and those with GeoMean greater than 0.01 were retained (following exclusion of structural and non-murine proteins). These remaining proteins were subjected to STRING analysis for each condition to better understand the role and interactions of these associated proteins (Fig. 4D and Fig. S15A-B). VF_Hx HIF-1α possesses a reduced interactome, despite greater levels of HIF-1α relative to WT_Hx and VF_Nx (5.42 and 3.15-fold greater respectively), suggesting a significant alteration in HIF-1α protein confirmation in the combined presence of JVF and hypoxic conditions. Most interestingly, an emergent group of spliceosomal factors were uniquely enriched in interaction with HIF-1α in JVF cells under both conditions, (including TDP-43, KHDRBS1/Sam68) along with ribosomal factors in normoxic treated cells.

Novel JVF-unique interacting partners identified through DOCIA were then validated by endogenous co-immunoprecipitation assays conducted in WT/JVF UT-7/TPO cells at normoxia (20% $O_2$) or hypoxia (1% $O_2$, 6 Hours) (Fig. E and Fig. 4F(I)-[II]). This confirmed the interaction of TDP-43, GOLGA3, SIK2 and IMPDH with endogenous HIF-1α. Phosphoproteomic investigation of HIF-1α phosphorylation (Fig. 3A), also identified GOLGA3 as a phosphorylated co-immunoprecipitated protein, with several distinct phospho-sites detected in JVF cells (Fig. S16). Together, these data identify that differential HIF-1

transcription complexes form as a direct result of the JVF mutation, comprising non-traditional co-regulatory proteins and significant enrichment of pre-mRNA processing factors.

## HIF-1 is genomically redistributed in JAK2V617F cells.

We next sought to determine whether the binding loci of HIF-1 throughout the genome was altered as a result of activation via JVF signalling. Continuing our single-input, dual output chromatin interactome approach (Fig. 5A), we interrogated the genomic sequences immunoprecipitated with the complexes analysed in Fig. 4. First, we identified a largely canonical HIF-1 signature [44,45] associated with HIF-1 in BaF3 cells exposed to 1% O2 for 6 hours (WT_Hx) (Fig. S17), including classical signature genes such as *Vegfa*, *Slc2a1, Eno1* and *Gapdh* (Fig. S18). Globally, we observed a reduction in median peak intensity (MPI) for HIF-1α in JVF cells (Fig. 5B, Fig. S19), marked by the emergence of a population of loci of low intensity (MPI<2), unobserved in WT_Hx condition, despite HIF-1α protein levels being higher (Fig. 4A[II]). Concomitant with this, we observed very few HIF-1α loci that were unique to JVF mutant cells, rather the binding loci were a subset of those bound by HIF-1α in WT_Hx conditions (Fig. S20). These data indicate that the DNA-binding capacity and/or the proximity of HIF-1α to DNA is reduced in JVF mutant cells at particular sites compared to in hypoxic WT JAK2 cells.

To calculate the priority of HIF-1 distribution across the genomic within a given cellular context, peak intensity for HIF-1 at loci was rank-scored for each condition WT_Hx, VF_Nx and VF_Hx; Δrank-score for VF_Nx/VF_Hx was calculated to identify loci that were higher or lower ranked relative to WT_Hx. First, we observe global priority redistribution of HIF-1, with the intensity ranking of 42% and 26% of sites in VF_Nx and VF_Hx, respectively, conferring Δrank-score greater than a quartile (Fig. 5C). Analysing the chromosomal distribution of intensity ranking, a population of depreciated HIF-1 bound sites in VF_Nx were evident in chromosomes 1-4 and prioritised sites at chromosome 8 and 14 (Fig. 5D and Fig. S21); notable genetic loci losses and gains included *Usf1* and *Dusp4*, respectively (Fig. 5E). In VF_Hx cells HIF-1α binding was overall enhanced on chromosome 12 (Fig. 5D and Fig. S21); these sites included *Bag5*, *Coa8, Mdm2* and *Hectd1* (Fig. 5E). To determine whether chromatin accessibility alterations mediated by JVF signalling was a factor in the redistribution in HIF-1α, we cross-analysed VF_Nx/VF_Hx ChIPseq data with a JVF scATAC-Seq dataset (Fig. 5F and Fig. S22) [19]. No significant difference in accessibility at HIF-1α binding loci was observed, suggesting that HIF-1α redistribution was not mediated by site accessibility. Feature analysis of HIF-1 bound loci demonstrated a 14% reduction in hypoxia-responsive elements in VF_Nx/VF_Hx compared to WT_Hx (Fig. 5G) and a modest increase in binding in intergenic regions and introns in VF_Nx cells (Fig. 5H).

## JAK2VF-HIF-1 gene-signatures diverge from canonical HIF-1 targets and correlate with MPN disease progression and survival.

Next, HIF-1 gene-signatures were generated from the top 200 (q<0.03) enriched binding loci in VF_Nx/VF_Hx relative to WT_Hx; a WT_Hx gene signature was generated relative to WT_Nx as a control canonical hypoxia signature (Fig. 6A). Gene ontology pathway analysis of the WT_Hx signature demonstrated canonical HIF-1 hallmark gene pathways [44,45], including glycolysis, response to oxidative stress and response to hypoxia. (Fig. 6B[I]). The VF_Nx gene-signature included non-canonical HIF-1/Hypoxia pathways including DNA metabolism, DNA damage response, and RNA processing, with a reduction of glycolysis pathways observed (Figure 6B[II]); strikingly, the VF_Hx gene-signature was even further separated in gene ontology from canonical WT_Hx (Fig. 6B[III]) pathways, with cell cycle progression and checkpoint pathway genes demonstrating the greatest contribution to the signature. Furthermore, VF_Nx and VF_Hx gene-signatures contained only 9 and 2 genes, respectively, of the HIF gene metascore - a recently identified core set of 48 HIF target genes highly conserved across cell/cancer types exposed to hypoxia (Fig. S23), underscoring the functional divergence incurred by the modality of HIF-1 activation in JVF mutant cells [20].

To investigate whether the redistribution of HIF-1 in response to JVF signalling was reflected in the transcriptome, we next interrogated the expression of the VF_Nx and VF_Hx HIF-1 signatures in primary haematopoietic stem and progenitor cells (HSPCs) from wildtype and JVF homozygous C57/BL6 mice (Fig. 7B) [14]. This analysis identified that 74.6% of VF_Hx signature genes were differentially expressed in multipotent JVF homozygous MEP cells, whereas only 4.6% of the signatures were differentially expressed in the more primitive LSK population. The cell type-specific activation of the HIF-1 VF_Hx signature within MEPs in mice mirrors recent findings identifying epigenetic changes in the erythroid and megakaryocytic progenitors of JVF patient samples, the cell types that undergo significant clonal expansion, which increase accessibility of particular transcription factor motifs in late erythroid progenitor populations [19]. Of note, we observe that a significant proportion of differentially expressed VF_Hx signature genes were downregulated in MEPs. HIFs are not known to confer transcription-repressive functions [46,47], suggesting that peri- or post-transcriptional mechanisms mediated by HIF-1 and/or co-factors confer the observed transcript repression. In concert with these findings, cross analysis with ATACseq data showed no correlation between VF_Hx signature gene expression and accessibility and illustrated that very few of the VF_Hx signature genes showed increased site accessibility in JVF samples (Fig. S24 and Fig. S25).

Having determined differential expression of the VF_Nx and VF_Hx signatures at the transcriptome level, we next sought to determine whether adverse HIF-1 transcriptional output in response to JVF mutation conferred pathophysiological effects in MPN disease. We therefore interrogated the expression of the HIF signatures in a 172-patient cohort of JVF-positive MPNs with matched RNAseq and disease progression/survival data [48]. First, we determined that there was no correlation between expression of the WT_Hx signature or a classical hypoxia signature (Hallmark Hypoxia) or in either disease progression or survival of these patients (Fig. 6C and Fig. 6D-E). However, interrogation of the VF_Nx/ VF_Hx signatures demonstrated a significant correlation between expression and disease progression from intermediate to high MIPSS70 score (Fig. 6D) [48–51]. Correlation of the VF_Hx signature (but not the VF_Nx signature) with disease severity was reflected in the overall survival of the cohort, for whom those in the upper median group of VF_Hx gene signature expression (VF_Hx $^{HIGH}$) demonstrated significantly worse overall survival, with a median survival of 4 years compared to 8 years for VF_Hx$^{LOW}$ patients (Fig. 6E).

### JAK2V617F-activated HIF-1 target genes contribute to disease progression and outcome.

To identify whether particular genes in the VF_Hx signature were responsible for survival outcome, we next analysed variable expression of these genes in biologically motivated gene sets, including ATAC-seq of CD34+ JVF stem and progenitor cells [52], MEPs bulk RNAseq [53], scRNA-seq profiles of Lin-CD34+ stem and progenitor cells from 11 JVF MF patients [54] and our patient cohort. We first identified the disparate genes between the VF_Hx/VF_Nx signatures (n=158), and the VF_Hx/WT_Hx signatures (n=144), representing those genes gained and lost, respectively, HIF-1 target genes in the VF_Hx context (Fig. 7A). To delineate genes that are acquired as HIF-1 targets as a result of chromatin alterations and not aberrant HIF-1 function, we next screened out those with altered accessibility [52]. These genes were then analysed for differential expression in bulk and scRNAseq JVF vs WT [53,54], and finally differentially expressed genes were analysed for correlation with progression/survival and AML transformation in the JVF MPN patient cohort. First, we observed that the JVF-HIF-1 target genes significantly associated with disease severity (MIPSS70 score) and overall survival of JVF patients, were differentially expressed within the disease-driving megakaryocyte progenitor populations in both humans (MkPs) and mice (MEPs) (Fig. 7C(I)-[II]). A notable cellular pathway emergent from this analysis was the DNA damage response [45,55], with JVF-HIF-1 target genes including proliferating cell nuclear antigen (PCNA), BLM RecQ Like Helicase (BLM), aurora kinase B (AURKB), EIF4EBP1 and BCL2L1 (BCL2XL) (Fig. S26) upregulated in transcript expression in MEPs/MkP in the JVF setting and associated with disease progression/survival. JVF-HIF-1 genes that were globally upregulated throughout HSPC clusters, for example TNKS,

HECTD1, WIPF1, PPID (Fig. S27) were not correlated with disease progression or survival. Additionally, we noted a small cohort of genes that were significantly upregulated in more primitive progenitor populations in patients (HSPC3), that were inversely correlated with disease severity and survival, including Immediate Early Response 3 (IER3), which regulates cell cycle/apoptosis decisions (Fig. S28) [56]. These data support previous findings that the disease-specific expanded MkP population drives disease in JVF MF patients [54], and also identify that disease co-opted HIF-1 downstream of JVF signalling induces DNA damage response genes that contribute to MPN disease progression and patient survival.

### JAK2VF-HIF-1 regulon correlates with transformation of MPNs to AML

JVF positive MPN patients who develop myelofibrosis are at risk of spontaneous conversion to acute myeloid leukaemia; however, the molecular mechanisms underpinning this pathobiological event are not well characterised [21]. We therefore applied the above sequential analysis to 11 patients from the JVF MPN cohort that transformed to AML, analysing expression of JVF-HIF-1 variable genes in matched pre-/post-transformation samples. As expected, no significant difference in expression of the gene signatures as a whole was observed in these patients pre-/post-transformation (Fig. S29), however, applying the above analysis pathway through biologically motivated gene-sets, we identified 13 variable HIF-1 genes that were significantly associated with transformation, comprising 5 up-regulated and 8 down-regulated genes (Fig. 8A). Notably, analysis of the upregulated genes identified the DNA damage response as a dominant HIF-1 mediated pathway associated with leukemic transformation. Downregulated pathways included negative feedback of the hypoxic response (*EGLN1*) and regulators of glucose metabolism (*IER3, HK2*). Analysis of these genes as a unified regulon demonstrated an extremely strong correlation with disease progression (MIPSS70 classification), myelofibrosis (overt, post-ET and post-PV), and significantly worsened survival (Fig 8B). Together, these results uncover a hitherto unidentified, non-canonical HIF-1 regulon in JVF-mutant MPNs that drive progression, leukemic transformation and survival outcome for patients.

## Discussion

HIF-1 is a master transcriptional regulator integral to normal oxygen homeostasis in healthy cells. In the malignant setting, HIF-1 activated by microenvironmental hypoxia or aberrant signalling cascades contributes to disease progression and treatment resistance, however the directionality and potency of its role is disease-context dependent; this is particularly evident within myeloid neoplasia [4,5,24,57]. We therefore sought to determine whether the modality of HIF-1 activation - either physiologically by hypoxia or pathologically as a result of

oncogenic signalling- could alter its transcriptional function and role within disease pathobiology, interrogating JVF-driven MPNs as a disease model system.

Whilst JVF mutation is known to activate JAK-STAT signalling in a cytokine-independent manner, recent studies by our groups and others have revealed that structural conformation of the TPO-MPL-JAK2 complex controls downstream signalling outcomes [22], and that the JVF mutation alters and strengthens the intermolecular interactions in the pseudokinase domain dimerization interface [23]. High-throughput phospho-flow cytometry reveals that STAT1 and STAT5 are disproportionately activated by JVF compared to TPO-stimulated JAK2, with relative suppression of ERK signalling. These data reveal that JVF mutation confers not only cytokine-independent JAK-STAT signalling but deregulation of this cascade, driving mutant-specific transcriptional effects via STAT1 and STAT5, upon which JVF MPNs become reliant [24]. These data provide the mechanism for recent single-cell multi-omic analyses that describe enhanced activity of STAT1/STAT5 promoters in JVF mutant patient CD34+ cells [19].

PIM1 is a direct transcriptional target of STAT1 and STAT5, and was previously described as a kinase acting upon HIF-1α in colorectal cancer [42]. Additionally, PIM1 was identified as conferring phenotypic effect in murine and *in vitro* models of JVF malignancy [13,25] and more widely has been extensively linked to haematological malignancies.[58–60]. Aberrant expression of the mixed-line-age leukaemia (MLL) gene caused by FLT3 or Hoxa9 activation in AML has been shown to be associated with elevated levels of PIM1 [61], whilst PIM1 expression has been shown to be predictive of patient prognosis in mantle cell lymphoma treated with high dose therapy, stem cell transplantation and Rituximab [62]. PIM kinases have also been shown to be solid progression markers in diffuse large B-cell lymphoma (DLBCL) [63] with pan-PIM inhibition shown to be cytotoxic to DLBCL cell lines [64]. Concurrent with these data, meta-analysis of murine and human RNAseq identify upregulation of PIM1 transcript, as well as direct analysis of murine BM-derived HSPCs by qRT-PCR. Mechanistically we determine that HIF-1α is stabilised in JVF cells by a PIM1 dependant mechanism through inhibition of proteasomal degradation via the PHD/VHL hydroxylation/ubiquitination couplet, the same route by which HIF-1α is stabilised by PIM1 in prostate cancer [42]. Notably, we identify a previously undescribed phosphorylation event on HIF-1α in JVF cells occurring within the oxygen dependent degradation (ODD) domain (Thr498/Ser500), which is distinct from the previously described PIM1 site (Thr455) [42]. Whilst well-characterised in terms of post-translational modifications and interactors [65], the ODD domain of HIF-1α is inherently unstructured. This is a typical feature of transcription factors to enable their function to be pliable in response to co-regulator protein interactors [66]. Phosphorylation of the Thr498/Ser500 sites might sterically block interaction of PHD

enzymes, however their proximity to the hydroxy-target proline residues (P402/P564) indicates an intermediate conformational alteration or protein interaction may be involved [67–69]. Further studies are warranted to determine the effects of Thr498/Ser500 phosphorylation on HIF-1α structure and function in JVF MPNs, and also to identify if this pathological phosphorylation event occurs in haematological or solid cancers of other origin.

Despite its potency within malignant transformation and progression, pharmacological inhibition of HIFs has been largely unsuccessful, with the exception of the recent FDA-approved HIF-2α inhibitor Belzutifan (MK-6482), indicated for advanced clear cell renal cell carcinoma [26]. Unlike HIF-1α, the HIF-2α isoform is exclusively oncogenic in a malignant context, suggesting that its regulation is less context-specific. HIF-1α inhibition, conversely, has not been successful as a therapeutic avenue in malignancy, largely due to the negative side effects of impaired canonical HIF activity in healthy cells [70–72]. The ability to delineate physiological from pathological activation or function of HIF-1α therefore creates new avenues to target HIF-1 within a specified disease context. Our study demonstrates that PIM1 inhibition eradicates HIF-1α in JVF cells and corrects aberrant lineage committal decisions within JVF HSPCs. These data therefore present mechanistic insights into the downstream effects of PIM1 inhibition on transcription, which include reversing the pathological activation of HIF-1. Future studies investigating alterations in the phospho/total-proteome in JVF cells treated with PIM1 inhibitors would bring further value into the modality of action of this therapeutic approach within MPNs.

ChIP-MS/RIME performed on HIF-1α in triple negative breast cancer [16] and renal cell carcinoma [17] cell lines exposed to hypoxia demonstrated that with a few notable exceptions (e.g. HIF-1β/ARNT and TRIM28), the transcription partners of HIF-1α are heavily dictated by the tissue/cancer-context. By applying DOCIA to isogenic paired WT JAK2/JVF haematopoietic progenitor cell lines, our study approach provided a clean genetic system to identify those partners specifically recruited to HIF-1 by JVF signalling in haematopoietic progenitor cells, as opposed to identifying tissue- or cancer-context associated factors. These findings hold particularly pertinent implications for targeting HIF-1 within haematopoietic malignancies, where eradication of the malignant clone whilst sparing normal haematopoiesis is the gold standard therapeutic approach [39,73].

We observed significantly higher HIF-1α protein levels at the chromatin in JVF cells compared to WT JAK2 cells by mass spectrometry, despite equal input into DOCIA assays across experimental conditions. Unexpectedly, this was paired with reduced peak intensity of associated genomic DNA as determined by NGS (ChIP-Seq). STRING analysis of the protein partners of HIF-1α in JVF cells (normalised against the geometric mean of HIF-1α

spectral counts to account for the above increased HIF-1 protein observed in these cells) identified an enrichment of RNA-binding/processing factors including TDP-43, Khdrbs1/Sam68, Fau and Znf638. Taken together, these data suggest that HIF-1 may perform a different role at the chromatin in JVF mutant HSPCs compared to WT JAK2, one that is more distal to DNA. This may account for a reduced association with DNA, coupled with enhanced interaction with post-transcriptional RNA processing factors. This hypothesis is also supported by the identification that HIF-1 binds to intron/exon regions of target genes, and that VF_Hx HIF-1 target genes are both up- and down-regulated at the transcript level, which both also suggest that HIF-1 is performing a transcript regulatory role beyond canonical transcription initiation in the JVF context. A subset of transcription factors, historically referred to as “coupling proteins" for their role in mechanically and functionally coupling the steps from transcription to translation, regulate pre-mRNA processing via regulation of elongation rates and pre-mRNA imprinting (binding to nascent RNA) [27,28]. Notable examples include the Wilms tumour-suppressor protein (WT1), originally identified as a transcription factor initiating growth and development gene expression profiles, which was subsequently demonstrated to localise to nuclear speckles, bind to RNA and splice factors, and regulate gene-expression via splicing [29–32]. In triple negative breast cancer cell lines, HIF-1α can bind to TRIM28/DNA-dependent protein kinase (DNAPK) to release paused RNA Pol II, thereby regulating elongation rate and, it is rational to presume, splicing, although this was not investigated in this study [16]. Our findings further implicate HIF-1 as adopting pre-mRNA splice-regulatory roles in JVF HSPCs to produce the observed disease-driving regulon of suppressed and activated genes in MPN disease, however further investigation is required to fully elucidated this non-canonical mechanism of HIF-mediated gene expression.

Meta-analysis of ChIP-seq, RNAseq and MPN patient cohort survival studies identify a set of DNA damage response genes that are deregulated by HIF-1 and significantly associated with overall survival of JVF MPN patients. JVF-carrying HSPCs are known to accumulate spontaneous DNA damage compared to healthy counterparts due to replication stress and the burden of metabolic products [33–36] and activate the DNA damage response (DDR) [33,35]. Our findings identify that malignant co-option of HIF-1 facilitates in part the enhanced DDR via upregulation of PCNA (nucleotide excision repair), [37], BLM helicase (*BLM*; double-strand break repair by homologous recombination (HR)) [38], Aurora Kinase B (*AURKB*; mitotic DNA damage checkpoints) [39] expression and Tankyrase 1 (*TNKS*, HR) [40], each of which is significantly associated with worsened patient survival. Furthermore, we identify these DDR genes are significantly upregulated in patients undergoing spontaneous leukemic transformation.

Lastly, our study identifies a 13-gene HIF-1 signature comprising the aforementioned pathways, significantly associated with both spontaneous leukaemic transformation and overall survival of JVF positive MPN patients. To our knowledge, these genes have not previously been implicated in MPN disease pathogenesis and therefore represent both novel pathogenic mechanisms and therapeutic targets.

Through direct experimental analysis of the HIF-1 transcription complex and regulon, our study identifies a hitherto unknown co-option of HIF-1 in JVF MPNs mediated by aberrant phosphorylation of HIF-1 via PIM1 kinase. We identify that in the setting of MPN, HIF-1 is reprogrammed to perform non-canonical roles as a direct result of oncogene signalling pathways, driving malignant phenotypes and revealing new prognostic signatures for MPNs. These findings also illuminate the value of direct analysis of TF complexes within a disease setting, highlighting the discrepancy between canonical HIF-1 regulons and those induced by oncogenic signalling pathways in the context of JVF MPNs. These identifications provide evidence that functional delineation of the essential homeostatic roles of HIF-1 within normal physiology from those roles co-opted by malignancy is possible and identifies tractable handles for this as a therapeutic approach within MPNs. Finally, our study warrants future investigations into the malignant co-option of HIFs and the resultant regulons in the pathogenesis of other haematological and solid cancers.

## Methods

### Patient data

We obtained bulk RNA-sequencing data and clinical annotations from 230 patients with a positive JAK2V617F mutation from the Princess Margaret Cancer Centre MPN cohort [48]. Individual gene expression counts were subjected to VST normalisation using the 'DESeq2' R package whereas gene sets were scored using gene set variation analysis (GSVA) using the 'GSVA' R Package [50,74]. Survival analysis was performed using the 'survival' and 'survminer' packages in R and visualised with Kaplan Meier plots to depict differences in survival outcomes between patients with high or low gene expression or gene set enrichment. MIPSS70 analysis was performed within 172 patients with available genomic annotations [51].

### Animal models

Animals used in this study were C57BL/6 mice (WT) and Jak/2E/B6 Stella Cre heterozygous and homozygous. All mice were bred and housed under specific pathogen-free conditions at the University of York. All animal procedures were approved by the University of York Animal Welfare and Ethical Review Board and carried out under United Kingdom Home Office

license (PEAD116C1). Animals were euthanized by $CO_2$ asphyxia and cervical dislocation. All the mice were 8 to 12 weeks old.

**Lineage negative HSPC isolation and expansion**

Lineage negative cells were isolated from the pelvis, femurs and tibias of C57BL/6 (WT) and Jak/2E/B6 Stella Cre mice using EasySep™ Mouse Hematopoietic Progenitor Cell Isolation Kit (STEMCELL Technologies 19856) according to the manufacturer's protocol, and were either used directly in downstream experiments or FACS sorted into Fibronectin-coated plates (Corning) containing PVA mouse expansion media [75]: Ham's F12 media (Gibco) supplemented with 1X penicillin-streptomycin-glutamine (Gibco), 1X HEPES (Gibco), 1X insulin-transferrin-selenium-ethanolamine (Gibco), 1 mg/ml polyvinyl alcohol (Sigma), 100 ng/ml recombinant mouse thrombopoietin (TPO; Peprotech), and 10 ng/ml recombinant mouse stem cell factor (SCF; Peprotech)1,2. 20 nM, IACS-010759 (Selleck). Gating strategy for FACS sorting of ESLAMS ($CD48^-$, $CD45^+$, $Sca1^+$, $CD150^+$, $EPCR^+$) HSCs as follows (Fig. S13); FSC-A vs SSC-A plotted to gate cells and exclude debris, FSC-H vs FSC-A plotted to gate 'singlets' and exclude 'doublet' events, SSC-H vs SSC-A plotted to gate 'singlets' and exclude 'doublet' events, Live/Dead Violet (LIVE/DEAD™ Fixable Violet Dead Cell Stain (Invitrogen L34955)) vs FSC-A plotted to gate for live cells and exclude dead cells, CD150 (PE/Cyanine7 anti-mouse CD150 (SLAM) Antibody (Biolegend)) vs CD48 (APC anti-mouse CD48 Antibody (Biolegend)) plotted to gate $CD150^+$ $CD48^-$ (SLAM) cells, EPCR (CD201 (EPCR) Monoclonal Antibody (eBio1560 (1560)), PE, eBioscience™ (Invitrogen)) vs CD45 (Alexa Fluor® 488 anti-mouse CD45 Antibody (Biolegend)) plotted to gate for $EPCR^+$ $CD45^+$ (ESLAM) cells, EPCR vs Sca-1 (Brilliant Violet 605™ anti-mouse Ly-6A/E (Sca-1) Antibody (Biolegend)) plotted to gate for Sca-$1^+$ cells (ESLAMS). Endpoint immunophenotyping of expanded cultures was performed after 14 days by flow cytometry with panel of antibodies as previously described [76] including ViaKrome 808 Fixable Viability Dye (Beckman Coulter), CD34 - CD34 Monoclonal Antibody (RAM34) Alexa Fluor™ 488, eBioscience™ (Invitrogen), CD16/32 - PE/Cyanine7 anti-mouse CD16/32 Antibody (Biolegend), CD41 - APC anti-mouse CD41 Antibody (Biolegend), Lineage - PE anti-mouse Lineage Cocktail (Biolegend) (Fig. S14 for gating strategy).

For drug treatments of expansion cultures, 100 nM (or dose as on figure μM) GN44028 (MedChemExpress or Tocris-Biotechne), SMI-4a (Cayman Chemical) (dose as shown on figure μM), TCS7009 (Tocris-Biotechne) (dose as shown on figure μM) or DMSO (Sigma) were added to the HSC media where indicated. Cells were incubated at 5% $CO_2$ and either 1% $O_2$, 5% $O_2$ or 20% $O_2$ (Invivo 500 hypoxic workstation or Binder CO2 incubator) for 6 hours as previously described [7]. Re-plating assays were performed by FACS sorting

cultured live (PI-) cells into fresh wells of complete media and then assessing the derived cell cultures after 14 days. We used >4000 live cells/well with >10% c-Kit+Sca1+Lineage- cells as the cut-off for replating activity. Extreme limiting dilution analysis was used to estimate culture replating cell frequencies.

**Flow cytometry.**

Following bone marrow isolation and lineage depletion, cells were resuspended in HSC culture media (see above) and cultured at 5% $CO_2$ and either 1% $O_2$ or 20% $O_2$ (Invivo 500 hypoxic workstation or Binder CO2 incubator) for 4 hours as previously described [7]. Cells were then fixed (16% PFA (2% PFA final concentration)), permeabilised in methanol and stained with LIVE/DEAD™ Fixable Violet Dead Cell Stain (Invitrogen L34955) and either HIF-1α (D1S7W) XP® rabbit mAb (Alexa Fluor® 488 conjugate) (Cell Signalling Technologies) or HIF-1 alpha Monoclonal Antibody (Mgc3), PE, eBioscience™ (Invitrogen) with appropriate isotype control (Rabbit (DA1E) mAb IgG XP® Isotype Control (Alexa Fluor® 488 conjugate) (Cell Signalling Technologies) or Mouse IgG1 kappa Isotype Control (P3.6.2.8.1), PE, eBioscience™ (Invitrogen)). Samples were washed with FACS buffer and run on CytoFlex LX flow cytometer (Beckman Coulter) and data analysed using FlowJo software (BD).

**Multiplex fluorescent barcoding and phospho-flow cytometry.**

UT7/TPO cells were cultured as indicated and then starved overnight in 2% FBS RPMI (Roswell Park Memorial Institute (RPMI) 1640 Medium (Gibco)) media with no TPO prior to treatment. Cells were treated as indicated with 2.5µm SMI-4a (Cayman Chemical) for 6hrs, 2µm Ruxolitinib (Rux) (Cell Guidance Systems) for 6hrs, DMSO (Sigma) vehicle control for 6hrs and/or 50ng/ml TPO (Peprotech) 30 minutes in either 6hrs of hypoxic (1% $O_2$) conditions or in normoxia (20% $O_2$). Cells were then fixed in 16% PFA (16% Formaldehyde, Methanol-Free #12606 Cell Signalling Technology) (2% PFA final concentration), resuspended in methanol for permeabilization and stored at -80℃ prior to barcoding. Compensation controls prepared prior to barcoding using cells for dye single stains and VersaComp beads (Beckman Coulter B22804) for signalling antibodies' single stains. Barcoding and flow cytometry was performed as previously described (including antibodies specified), [32]. Fig. S6 for gating strategy.

**Cell culture**

Murine BaF3 cells stably expressing the human MPL and human JAK2 (BaF3 hMPL hJAK2 WT) or the JAK2V617F mutant (BaF3 hMPL hJAK2 VF) were grown in RPMI media (Gibco) (10% FBS (Gibco), 1% penicillin (Gibco)/streptomycin/L-glutamine (Gibco)) (plus murine IL-3

(Peprotech) for hJAK2 WT cells). Human UT7/TPO cells expressing JAK2 (UT7/TPO JAK2 WT) or the JAK2V617F mutant (UT7/TPO JAK2 VF) were grown in RPMI media (Gibco) (10% FBS (Gibco), 1% penicillin (Gibco)/streptomycin/L-glutamine (Gibco)) (plus human TPO (Peprotech) for JAK2 WT cells). Human SET2 cells heterozygous for the JAK2V617F mutation were grown in RPMI media (Gibco) (20% FBS (Gibco), 1% penicillin/streptomycin (Gibco)/L-glutamine (Gibco)) and human HEL cells homozygous for the JAK2V617F mutation were grown in RPMI media (Gibco) (10% FBS (Gibco), 1% penicillin/streptomycin (Gibco)/L-glutamine (Gibco)). Cells were incubated at 5% $CO_2$ and the indicated $O_2$ concentrations.

**Western blot**

Cells were cultured as above and treated with either 4mM NAC (Biotechne), 75μM DMF (Stratech Scientific), 10μM SMI-4a (Cayman Chemical), (dose as on figure μM) TCS PIM1.1 (Santa Cruz Biotechnology), (dose as on figure μM) PIM447 (Sellachem), 2μM Ruxolitinib (Rux) (Cell Guidance Systems), 10μM MG132 (MedChemExpress), 50ng/ml human TPO (Peprotech) or (dose as on figure nM) SCH874 (Sellachem) as indicated. Cells were lysed in cell lysis buffer (20 mM Tris-HCl (pH 7.5), 150 mM NaCl, 1 mM $Na_2EDTA$, 1 mM EGTA, 1% Triton) plus Halt™ Protease and Phosphatase Inhibitor Cocktail, EDTA-free (ThermoFisher Scientific). Lysate (20 μg) was separated on 4-20% Mini-PROTEAN® TGX Stain-Free™ protein gels (Biorad) and transferred onto Immun-Blot® Low Fluorescence PVDF membrane (Biorad). Membranes were probed for the indicated antibodies (list below).

Isotype control - Rabbit (DA1E) mAb IgG XP® isotype control (Cell Signalling Technology)

HIF-1α - HIF-1α (D1S7W) XP® Rabbit mAb (Cell Signalling Technology)

pHIF-1α (Thr455) - Rabbit mAb (Generously donated by Prof. Noel Warfel)

β-Actin - Anti-actin hFAB Rhodamine (Biorad)

TDP-43 - TARDBP Antibody (H-8): sc-376532 mouse mAb (Santa Cruz)

ERK1/2 - p44/42 MAPK (Erk1/2) (L34F12) mouse mAb #4696 (Cell Signalling Technologies)

pERK1/2 - Phospho-p44/42 MAPK (Erk1) (Tyr204)/(Erk2) (Tyr187) (D1H6G) Mouse mAb #5726 (Cell Signalling Technologies)

Golga3 - Golgin 160 Antibody (C-8): sc-374596 mouse mAb (Santa Cruz)

SIK2 - SIK2 Antibody (B-12): sc-393139 mouse mAb (Santa Cruz)

IMPDH -IMPDH Antibody (F-6): sc-166551 mouse mAb (Santa Cruz)

p70 S6K - p70 S6 kinase α Antibody (H-9): sc-8418 mouse mAb (Santa Cruz)

pp70 S6K (T389) - Phospho-p70 S6 Kinase (Thr389) (108D2) Rabbit mAb #9234 (Cell Signalling Technologies)

PIM1 - PIM1 Recombinant Polyclonal Antibody (19HCLC) (Invitrogen)

NRF2 - Nrf2 Antibody (A-10): sc-365949 mouse mAb (Santa Cruz)

STAT3 - STAT3 (124H6) mouse mAb (91395) (Cell Signalling Technologies)

pSTAT3 (Y705) - Phospho-STAT3 (Tyr705) (D3A7) XP® rabbit mAb (91455) (Cell Signalling Technologies)

JAK2 - JAK2 Monoclonal Antibody (691R5) mouse mAb (Invitrogen)

pJAK2 (Y1007/8) - Phospho-Jak2 (Tyr1007/1008) (C80C3) Rabbit mAb #3776 (Cell Signalling Technologies)

**Immunoprecipitation**

Cells were cultured as above with the indicated conditions. Cells were lysed in cell lysis buffer (20 mM Tris-HCl (pH 7.5), 150 mM NaCl, 1 mM $Na_2EDTA$, 1 mM EGTA, 1% Triton) plus Halt™ Protease and Phosphatase Inhibitor Cocktail, EDTA-free (ThermoFisher Scientific). 200 µg of cell lysate used as input for immunoprecipitation. Cell lysates were precleared by addition of Protein A magnetic beads (Cell Signaling Technologies) for 20 minutes at RT with rotation followed by magnetic separation. Proteins were captured by addition of HIF-1α (D1S7W) XP® Rabbit mAb (Cell Signaling Technology) or TDP-43 sc-376532 mouse mAb (Santa Cruz) and incubated overnight at 4°C with rotation followed by immunoprecipitation by addition of Protein A magnetic beads and incubation for 20 minutes at RT, followed by magnetic separation and washing. Immunoprecipitated protein as then analysed by western blotting.

**Dual Output Chromatin Interactome Assay (DOCIA)**

$5x10^7$ BaF3 hMPL hJAK2 WT or BaF3 hMPL hJAK2 VF cells were incubated at the indicated $O_2$ concentrations for 6 hours. Cells were fixed by addition of 2mM Disuccinimidyl glutarate (DSG) (Chem Cruz - Santa Cruz) for 20 minutes with agitation, pelleted by centrifugation at 500xg for 5 minutes RT, and then resuspended into 1% formaldehyde (Cell Signalling Technology) for 10 minutes at room temperature (RT), then neutralised by the addition of 10x Glycine for 5 minutes at RT. Sample processing and immunoprecipitations were performed as described previously [41,42]. **Chromatin-Immunoprecipitation:** Samples were then processed using SimpleChIP® Enzymatic Chromatin IP Kit, Magnetic

Beads (Cell Signaling Technology) according to the manufacturer's protocol. ChIP was performed with HIF-1α (D1S7W) XP® Rabbit mAb (Cell Signaling Technology). DNA was isolated using a ChIP DNA Clean & Concentrator (Zymo Research). **Next Generation Sequencing:** Library preparation was performed using the NEBNext DNA Ultra II library preparation kit for Illumina and performing 12 cycles PCR amplification with unique dual indexed primers. Libraries were pooled at equimolar ratios, and subject to 150 base paired end sequencing on an Illumina NovaSeq 6000 at Azenta Life Sciences. Read quality was assessed with FastQC v0.11.7 [77], removing any retained adapters and poor quality reads using a sliding window approach with trimmomatic v0.36 [78]. Reads were discarded when trimmed to less than 50 base pairs and only intact read pairs were retained. Reads were aligned to the GRCm39 primary mouse assembly with STAR v2.7.10a [79] and annotated with SAMtools v1.15 [80] fixmate and markdup. ENCODE mm10 'blacklist' regions [81]) were removed after GRCm39 UCSC liftOver using BEDTools v2.30.0 [82]. Peaks were called with MACS v2.2.7.1 [83] and pairwise differential binding assessed using DiffBind v3.14.0 [84] in R v4.3.3 using all replicates and input controls. Absolute $\log_2$ fold changes greater than 1 and FDR-corrected p values less than 0.05 were considered in the first instance, with FDR-based ranking also used to assess condition-specific HIF-1α binding importance. Relevant peak locations were plotted using karyoploteR v1.3.0 [85]. Peak locations were annotated using ENCODE and GENCODE GRCm39 annotations and HREs detected using Jellyfish 2.3.0 [86].

**Mass spectrometry:** Protein was on-bed digested with trypsin, without reduction or alkylation. Peptides were desalted by C18 ZipTip before drying and resuspending in aqueous 0.1% TFA for LC-MS. Peptides were acquired over a 1 h acquisition with elution from a 50 cm EN PepMap C18 column driven by a Waters mClass UPLC onto an Orbitrap Fusion Tribrid mass spectrometer operated in DDA mode. MS1 spectra were acquired in the Orbitrap mass analyser at 120K resolutions and a cycle time of 1 s, with MS2 spectra acquired in parallel in the linear ion trap using TopSpeed selection. LC-MS chromatograms in. raw format were imported into Progenesis QI for peak picking and chromatographic alignment, before exporting a concatenated tandem mass list in .mgf format for Mascot database searching. Searching was performed against the mouse subset of the SwissProt database appended with common proteomic contaminants. Peptide spectral matches were filtered to 1% FDR using the percolator algorithm and as assessed empirically against a reverse database search. Accepted peptide identifications were imported into Progenesis QI, associated with the chromatographic data and mapped between runs. Data were further filtered to require a minimum of two unique peptides per protein quantification. Relative protein quantification was inferred from peptide precursor ion areas using unique, non-

conflicting peptides only and after normalisation to total peptide intensity among runs. Statistical testing between groups was done using anova with the null hypothesis being that proteins are of equal abundance between all samples. The Hochberg and Benjamini FDR methodology was used for multiple test correction of p-values to q-values.

**Phosphoproteomics**

Samples immunoprecipitated for HIF-1α (see above) were digested on-bead using the RIME protocol and trypsin as the protease, before $TiO_2$ (MagReSyn) phosphopeptide enrichment. Resulting peptides were loaded onto an EvoTip Pure for introduction onto an 8 cm performance column. Elution was carried out using a 60 SPD pre-set gradient on an EvoSep One UPLC. DDA-PASEF data were acquired using a Bruker timsToF HT. Data were searched through FragPipe for phosphopeptide identification and relative quantification at 1% FDR. Statistical testing was performed for all pairwise comparisons using limma via FragPipe-Analyst. Zero value imputation was applied and the Hochberg and Benjamini approach was used for multiple test correction. Significance threshold was set at $q < 0.05$.

**Bulk RNAseq and analysis**

Bulk RNAseq data of JAK2V617F knock-in mice re-analysed from publicly available dataset (GEO: GSE180853). RNA extracted, prepared and sequenced as per method specified in paper [53]. Briefly, RNA extracted by TRIzol extraction from sorted-cell populations as indicated. RNA-seq libraries were generated by 3′ sequencing and SMART-Seq2 amplification and sequenced on an Illumina HiSeq 4000. SRA short read RNA-seq analysis performed as follows; raw, paired-end Illumina reads downloaded from NCBI SRA were first trimmed with Cutadapt (version 2.10) [87] to remove the Illumina universal adapters and any low-quality sequence, with a minimal length threshold of 20bp. Trimmed reads were mapped and quantified using the Salmon (version 1.10) [88] pseudo-aligner, using the GENCODE M32 (GRCm39) [89] Mus musculus transcriptome, specifying the ISR library type, 100 bootstraps, and the “validateMappings” option. Differential expression analysis was run using the Sleuth (version 0.30.1) [90] and Wasabi (version 1.0.1) [91] packages in R, on a gene-wise basis, and using the Wald test to find statistically significant, differentially expressed genes. Genes with a log2 fold change of greater than +/-1 and with a q value of less than 0.1 were taken to be significantly differentially expressed.

**scRNAseq and analysis**

scRNAseq of MPN patients and healthy controls taken from publicly available dataset (GEO: GSE144568). RNA extracted, prepared and sequenced as per method specified in paper [54]. SRA single cell RNA-seq analysis performed as follows; CellRanger files downloaded from NCBI SRA were loaded into the Seurat package (version 5.1.0) [92] and the Read10X

function. Samples read in separately and were filtered to exclude genes expressed in fewer than 3 cells, and to exclude cells with fewer than 500 genes expressed. Cells with greater than 10% mitochondrial gene expression were excluded. Filtered samples were merged and then normalised, scaled, and variable features identified. Layers in the merged object were integrated with the “RPCAIntegration” method. The “FindNeighbors” function was run using the first 30 principal components, followed by FindClusters function with a resolution of 0.25. The RunUMAP function was used to calculate the UMAP dimensional reduction, again with the first 30 principal components. Marker genes for the UMAP clusters were found by first joining the layers with the JoinLayers function and then using the FindAllMarkers function. The UMAP clusters were renamed according to their cell types, by manually assessing the marker genes for each cluster. HIF gene module scores were calculated by providing a list of HIF-associated genes to the R UCell package [93] and the “AddModuleScore_UCell” function, and added to the Seurat object to visualise the HIF gene module scores for the cells in their respective UMAP clusters.

**RT-qPCR**

RNA was extracted from samples using Monarch® Total RNA Miniprep Kit #T2010S and RT performed using LunaScript RT Master Mix Kit (Primer-free) #E3025S (New England Biolabs) as per manufacturer protocols with SimpliAmp™ Thermal Cycler (Applied Biosystems™ #A24811). qPCR was performed with SYBR™ Green PCR Master Mix (Applied Biosystems™ #4309155) and primers: Ms GAPDH (F): CATCACTGCCACCCAGAAGACTG, Ms GAPDH (R): ATGCCAGTGAGCTTCCCGTTCAG, Ms PIM-1 (F): CGCGACATCAAGGACGAGAACA, Ms PIM-1 (R): CGAATCCACTCTGGAGGACTGT on StepOnePlus™ Real-Time PCR System (Applied Biosystems™ #4376600). Analysis performed on StepOne Software.

**Figure legends:**

**Figure 1**

(A) JVF stabilises HIF-1α independent of oxygen levels in monogenic JVF and JVF MPN immortalised cell lines. Immunoblot of HIF-1α levels in normoxic cultured wildtype and JVF-monogenic UT7/TPO and hMPL BaF3 cells, JVF heterozygous MPN-patient derived SET2 cells and JVF homozygous MPN-patient derived HEL cells. Immunoblotting carried out using HIF-1α antibody with β actin as a loading control (n=3).

(B) In wildtype primary mouse HSCs, HIF-1α is stabilised by physioxic (5% O2) and hypoxic (1% O2) conditions correlative to oxygen levels. Representative intracellular flow cytometry plot for anti- HIF-1α -PE staining in wildtype mouse HSC-derived 20%, 5%, or 1% O2 cultures.

(C) Treatment with HIF-1α inhibitor reduces the population of CD201+CD150+LSK cells and overall cell viability whilst increasing the percentage of lineage committed cells in 10-day PVA expansion culture. Mean frequency of CD201+CD150+LSK cells (left), mean number of live cells per well (middle), and mean frequency of Lineage+ cells (right) within 10-day HSC-derived cultures at 20% O2, 5% O2, or 1% O2, cultured with either DMSO or the HIF-1α-specific transcription inhibitor GN44028 (100 nM) (n=10).

(D) JVF stabilises HIF-1α in primary mouse lineage depleted bone marrow cells. Flow cytometry histogram distribution of channel fluorescent intensity (normalised to mode) and cell count (table below) from JVF homozygous (n=1), heterozygous (n=2) and wildtype (n=2) C57/BL6 mouse lineage-depleted bone marrow cells probed with fluorescently labelled HIF-1α antibody, following ex-vivo culture in 4hrs hypoxic 1% O2 (blue) or normoxic 20% O2 (purple) conditions (n=2).

(E) Treatment with ROS scavenger NAC (N-acetyl-L-cysteine) fails to inhibit JVF-induced HIF-1α stabilisation (whereas PIM1 inhibition with SMI-4a, does inhibit JVF-induced HIF-1α stabilisation). Immunoblot of HIF-1α, PIM1 and PIM1 substrate (p70 S6K) levels in wildtype and JVF UT7/TPO cells starved overnight and treated as indicated with either NAC (from the onset of starvation - 24hr treatment), SMI-4a (6hr treatment) or vehicle control. Immunoblotting carried out using HIF-1α, T389 p70 S6K, p70 S6K and PIM1 antibodies with β actin as a loading control (n=3).

(F)(I) Kinase cascade activity downstream of JAK2 shows significant differences between TPO-stimulated JAK2 and JVF-mediated constitutive signalling. Wildtype and JVF UT7/TPO cells overnight starved or treated with TPO (thrombopoietin) and analysed by multiplex fluorescent phospho-flow cytometry. Heatmap of mean fold change of channel fluorescence intensity (MFI), data normalised based on fold change to mean value of wildtype starved, no TPO, normoxic condition (±SEM) (n=3).

(II) Proportional representation of kinase activity as detected by phospho-flow cytometry relative to total kinase cascade signalling downstream of JAK2 shows an increase in the relative amount of STAT1 and STAT5 activation in JVF cells compared to TPO/MPL stimulation of wildtype JAK2 (n=3).

(G) Database analysis of STAT1 and STAT5 target genes show PIM1 as the sole known kinase of HIF-1α. STAT1 gene targets indicated in purple, STAT5 gene targets indicated in blue, shared STAT1 and STAT5 targets indicated in green, of which are kinases shown in yellow.

(H) PIM1 transcript expression is significantly higher in JVF mouse MEPs (Megakaryocytic-erythroid progenitors) compared to wildtype. Bulk RNA-seq analysis of mouse MEPs from wildtype (n=3) and JVF heterozygous mice (n=3).

(I) PIM1 transcript expression is significantly higher in both total and lineage negative JVF mouse bone marrow. qRT-PCR of PIM1 transcript levels in homozygous JVF (n=3) and wildtype (n=3) mouse bone marrow HSPCs (total and lineage negative) with GAPDH as a housekeeping gene control.

(J) PIM1 transcript levels are elevated and localised to the megakaryocyte progenitor (MkP) population in JVF positive MPN patients when compared to healthy controls. UMAP scRNAseq plots of control (top row) and myelofibrosis (bottom row) HSPCs with PIM1 transcript highlighted in purple.

**Figure 2**

(A)(I) Treatment with a variety of PIM1 inhibitors inhibits JVF-mediated HIF-1α stabilisation. Immunoblot for HIF-1α, HIF-1β, PIM1 and PIM1 substrate (p70 S6K) of JVF UT7/TPO cells starved overnight and treated with the indicated PIM inhibitor for 6hrs at the indicated dose. Immunoblotting carried out using HIF-1α, HIF-1β, pT389 S6, p70 S6K and PIM1 antibodies with β actin as a loading control (n=3).

(II) Treatment with SMI-4a restores JVF-stabilised HIF-1α levels closer to those of wildtype TPO-treated cells and leaves wildtype TPO-treated cells unaffected, whilst treatment with Rux ablates both JVF-mediated and wildtype TPO-induced HIF-1α levels. Barcoded phospho-flow cytometry of HIF-1α levels in JVF and wildtype UT7/TPO cells, cultured in normoxic (20% O2) or hypoxic (1% O2) conditions, starved overnight or treated with TPO and SMI-4a, Rux or vehicle control as indicated. Heatmap of mean channel fluorescence intensity (MFI), data normalised based on fold change to mean value of wildtype starved, no TPO, normoxic condition (n=3).

(B)(I) Treatment with SMI-4a effectively lowers levels of JVF-stabilised HIF-1α whilst leaving JAK2 signalling cascades untouched, whilst treatment with Rux ablates both JVF-stabilised HIF-1α and JAK2 downstream signalling. Immunoblot for HIF-1α, JAK2, and various kinase cascade constituent proteins downstream of JAK2 of SET2 and HEL cells treated with Rux, SMI-4a or vehicle control as indicated. Performed using HIF-1α, pY1007/8 JAK2, JAK2, pY705 STAT3, STAT3, pT389 p70 S6K, p70 S6K, pY204/Y187 ERK1/2 and ERK1/2 antibodies and using β actin as a loading control (n=3).

(II) Treatment with SMI-4a effectively leaves JAK2 signalling cascades untouched, whilst treatment with Rux ablates JAK2 downstream signalling. Barcoded phospho-flow cytometry

of kinase cascade constituent proteins downstream of JAK2 in JVF and wildtype UT7/TPO cells, cultured in normoxic (20% O2) or hypoxic (1% O2) conditions, starved overnight or treated with TPO and treated with SMI-4a, Rux or vehicle control as indicated. Heatmap of mean channel fluorescence intensity (MFI), data normalised based on fold change to mean value of wildtype starved, no TPO, normoxic condition (±SEM) (n=3).

(C) PIM1 inhibition rescues HSC expansion culture phenotype in JVF cells as determined by proportion of LSK ((lineage negative, Sca-1 positive, c-kit positive) and progenitors in culture, returning the LSK/Prog ratios to those observed in wildtype expansion cultures, whilst leaving wildtype expansion cultures unaffected. Ex vivo expansion of long-term HSCs from wildtype (purple) and JVF heterozygous (blue) mice in the PVA culture system treated with the indicated dose (μM) of SMI-4a or vehicle control and immunophenotyped (by gating strategy following previously described HSC populations [76]) after 14 days of expansion and expressed as percentage of lineage negative cell population (n=3).

**Figure 3**

(A)(I) Two novel JVF-exclusive phosphorylation sites identified on HIF-1α (Thr498 and Ser500), compared to wildtype hypoxia-treated cells. Phosphoproteomic mass spectrometry analysis of hypoxia-treated JVF and wildtype UT7/TPO cell lysate enriched for phosphoproteins by TiO2 and enriched for HIF-1α by immunoprecipitation (n=3).

(II) Two novel JVF-exclusive phosphorylation sites identified on HIF-1α (Thr498 and Ser500), compared to wildtype hypoxia-treated cells. Volcano plot of phospho-site signal intensity in hypoxic JVF cell lysate vs hypoxic WT cell lysate plotted vs statistical significance (-log10 adj p value).

(B) Ser500 site is highly evolutionarily conserved across species whereas Thr498 is not. Sequence alignment of various species at Thr498/Ser500 site highlighted by blue dotted box as shown.

(C) Novel JVF-exclusive phosphorylation sites (Thr498 and Ser500) fall in HIF-1αs ODD (oxygen-dependent degradation) domain between canonical HIF-1α hydroxylation sites (P402 and P564). Ribbon diagram (top) and domain diagram (bottom) of HIF-1α, both coloured by domain. Amino acid residues of interest marked in red on both.

(D) Treatment with proteasome-inhibitor MG132 inhibits SMI-4a-mediated destabilisation of JVF-mediated HIF-1α stabilisation. Immunoblot for HIF-1α of JVF and wildtype UT7/TPO cells cultured in normoxic (20% O2) or hypoxic (1% O2) conditions treated with SMI-4a, MG132 or a combination of the two as indicated, using HIF-1α antibody and using β actin as a loading control (n=2).

**Figure 4**

(A)(I) Diagram of DOCIA method: wildtype or JVF hMPL BaF3 cells cultured in normoxic (20% O2), or hypoxic conditions (1% O2) have their nuclear material crosslinked to retain DNA-bound proteins, fragmented and HIF-1α containing fragments immunoprecipitated by the addition of HIF-1α antibody. The sample is then divided for concurrent analysis by both ChIP-seq (to determine HIF-1αs genomic binding loci) and mass spectrometry (RIME- Rapid immunoprecipitation mass spectrometry of endogenous protein) (to determine HIF-1αs associated transcription cofactors).

(II) JVF causes significantly increased abundance of HIF-1α protein at the chromatin in hypoxic conditions yet is significantly less bound to it compared to wildtype cells cultured in hypoxia in both normoxia and hypoxia. RIME-mass spec analysis of HIF-1α abundance at the chromatin (left) and ChIPseq analysis of the general peak intensity of chromatin bound by HIF-1α (right) in wildtype and JVF hMPL BaF3 cells cultured in either normoxic or hypoxic conditions. Coloured by condition as described in Fig. 4A(I) (n=3).

(B) Whilst several cofactors are found to be common between all conditions, a number are identified as unique to JVF in both normoxia and hypoxia. Venn diagram displaying number of cofactors unique to each condition shown as determined by RIME-mass spec. Coloured by condition as described in Fig. 4A(I) (n=3).

(C) RIME-mass spec-identified HIF-1α cofactors displayed as a heatmap by binding intensity (Log2FC), normalised to HIF-1α protein levels. Wildtype and JVF hMPL BaF3 cells cultured in either normoxic (20% O2) or hypoxic (1% O2) conditions and subjected to RIME-mass spectrometry wing of DOCIA procedure (n=3).

(D) Distinct JVF-unique functional protein clusters are enriched in HIF-1α cofactor analysis. STRING analysis was performed on RIME-mass spec protein hits. For each treatment condition, structural and non-mouse proteins were discarded, RIME hit proteins were sorted by geomean (relative to HIF-1α) and those less than 0.01 discarded. The remaining proteins were then run through the STRING analysis online database and clustered via MCL clustering (stringency 3). Resulting connections plotted by confidence (cutoff ‘medium’ – 0.04).

(E) Key cofactors were identified as uniquely up or downregulated in association with HIF-1α in JVF cells in both normoxia and hypoxia. Wildtype and JVF hMPL BaF3 cells cultured in either normoxic (20% O2) or hypoxic (1% O2) conditions and subjected to RIME-mass spectrometry wing of DOCIA procedure, the top 20 most significantly up or down regulated

proteins in both JVF normoxic and hypoxic cells plotted on chart by Log2FC relative to wildtype (n=3).

(F)(I) Key cofactors identified by DOCIA validated by HIF-1α immunoprecipitation. Immunoblot of HIF-1α, HIF-1β and key JVF-unique cofactors identified by RIME mass spec in HIF-1α-immunoprecipitated wildtype and JVF UT7/TPO cells cultured in either normoxic (20% O2) or hypoxic (1% O2) conditions, treated with or without SMI-4a as shown and with TPO-treated wildtype normoxic cells as additional control. Input on left, IP on right. Antibodies for HIF-1α, HIF-1β, TDP-43, Golga3, SIK2 and IMPDH used with β-actin used as loading control (n=2).

(II) The JVF-unique cofactor TDP-43, identified by DOCIA, validated by TDP-43 immunoprecipitation of HIF-1α. Immunoblot of HIF-1α and TDP-43 in TDP-43-immunoprecipitated wildtype and JVF UT7/TPO cells cultured in either normoxic (20% O2) or hypoxic (1% O2) conditions, with HIF-1α and TDP-43 antibodies used and with β-actin as loading control. Input on left, IP on right (n=2).

**Figure 5**

(A) Diagram of DOCIA method: wildtype or JVF hMPL BaF3 cells cultured in normoxic (20% O2), or hypoxic conditions (1% O2) have their nuclear material crosslinked to retain DNA-bound proteins, fragmented and HIF-1α containing fragments immunoprecipitated by the addition of HIF-1α antibody. The sample is then divided for concurrent analysis by both ChIP-seq (to determine the genomic binding loci of HIF-1α) and mass spectrometry (RIME-Rapid immunoprecipitation mass spectrometry of endogenous protein) (to determine the associated transcription factors of HIF-1α).

(B) Weaker overall binding of HIF-1α to chromatin observed in normoxic and hypoxic JVF cells compared to hypoxic-treated wildtype cells. Heatmap of normalised ChIPseq signal for the entire genome from wildtype and JVF hMPL BaF3 cells cultured in normoxic (20% O2) or hypoxic (1% O2) conditions and subjected to the ChIP-seq wing of the DOCIA procedure, as displayed by median peak intensity (n=3). Each row of the heatmap is a genomic region, centred to peaks of binding signals. Binding is summarized with a gradient colour code key with 0 representative of no binding (white) to maximum binding 30 (blue). Plots at the top of the heatmaps show the median signal at genomic regions centred at peaks of binding signals.

(C) Whilst the genomic loci bound by HIF-1α in JVF cells are minimally altered when compared to wildtype hypoxic-treated cells, the priority in which those sites are bound by HIF-1α is significantly altered in both normoxic and hypoxic JVF cells, with a number of loci

whose HIF-1α binding priority relative to WT_Hx binding is altered by more than a quartile in both VF_Nx and VF_Hx conditions. Δrank-score analysis of HIF-1α-bound genomic loci for VF_Nx (left) VF_Hx (right) denoting loci higher or lower ranked in HIF-1α binding priority than WT_Hx, as determined by ChIP-seq, plotted in order of score, with those loci with Δrank-score greater than a quartile highlighted.

(D) Across the mouse genome, the priority of HIF-1α binding appears lessened between chromosomes 1-4 and sites at chromosomes 8 and 14 appear prioritised in VF_Nx when compared to WT_Hx whilst the priority of HIF-1α binding appears enhanced in the region of chromosome 12 when compared to WT_Hx. Δrank-score analysis of HIF-1α-bound genomic loci for VF_Nx (light blue) VF_Hx (dark blue) denoting loci higher or lower ranked in HIF-1α binding priority than WT_Hx, as determined by ChIP-seq, plotted by genomic location (chromosome).

(E) Key genes found to be differently bound by HIF-1α in VF_Nx and VF_Hx compared to WT_Hx include a loss in Usf1 and a gain in Dusp4 HIF-1α binding in VF_Nx and a loss in Mdm2 and a gain in Bag8, Coa8 and Hectd1 HIF-1α binding in VF_Hx. Gene tracks of genomic loci where significant loss or gain of HIF-1α binding as determined by ChIP-seq can be observed in VF_Hx (green) or VF_Nx (yellow) compared to WT_Hx (blue).

(F) Cross analysis of ChIP-seq data with scATAC-Seq data demonstrates no correlation between gene loci accessibility and HIF-1α binding in JVF compared to wildtype. Plot of genome-wide gene accessibility (as derived from [52] Supplementary Figure 4 'Differential gene accessibility score in HSC and HSCMY clusters in untreated patients with myelofibrosis.') in primary JVF-mutation carrying patient cells plotted against genome-wide genomic loci binding (as determined by ChIP-seq of hMPL BaF3 VF_Hx cells).

(G) Analysis of ChIP-seq-derived HIF-1α binding loci shows reduced binding to canonical HREs (Hypoxic Response Elements) in JVF cells in both normoxia and hypoxia. HIF-1α HRE binding analysis of wildtype and JVF hMPL BaF3 cells cultured in normoxic (20% O2) or hypoxic (1% O2) conditions and subjected to the ChIP-seq wing of the DOCIA procedure, shown as percentage of HIF-1α binding loci localised to HREs.

(H) Analysis of ChIP-seq-derived HIF-1α binding loci shows increased binding in intergenic regions of the DNA in JVF cells in both normoxia and hypoxia and decreased exon binding in normoxia. Genomic feature binding analysis of wildtype and JVF hMPL BaF3 cells cultured in normoxic (20% O2) or hypoxic (1% O2) conditions and subjected to the ChIP-seq wing of the DOCIA procedure, shown as percentage of HIF-1α binding loci localised to the indicated genomic features.

**Figure 6**

(A) Diagram of derivation of ‘gene signatures’: Top 200 enriched genomic loci from HIF-1α ChIP-seq analysis with q<0.03 for each condition selected for further analysis.

B)(I) GO (gene ontology) analysis of WT_Hx ‘gene signature’ shows key canonical HIF-1 pathway associations. GO data of WT_Hx ‘gene signature’ displayed both as enrichment bubble plot (top) and chord plot (bottom). Enrichment bubble plot plotted in descending order of statistical significance as designated by p-value (from 0.01 to 0.04) with ‘bubble’ size indicating number of genes associated with the indicated function. Enrichment chord plots plotted by gene within signature in order of fold change (LogFC) and its associated GO function (colour-coded).

(II) GO (gene ontology) analysis of VF_Nx ‘gene signature’ shows loss of key canonical HIF-1 pathway associations (such as glycolysis) and gain of novel pathway associations never before ascribed to HIF-1α including DNA metabolism, DNA damage response and RNA processing. GO data of VF_Nx ‘gene signature’ displayed both as enrichment bubble plot (top) and chord plot (bottom).

(III) GO (gene ontology) analysis of VF_Hx ‘gene signature’ shows more extensive loss of key canonical HIF-1 pathway associations and gain of novel pathway associations never before ascribed to HIF-1α including RNA splicing, RNA processing, cell cycle progression and checkpoint pathway genes. GO data of VF_Nx ‘gene signature’ displayed both as enrichment bubble plot (top) and chord plot (bottom).

(C) ‘Hallmark hypoxia gene set’ shows no correlation with JVF MPN patient cohort survival.

(D) Neither WT_Hx nor VF_Nx ‘gene signatures’ show correlation with MPN patient disease severity as defined by MIPSS70 classification whereas the VF_Hx signature does. MPN patient cohort (172 JVF mutation carrying MPN patients) expression enrichment of WT_Hx, VF_Nx and VF_Hx gene signatures plotted by MIPSS70 (Mutation-Enhanced International Prognostic Score System for transplantation eligible-aged patients with overt PMF) classification. The score takes into account haemoglobin <10 g/dL (1 point), leukocyte count >25×109/L (2 points), platelet count <100×109/L (2 points), circulating blasts ≥2% (1 point), MF-2 or higher bone marrow fibrosis grades (1 point), presence of constitutional symptoms (1 point), absence of CALR type-1 mutation (1 point), and presence of HMR mutations (ASXL1, EZH2, SRSF2, and IDH1/2; 1 point for single mutation and 2 points for ≥2 HMR mutated genes) as independent prognostic factors of inferior OS. The MIPSS70 classified the MF patients into three groups: low-risk (0–1 point), intermediate-risk (2–4 points), and high-risk (≥5 points).

(E) MPN patient cohort expression enrichment of neither the WT_Hx nor the VF_Nx 'gene signatures' show correlation with JVF MPN patient cohort survival whereas patient enrichment of VF_Hx 'gene signature' expression show significant correlation with poorer survival outcomes. MPN patient cohort survival curves subdivided into populations with high (blue) or low (red) expression of WT_Hx, VF_Nx or VF_Hx gene signatures with significance of difference between the populations shown on graph (p-value). Remaining patients in each population shown in table below with number of censoring (i.e. number of patients leaving the study whose fate is unknown).

**Figure 7**

(A) Diagram illustrating identification of specific genes responsible for differential survival in patients with high VF_Hx signature expression compared to patients with high VF_Nx signature expression. Genes unique to VF_Hx signature were run through JVF MPN patient scATACseq, bulk mouse RNAseq and scRNAseq human datasets, any genes significantly upregulated in all three were run through the MPN patient cohort dataset and remaining genes associated with poorer patient survival examined.

(B) The transcripts of 74.6% of the genes in the VF_Hx gene signature are detectable in mouse MEP (megakaryocytic-erythroid progenitor) cells in bulk RNAseq experiments, whilst transcripts of only 4.6% of the signature are detectable in mouse LSK (lineage negative, Sca-1 positive, c-kit positive) cells. Volcano plots of bulk RNAseq from mouse primary haematopoietic stem and progenitor cells (HSPCs) from wildtype (n=3) and JVF homozygous (n=3) C57/BL6 mice, (LSKs top and MEPs bottom). VF_Hx gene signature transcripts highlighted in blue with transcripts with significance higher than -log10 adj p value of 1 labelled.

(C)(I) Genes identified as responsible for differential survival in MPN patients with high VF_Hx expression include genes associated with DNA damage response and are found to be upregulated specifically in patient MkP cell populations. High expression of these individual genes is also correlated with MPN patient disease severity. UMAP scRNAseq plots of control (top row) and myelofibrosis (bottom row) HSPCs with transcripts of genes of interest (PCNA, BLM and AURKB) highlighted in purple. The correlation of the individual genes of interest with MIPSS70 MPN patient classification displayed below.

(II) High expression of the individual genes PCNA, BLM and AURKB is associated with significantly poorer MPN patient survival outcomes.

**Figure 8**

(A) Of the genes identified by the process outlined in Fig. 7A, the high expression of a subset of them were found to be associated with increased risk of spontaneous AML transformation. Paired transcript expression of the genes of interest pre (red) and post (blue) spontaneous AML (sAML) transformation plotted by MPN patient. The top and middle rows of the figure illustrate genes whose expression were elevated in patients post-spontaneous AML transformation and the bottom row illustrates genes whose expression levels were lowered upon spontaneous AML transformation.

(B) Taken together as a novel 'sub-signature', high expression of the genes that show elevated expression in MPN patients who suffered spontaneous AML transformation are significantly associated with MPN patient disease severity, increased myelofibrosis, AML transformation and poorer patient survival. From left to right, MPN patient cohort expression enrichment of the spontaneous AML transformation associated 'gene signature' plotted by MIPSS70 classification, expression of the signature plotted by severity of patient myelofibrosis, expression of the signature in patients pre and post spontaneous AML transformation and survival of patients stratified into those with high or low expression of the signature.

**Supplementary Figures:**

S1 Replating efficiency from cultures described in Fig. 1(C).

S2(A) Cell count data for Fig. 1D

(B) Violin plot of flow cytometry data from Fig. 1D normalised to isotype.

(C) Immunoblot for HIF-1α in primary mouse lineage depleted HSCs from wildtype, heterozygous and homozygous JVF mice cultured in 1% O2 hypoxic conditions for the indicated length of time. HIF-1α antibody used with β-actin as loading control (n=2). Quantification by densitometry (below).

S3(A) HIF-1 inhibition partially rescues HSC expansion culture phenotype in JVF cells as determined by proportion of LSK cells in culture, returning the LSK cell percentage closer to those observed in vehicle treated wildtype expansion cultures. In wildtype cultures however, HIF-1 inhibition decreased LSK percentage. Ex-vivo expansion of long-term HSCs from wildtype (purple) and JVF heterozygous (blue) mice in the PVA culture system treated with the indicated dose (μM) of GN44028 or vehicle control and immunophenotyped (by gating strategy following previously described HSC populations [76]) after 14 days of expansion and expressed as percentage of lineage negative cell population (n=3).

(B) HIF-1 inhibition partially rescues HSC expansion culture phenotype in JVF cells as determined by proportion of progenitor cells in culture, returning the progenitor cell percentage to those observed in vehicle treated wildtype expansion cultures. In wildtype cultures, HIF-1 inhibition leaves progenitor cell percentage unaffected.

S4(A) Confirmatory representative western blots of Fig. 1C NAC ROS inhibition assay in SET2 and HEL cell lines.

(B) Treatment with ROS scavenger NAC (N-acetyl-L-cysteine) fails to inhibit JVF-induced HIF-1α stabilisation, whereas treatment with the ROS inhibitor DMF (dimethyl fumarate) does inhibit JVF-induced HIF-1α stabilisation. Representative immunoblot of HIF-1α, PIM1 and DMF-target NRF2 levels in wildtype and JVF UT7/TPO cells, SET2 cells and HEL cells treated as indicated with either NAC, DMF or vehicle control. Immunoblotting carried out using HIF-1α, NRF2 and PIM1 antibodies with β-actin as a loading control (n=3).

S5 Treatment with ERK inhibitor SCH874 fails to destabilise JVF-induced HIF-1α stabilisation. Immunoblot of HIF-1α, pJAK2, ERK1/2 and pERK1/2 in JVF UT7/TPO cells, treated as indicated with either SCH874, Rux or vehicle control. Immunoblotting carried out using HIF-1α, pJAK2 Y1007/Y1008, pERK1/2 Y204/Y187 and ERK1/2 antibodies with β-actin as a loading control (n=2).

S6 Gating strategy for multiplex fluorescent barcoding and phospho-flow cytometry.

S7 PIM1 transcript expression is higher in JVF mouse LSKs compared to wildtype. Bulk RNA-seq analysis of mouse LSKs from wildtype (n=3) and JVF heterozygous mice (n=3).

S8 Confirmatory representative western blot of Fig. 2A(I) PIM1 inhibition assay in wildtype UT7/TPO cells (n=3).

S9 Confirmatory representative western blot of Fig. 2A(I) PIM1 inhibition assay in wildtype and JVF hMPL BaF3 cells (n=3).

S10 Remaining panel of kinase cascade constituent proteins downstream of JAK2 from barcoded phosflow flow cytometry experiment in Fig. 2B(II).

S11 HIF-2 inhibition has no significant effect on expansion culture phenotype as determined by proportion of LSK/progenitor cells in culture in either wildtype or JVF cells. Ex vivo expansion of long-term HSCs from wildtype (purple) and JVF heterozygous (blue) mice in the PVA culture system treated with the indicated dose (μM) of TCS7009 or vehicle control and immunophenotyped after 14 days of expansion and expressed as percentage of lineage negative cell population (n=3).

S12 HSC gating strategy for immunophenotyping of expansion cultures in Fig. 2C, Fig. S3(A)-(B) and Fig. S14.

S13 Exemplary plots of HSC gating for immunophenotyping in cells treated with vehicle control (DMSO), GN44028 or SMI-4a.

S14 Levels of HIF-1α at 6hrs of hypoxic exposure are equal between wildtype and JVF hMPL BaF3 cells. Immunoblot of HIF-1α in wildtype and JVF hMPL BaF3 cells cultured in hypoxia for the indicated number of hours, blotted for HIF-1α with β-actin as loading control. Quantification by densitometry included.

S15(A) Full STRING functional cluster analysis of all cofactor proteins across all conditions identified by RIME-mass spec from Fig. 4D.

(B) STRING functional cluster analysis of cofactors de-enriched (geomean relative to WT_Hx 0.01<0.005) for VF_Hx HIF-1α (left) and VF_Nx HIF-1α (right).

S16 Full panel of phosphorylated proteins identified by phospho mass spec as immunoprecipitated with HIF-1α in JVF and wildtype hypoxic UT7/TPO cells from Fig. 3A(I) (n=3).

S17 Analysis of WT_Hx hMPL BaF3 cells by ChIP-seq shows canonical HIF signature gene loci binding. Volcano plot of loci binding intensity in WT_Hx cells relative to WT_Nx plotted by statistical significance (1/log10(BH-p)) with canonical HIF-1α target genes indicated by a cross and key signature genes and highly expressed non-signature genes labelled.

S18 Key HRE genes found to be differentially bound by HIF-1α in WT_Hx compared to WT_Nx include Vegfa and Slc2a3. Gene tracks of genomic loci where significant gain of HIF-1α binding as determined by ChIP-seq can be observed in WT_Hx (blue) compared to WT_Nx (purple).

S19 Weaker overall binding of HIF-1α to chromatin observed in normoxic and hypoxic JVF hMPL BaF3 cells compared to hypoxic-treated wildtype cells. Overlay of median genome-wide ChIP-seq binding signal at genomic regions centred at peaks of binding signals, in WT_Nx (purple), WT_Hx (blue), VF_Nx (yellow) and VF_Hx (green).

S20 JVF-stabilised HIF-1α binds to fewer genomic loci than wildtype hypoxia-stabilised HIF-1α, with no novel loci binding sites detected in JVF cells in either normoxia or hypoxia. Venn diagram of HIF-1α loci bound in the indicated conditions with number of genes unique to each condition labelled. Binding sites determined by ChIPseq in hMPL BaF3 cells (n=3).

S21 Across the mouse genome, HIF-1α binding appears lessened between chromosomes 1-4 and sites at chromosomes 8 and 14 appear prioritised in VF_Nx when compared to WT_Hx whilst the priority of HIF-1α binding appears enhanced in the region of chromosome 12 when compared to WT_Hx. Binding intensity of HIF-1α-bound genomic loci for VF_Nx (light blue) VF_Hx (dark blue) denoting bound more intensely by HIF-1α in JVF cells than WT_Hx, as determined by ChIP-seq, plotted by genomic location (chromosome).

S22 Cross analysis of mouse bulk RNA-seq data with JVF MPN patient scATAC-Seq data demonstrates no correlation between gene loci accessibility and gene transcription in JVF heterozygous mouse cells compared to wildtype. Plot of genome-wide gene accessibility (as derived from Izzo et al. Supplementary Figure 4 'Differential gene accessibility score in HSC and HSCMY clusters in untreated patients with myelofibrosis.') in primary JVF-mutation carrying patient cells plotted against gene expression (as determined by bulk RNA-seq of JVF heterozygous mice from publicly available dataset).

S23 A limited number of genes from canonical HIF-1 metagene signature (Lombardi et al.) identified in VF_Nx and VF_Hx gene signatures.

S24 Analysis of scATAC-seq data shows key VF_Hx 'signature' genes as more or less accessible in JVF-mutation carrying patient cells. Volcano plot of Log2FC (Fold Change) gene accessibility in JVF-carrying patients compared to healthy controls as determined by scATAC-seq, plotted against statistical significance (-Log10 FDR (False discovery rate)). Data derived from Izzo et al. Supplementary Figure 4 'Differential gene accessibility score in HSC and HSCMY clusters in untreated patients with myelofibrosis.'

S25 Log2 Fold Change expression of key genes with high expression in JVF cells, association with worse MPN patient disease severity and poorer survival outcomes from bulk RNA-seq analysis of JVF hypoxic cells compared to wildtype hypoxic mouse MEP and LSKs (n=3).

S26 BCL2L1 (BCL2XL) is significantly upregulated in transcript expression in MEPs/MkP and significantly associated with disease progression and survival. UMAP scRNAseq plot of control (top) and myelofibrosis (bottom) HSPCs with transcript of gene of interest (BCL2L1) highlighted in purple. The correlation of the individual genes of interest with MIPSS70 MPN patient classification and patient survival displayed below.

S27 TNKS, HECTD1, WIPF1, PPID are globally upregulated throughout HSPC clusters but were not significantly associated with disease progression and survival. UMAP scRNAseq plot of control (top) and myelofibrosis (bottom) HSPCs with transcript of genes of interest (TNKS, HECTD1, WIPF1, PPID) highlighted in purple. The correlation of the individual

genes of interest with MIPSS70 MPN patient classification and patient survival displayed below.

S28 IER3 is significantly upregulated in more primitive progenitor populations and is inversely correlated with MPN patient disease severity and survival. UMAP scRNAseq plot of control (top) and myelofibrosis (bottom) HSPCs with transcript of genes of interest (IER3) highlighted in purple. The correlation of the individual genes of interest with MIPSS70 MPN patient classification and patient survival displayed below.

S29 No significant difference in expression of the VF_Hx signature genes as a whole can be observed in the 11 MPN patients from the JVF MPN cohort who spontaneously converted to AML (blue) compared to those that didn't (red).

S30 Graphical abstract/illustration of JVF-mediated HIF-1α stabilisation.

**References**


1. Iliopoulos O, Levy AP, Jiang C, Kaelin WG Jr, Goldberg MA. Negative regulation of hypoxia-inducible genes by the von Hippel-Lindau protein. Proc Natl Acad Sci U S A. 1996;93: 10595–10599.
2. Semenza GL. HIF-1 and mechanisms of hypoxia sensing. Curr Opin Cell Biol. 2001;13: 167–171.
3. Lombardi O, Li R, Halim S, Choudhry H, Ratcliffe PJ, Mole DR. Pan-cancer analysis of tissue and single-cell HIF-pathway activation using a conserved gene signature. Cell Rep. 2022;41: 111652.
4. Deeb G, Vaughan MM, McInnis I, Ford LA, Sait SNJ, Starostik P, et al. Hypoxia-inducible factor-1α protein expression is associated with poor survival in normal karyotype adult acute myeloid leukemia. Leuk Res. 2011;35: 579–584.
5. Forristal CE, Brown AL, Helwani FM, Winkler IG, Nowlan B, Barbier V, et al. Hypoxia inducible factor (HIF)-2α accelerates disease progression in mouse models of leukemia and lymphoma but is not a poor prognosis factor in human AML. Leukemia. 2015;29: 2075–2085.
6. Pastoors D, Havermans M, Mulet-Lazaro R, Brian D, Noort W, Grasel J, et al. Oncogene *EVI1* drives acute myeloid leukemia via a targetable interaction with CTBP2. Science Advances. 2024;10: eadk9076.
7. Niktoreh N, Weber L, Walter C, Karimifard M, Hoffmeister LM, Breiter H, et al. Understanding WT1 Alterations and Expression Profiles in Hematological Malignancies. Cancers . 2023;15. doi:10.3390/cancers15133491
8. Coltella N, Percio S, Valsecchi R, Cuttano R, Guarnerio J, Ponzoni M, et al. HIF factors cooperate with PML-RARα to promote acute promyelocytic leukemia progression and relapse. EMBO Mol Med. 2014;6: 640–650.
9. Patel SA, Hirosue S, Rodrigues P, Vojtasova E, Richardson EK, Ge J, et al. The renal lineage factor PAX8 controls oncogenic signalling in kidney cancer. Nature. 2022;606: 999–1006.
10. Levine RL, Pardanani A, Tefferi A, Gilliland DG. Role of JAK2 in the pathogenesis and therapy of myeloproliferative disorders. Nat Rev Cancer. 2007;7: 673–683.
11. Dunbar AJ, Rampal RK, Levine R. Leukemia secondary to myeloproliferative neoplasms. Blood. 2020;136: 61–70.
12. Bhagwat N, Koppikar P, Keller M, Marubayashi S, Shank K, Rampal R, et al. Improved targeting of JAK2 leads to increased therapeutic efficacy in myeloproliferative neoplasms. Blood. 2014;123: 2075–2083.
13. Levine RL, Wadleigh M, Cools J, Ebert BL, Wernig G, Huntly BJP, et al. Activating mutation in the tyrosine kinase JAK2 in polycythemia vera, essential thrombocythemia, and myeloid metaplasia with myelofibrosis. Cancer Cell. 2005;7: 387–397.

14. Palacios R, Steinmetz M. Il-3-dependent mouse clones that express B-220 surface antigen, contain Ig genes in germ-line configuration, and generate B lymphocytes in vivo. Cell. 1985;41: 727–734.
15. Koga T, Suda K, Mitsudomi T. Utility of the Ba/F3 cell system for exploring on-target mechanisms of resistance to targeted therapies for lung cancer. Cancer Sci. 2022;113: 815–827.
16. Komatsu N, Kunitama M, Yamada M, Hagiwara T, Kato T, Miyazaki H, et al. Establishment and characterization of the thrombopoietin-dependent megakaryocytic cell line, UT-7/TPO. Blood. 1996;87: 4552–4560.
17. Uozumi K, Otsuka M, Ohno N, Moriyama T, Suzuki S, Shimotakahara S, et al. Establishment and characterization of a new human megakaryoblastic cell line (SET-2) that spontaneously matures to megakaryocytes and produces platelet-like particles. Leukemia. 2000;14: 142–152.
18. Zhou Y, Li F, Jin J. Establishment and Characterization of a Human Primary Myelofibrosis Cell Line. Blood. 2021;138: 4594.
19. Martin P, Papayannopoulou T. HEL cells: a new human erythroleukemia cell line with spontaneous and induced globin expression. Science. 1982;216: 1233–1235.
20. Yin A, Fu W, Elengickal A, Kim J, Liu Y, Bigot A, et al. Chronic hypoxia impairs skeletal muscle repair via HIF-2α stabilization. J Cachexia Sarcopenia Muscle. 2024;15: 631–645.
21. Fan X, Fan J, Yang H, Zhao C, Niu W, Fang Z, et al. Heterogeneity of subsets in glioblastoma mediated by Smad3 palmitoylation. Oncogenesis. 2021;10: 72.
22. Li J, Kent DG, Godfrey AL, Manning H, Nangalia J, Aziz A, et al. JAK2V617F homozygosity drives a phenotypic switch in myeloproliferative neoplasms, but is insufficient to sustain disease. Blood. 2014;123: 3139–3151.
23. Yoshida K, Kirito K, Yongzhen H, Ozawa K, Kaushansky K, Komatsu N. Thrombopoietin (TPO) regulates HIF-1alpha levels through generation of mitochondrial reactive oxygen species. Int J Hematol. 2008;88: 43–51.
24. Baumeister J, Chatain N, Hubrich A, Maié T, Costa IG, Denecke B, et al. Hypoxia-inducible factor 1 (HIF-1) is a new therapeutic target in JAK2V617F-positive myeloproliferative neoplasms. Leukemia. 2020;34: 1062–1074.
25. Koukoulas K, Giakountis A, Karagiota A, Samiotaki M, Panayotou G, Simos G, et al. ERK signaling controls productive HIF-1 binding to chromatin and cancer cell adaptation to hypoxia through HIF-1α interaction with NPM1. Mol Oncol. 2021;15: 3468–3489.
26. Kalousi A, Mylonis I, Politou AS, Chachami G, Paraskeva E, Simos G. Casein kinase 1 regulates human hypoxia-inducible factor HIF-1. J Cell Sci. 2010;123: 2976–2986.
27. Mylonis I, Chachami G, Paraskeva E, Simos G. Atypical CRM1-dependent nuclear export signal mediates regulation of hypoxia-inducible factor-1alpha by MAPK. J Biol Chem. 2008;283: 27620–27627.
28. Mylonis I, Chachami G, Samiotaki M, Panayotou G, Paraskeva E, Kalousi A, et al. Identification of MAPK phosphorylation sites and their role in the localization and activity of hypoxia-inducible factor-1alpha. J Biol Chem. 2006;281: 33095–33106.
29. Gradin K, Takasaki C, Fujii-Kuriyama Y, Sogawa K. The transcriptional activation function of the HIF-like factor requires phosphorylation at a conserved threonine. J Biol Chem. 2002;277: 23508–23514.
30. Lancaster DE, McNeill LA, McDonough MA, Aplin RT, Hewitson KS, Pugh CW, et al. Disruption of dimerization and substrate phosphorylation inhibit factor inhibiting hypoxia-inducible factor (FIH) activity. Biochem J. 2004;383: 429–437.
31. Cho H, Ahn D-R, Park H, Yang EG. Modulation of p300 binding by posttranslational modifications of the C-terminal activation domain of hypoxia-inducible factor-1alpha. FEBS Lett. 2007;581: 1542–1548.
32. Tsutsumi N, Masoumi Z, James SC, Tucker JA, Winkelmann H, Grey W, et al. Structure of the thrombopoietin-MPL receptor complex is a blueprint for biasing hematopoiesis. Cell. 2023;186: 4189-4203.e22.
33. Transcription Factor Target Gene Database. [cited 11 Jul 2024]. Available: https://tfbsdb.systemsbiology.net/
34. Dawson MA, Foster SD, Bannister AJ, Robson SC, Hannah R, Wang X, et al. Three distinct patterns of histone H3Y41 phosphorylation mark active genes. Cell Rep. 2012;2: 470–477.
35. KinHub. [cited 12 Jul 2024]. Available: http://kinhub.org/kinases.html
36. HIF1A (human). [cited 12 Jul 2024]. Available: https://www.phosphosite.org/proteinAction.action?id=4987&showAllSites=true

37. Quintás-Cardama A, Vaddi K, Liu P, Manshouri T, Li J, Scherle PA, et al. Preclinical characterization of the selective JAK1/2 inhibitor INCB018424: therapeutic implications for the treatment of myeloproliferative neoplasms. Blood. 2010;115: 3109–3117.
38. Mesa RA, Gotlib J, Gupta V, Catalano JV, Deininger MW, Shields AL, et al. Effect of ruxolitinib therapy on myelofibrosis-related symptoms and other patient-reported outcomes in COMFORT-I: a randomized, double-blind, placebo-controlled trial. J Clin Oncol. 2013;31: 1285–1292.
39. Vainchenker W, Yahmi N, Havelange V, Marty C, Plo I, Constantinescu SN. Recent advances in therapies for primary myelofibrosis. Fac Rev. 2023;12: 23.
40. Eghtedar A, Verstovsek S, Estrov Z, Burger J, Cortes J, Bivins C, et al. Phase 2 study of the JAK kinase inhibitor ruxolitinib in patients with refractory leukemias, including postmyeloproliferative neoplasm acute myeloid leukemia. Blood. 2012;119: 4614–4618.
41. Boldrini V, Vannucchi AM, Guglielmelli P. A safety evaluation of ruxolitinib for the treatment of polycythemia vera. Expert Opin Drug Saf. 2024;23: 1–7.
42. Casillas AL, Chauhan SS, Toth RK, Sainz AG, Clements AN, Jensen CC, et al. Direct phosphorylation and stabilization of HIF-1α by PIM1 kinase drives angiogenesis in solid tumors. Oncogene. 2021;40: 5142–5152.
43. Yang Y, Lu H, Chen C, Lyu Y, Cole RN, Semenza GL. HIF-1 Interacts with TRIM28 and DNA-PK to release paused RNA polymerase II and activate target gene transcription in response to hypoxia. Nat Commun. 2022;13: 316.
44. HALLMARK_HYPOXIA. [cited 12 Jul 2024]. Available: https://www.gsea-msigdb.org/gsea/msigdb/human/geneset/HALLMARK_HYPOXIA.html
45. Liberzon A, Birger C, Thorvaldsdóttir H, Ghandi M, Mesirov JP, Tamayo P. The Molecular Signatures Database (MSigDB) hallmark gene set collection. Cell Syst. 2015;1: 417–425.
46. Batie M, Del Peso L, Rocha S. Hypoxia and Chromatin: A Focus on Transcriptional Repression Mechanisms. Biomedicines. 2018;6. doi:10.3390/biomedicines6020047
47. Ortmann BM. Hypoxia-inducible factor in cancer: from pathway regulation to therapeutic opportunity. bmjonc. 2024;3. doi:10.1136/bmjonc-2023-000154
48. Medeiros JJF, Zeng AGX, Chan-Seng-Yue M, Woo T, Bansal S, Kim H, et al. Stem cell-derived gene expression scores predict survival and blastic transformation in myelofibrosis. bioRxiv. 2024. doi:10.1101/2024.07.09.24310101
49. Ali H, Aldoss I, Yang D, Mokhtari S, Khaled S, Aribi A, et al. MIPSS70+ v2.0 predicts long-term survival in myelofibrosis after allogeneic HCT with the Flu/Mel conditioning regimen. Blood Adv. 2019;3: 83–95.
50. Hänzelmann S, Castelo R, Guinney J. GSVA: gene set variation analysis for microarray and RNA-seq data. BMC Bioinformatics. 2013;14: 7.
51. Guglielmelli P, Lasho TL, Rotunno G, Mudireddy M, Mannarelli C, Nicolosi M, et al. MIPSS70: Mutation-Enhanced International Prognostic Score System for Transplantation-Age Patients With Primary Myelofibrosis. J Clin Oncol. 2018;36: 310–318.
52. Izzo F, Myers RM, Ganesan S, Mekerishvili L, Kottapalli S, Prieto T, et al. Mapping genotypes to chromatin accessibility profiles in single cells. Nature. 2024;629: 1149–1157.
53. Li B, An W, Wang H, Baslan T, Mowla S, Krishnan A, et al. BMP2/SMAD pathway activation in JAK2/p53-mutant megakaryocyte/erythroid progenitors promotes leukemic transformation. Blood. 2022;139: 3630–3646.
54. Psaila B, Wang G, Rodriguez-Meira A, Li R, Heuston EF, Murphy L, et al. Single-Cell Analyses Reveal Megakaryocyte-Biased Hematopoiesis in Myelofibrosis and Identify Mutant Clone-Specific Targets. Mol Cell. 2020;78: 477-492.e8.
55. HALLMARK_DNA_REPAIR. [cited 12 Jul 2024]. Available: https://www.gsea-msigdb.org/gsea/msigdb/human/geneset/HALLMARK_DNA_REPAIR.html
56. Arlt A, Schäfer H. Role of the immediate early response 3 (IER3) gene in cellular stress response, inflammation and tumorigenesis. Eur J Cell Biol. 2011;90: 545–552.
57. Lawson H, Holt-Martyn JP, Dembitz V, Kabayama Y, Wang LM, Bellani A, et al. The selective prolyl hydroxylase inhibitor IOX5 stabilizes HIF-1α and compromises development and progression of acute myeloid leukemia. Nat Cancer. 2024;5: 916–937.
58. Mazzacurati L, Lambert QT, Pradhan A, Griner LN, Huszar D, Reuther GW. The PIM inhibitor AZD1208 synergizes with ruxolitinib to induce apoptosis of ruxolitinib sensitive and resistant JAK2-V617F-driven cells and inhibit colony formation of primary MPN cells. Oncotarget. 2015;6: 40141–40157.
59. Dutta A, Nath D, Yang Y, Le BT, Rahman MF-U, Faughnan P, et al. Genetic ablation of Pim1 or pharmacologic inhibition with TP-3654 ameliorates myelofibrosis in murine models. Leukemia. 2022;36: 746–759.

60. Mondello P, Cuzzocrea S, Mian M. Pim kinases in hematological malignancies: where are we now and where are we going? J Hematol Oncol. 2014;7: 95.
61. Chen W, Kumar AR, Hudson WA, Li Q, Wu B, Staggs RA, et al. Malignant transformation initiated by Mll-AF9: gene dosage and critical target cells. Cancer Cell. 2008;13: 432–440.
62. Hsi ED, Jung S-H, Lai R, Johnson JL, Cook JR, Jones D, et al. Ki67 and PIM1 expression predict outcome in mantle cell lymphoma treated with high dose therapy, stem cell transplantation and rituximab: a Cancer and Leukemia Group B 59909 correlative science study. Leuk Lymphoma. 2008;49: 2081–2090.
63. Brault L, Menter T, Obermann EC, Knapp S, Thommen S, Schwaller J, et al. PIM kinases are progression markers and emerging therapeutic targets in diffuse large B-cell lymphoma. Br J Cancer. 2012;107: 491–500.
64. Gómez-Abad C, Pisonero H, Blanco-Aparicio C, Roncador G, González-Menchén A, Martinez-Climent JA, et al. PIM2 inhibition as a rational therapeutic approach in B-cell lymphoma. Blood. 2011;118: 5517–5527.
65. Albanese A, Daly LA, Mennerich D, Kietzmann T, Sée V. The Role of Hypoxia-Inducible Factor Post-Translational Modifications in Regulating Its Localisation, Stability, and Activity. Int J Mol Sci. 2020;22: 268.
66. Minezaki Y, Homma K, Kinjo AR, Nishikawa K. Human transcription factors contain a high fraction of intrinsically disordered regions essential for transcriptional regulation. J Mol Biol. 2006;359: 1137–1149.
67. Herzog J, Ehrlich SM, Pfitzer L, Liebl J, Fröhlich T, Arnold GJ, et al. Cyclin-dependent kinase 5 stabilizes hypoxia-inducible factor-1α: a novel approach for inhibiting angiogenesis in hepatocellular carcinoma. Oncotarget. 2016;7: 27108–27121.
68. Warfel NA, Dolloff NG, Dicker DT, Malysz J, El-Deiry WS. CDK1 stabilizes HIF-1α via direct phosphorylation of Ser668 to promote tumor growth. Cell Cycle. 2013;12: 3689–3701.
69. Hubbi ME, Gilkes DM, Hu H, Kshitiz, Ahmed I, Semenza GL. Cyclin-dependent kinases regulate lysosomal degradation of hypoxia-inducible factor 1α to promote cell-cycle progression. Proc Natl Acad Sci U S A. 2014;111: E3325-34.
70. Fallah J, Rini BI. HIF Inhibitors: Status of Current Clinical Development. Curr Oncol Rep. 2019;21: 6.
71. Liu J, Gao Y, Zhang X. A patent review on hypoxia-inducible factor (HIF) modulators (2021-2023). Expert Opin Ther Pat. 2024;34: 651–664.
72. Ban HS, Uto Y, Nakamura H. Hypoxia-inducible factor (HIF) inhibitors: a patent survey (2016-2020). Expert Opin Ther Pat. 2021;31: 387–397.
73. Mesa RA. The evolving treatment paradigm in myelofibrosis. Leuk Lymphoma. 2013;54: 242–251.
74. Love MI, Huber W, Anders S. Moderated estimation of fold change and dispersion for RNA-seq data with DESeq2. Genome Biol. 2014;15: 550.
75. Wilkinson AC, Ishida R, Kikuchi M, Sudo K, Morita M, Crisostomo RV, et al. Long-term ex vivo haematopoietic-stem-cell expansion allows nonconditioned transplantation. Nature. 2019;571: 117–121.
76. Nestorowa S, Hamey FK, Pijuan Sala B, Diamanti E, Shepherd M, Laurenti E, et al. A single-cell resolution map of mouse hematopoietic stem and progenitor cell differentiation. Blood. 2016;128: e20-31.
77. Andrews S. FastQC: a quality control tool for high throughput sequence data. 2010.
78. Bolger AM, Lohse M, Usadel B. Trimmomatic: a flexible trimmer for Illumina sequence data. Bioinformatics. 2014;30: 2114–2120.
79. Dobin A, Davis CA, Schlesinger F, Drenkow J, Zaleski C, Jha S, et al. STAR: ultrafast universal RNA-seq aligner. Bioinformatics. 2013;29: 15–21.
80. Danecek P, Bonfield JK, Liddle J, Marshall J, Ohan V, Pollard MO, et al. Twelve years of SAMtools and BCFtools. Gigascience. 2021;10: giab008.
81. Amemiya HM, Kundaje A, Boyle AP. The ENCODE blacklist: Identification of problematic regions of the genome. Sci Rep. 2019;9: 9354.
82. Quinlan AR, Hall IM. BEDTools: a flexible suite of utilities for comparing genomic features. Bioinformatics. 2010;26: 841–842.
83. Zhang Y, Liu T, Meyer CA, Eeckhoute J, Johnson DS, Bernstein BE, et al. Model-based analysis of ChIP-Seq (MACS). Genome Biol. 2008;9: R137.
84. Ross-Innes CS, Stark R, Teschendorff AE, Holmes KA, Ali HR, Dunning MJ, et al. Differential oestrogen receptor binding is associated with clinical outcome in breast cancer. Nature. 2012;481: 389–393.

85. Gel B, Serra E. karyoploteR: an R/Bioconductor package to plot customizable genomes displaying arbitrary data. Bioinformatics. 2017;33: 3088–3090.
86. Marçais G, Kingsford C. A fast, lock-free approach for efficient parallel counting of occurrences of k-mers. Bioinformatics. 2011;27: 764–770.
87. Martin M. Cutadapt removes adapter sequences from high-throughput sequencing reads. EMBnet J. 2011;17: 10.
88. Patro R, Duggal G, Love MI, Irizarry RA, Kingsford C. Salmon provides fast and bias-aware quantification of transcript expression. Nat Methods. 2017;14: 417–419.
89. Frankish A, Diekhans M, Ferreira A-M, Johnson R, Jungreis I, Loveland J, et al. GENCODE reference annotation for the human and mouse genomes. Nucleic Acids Res. 2019;47: D766–D773.
90. Pimentel H, Bray NL, Puente S, Melsted P, Pachter L. Differential analysis of RNA-seq incorporating quantification uncertainty. Nat Methods. 2017;14: 687–690.
91. Veidenberg A, Medlar A, Löytynoja A. Wasabi: An integrated platform for evolutionary sequence analysis and data visualization. Mol Biol Evol. 2016;33: 1126–1130.
92. Hao Y, Stuart T, Kowalski MH, Choudhary S, Hoffman P, Hartman A, et al. Dictionary learning for integrative, multimodal and scalable single-cell analysis. Nat Biotechnol. 2024;42: 293–304.
93. Andreatta M, Carmona SJ. UCell: Robust and scalable single-cell gene signature scoring. Comput Struct Biotechnol J. 2021;19: 3796–3798.

# Fig. 1

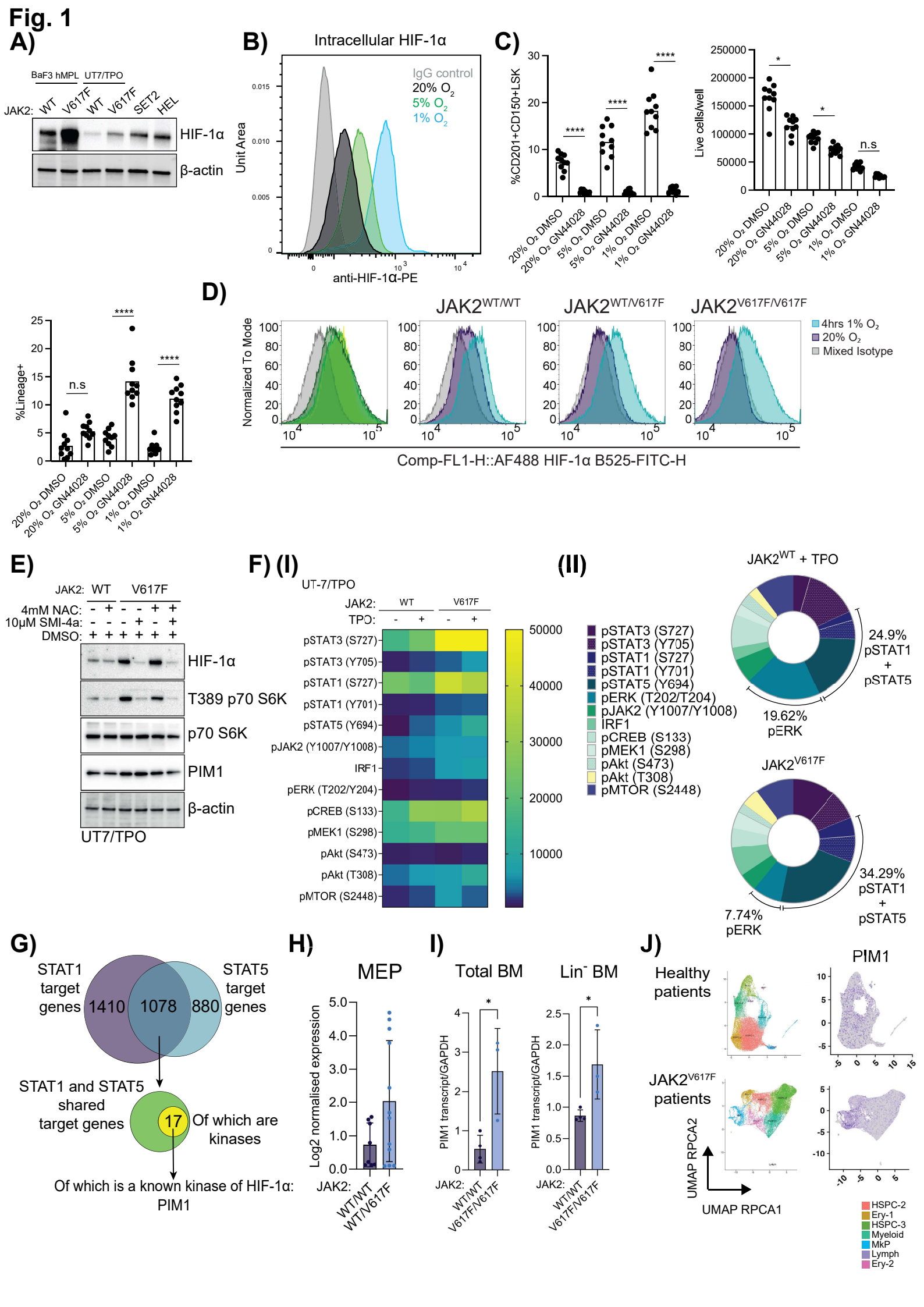
A)
BaF3 hMPL
UT7/TPO
JAK2: WT V617F WT V617F SET2 HEL
HIF-1α
β-actin
B)
Intracellular HIF-1α
IgG control
20% O2
5% O2
1% O2
Unit Area
anti-HIF-1α-PE
C)
%CD201+CD150+LSK
Live cells/well
****
*
n.s
20% O2 DMSO
20% O2 GN44028
5% O2 DMSO
5% O2 GN44028
1% O2 DMSO
1% O2 GN44028
D)
%Lineage+
JAK2WT/WT
JAK2WT/V617F
JAK2V617F/V617F
Normalized To Mode
4hrs 1% O2
20% O2
Mixed Isotype
Comp-FL1-H::AF488 HIF-1α B525-FITC-H
E)
JAK2: WT V617F
4mM NAC:
10μM SMI-4a:
DMSO:
HIF-1α
T389 p70 S6K
p70 S6K
PIM1
β-actin
UT7/TPO
F) (I)
UT-7/TPO
JAK2: WT V617F
TPO:
pSTAT3 (S727)
pSTAT3 (Y705)
pSTAT1 (S727)
pSTAT1 (Y701)
pSTAT5 (Y694)
pJAK2 (Y1007/Y1008)
IRF1
pERK (T202/Y204)
pCREB (S133)
pMEK1 (S298)
pAkt (S473)
pAkt (T308)
pMTOR (S2448)
(II)
JAK2WT + TPO
24.9% pSTAT1 + pSTAT5
19.62% pERK
JAK2V617F
34.29% pSTAT1 + pSTAT5
7.74% pERK
G)
STAT1 target genes
STAT5 target genes
1410
1078
880
STAT1 and STAT5 shared target genes
17
Of which are kinases
Of which is a known kinase of HIF-1α: PIM1
H)
MEP
Log2 normalised expression
JAK2: WT/WT WT/V617F
I)
Total BM
Lin- BM
PIM1 transcript/GAPDH
JAK2: WT/WT V617F/V617F
J)
Healthy patients
PIM1
JAK2V617F patients
UMAP RPCA2
UMAP RPCA1
HSPC-2
Ery-1
HSPC-3
Myeloid
MkP
Lymph
Ery-2

# Fig. 2

## A) (I)

DMSO: + + + + + + + +
TCS PIM 1.1 (μM): - 3 15 30 - - - -
TCS SMI-4a (μM): - - - - 0.1 1 10 -
PIM 447 (μM): - - - - - - - 3

HIF-1α
HIF-1β
pT389 p70 S6K
p70 S6K
PIM1
β-actin

UT7/TPO JAK2V617F

## (II)

HIF-1α

Starved
TPO
TPO + DMSO
TPO + Rux
TPO + SMI4

1.6
1.4
1.2
1.0

JAK2: WT VF
$O_2$: 20% 1% 20% 1%

## B) (I)

DMSO: + + + + + +
Ruxolitinib 2μM: - + - - + -
SMI-4a 2.5μM: - - + - - +

HIF-1α
pY1007/8 JAK2
JAK2
pY705 STAT3
STAT3
pT389 p70 S6K
p70 S6K
pY204/Y187 ERK1/2
ERK1/2
β-actin

Set2 Hel

## (II)

pJAK2 Y1007/1008
pSTAT1 Y701
pSTAT3 Y705
pSTAT3 S727
pSTAT5 Y694
IRF-1
pERK T202/Y204
pMEK1 S298
pAKT S473
pAKT T308
pCREB S133
mTOR pS2448

Starved
TPO
TPO + DMSO
TPO + Rux
TPO + SMI4

JAK2: WT VF
$O_2$: 20% 1% 20% 1%

## C)

LSK

Progenitors

jak2$^{wt/wt}$
jak2$^{wt/vf}$

% of Lin$^-$ cells

DMSO 0.1 1 5
SMI-4a

**
****

**Fig. 3**

**A) (I)**

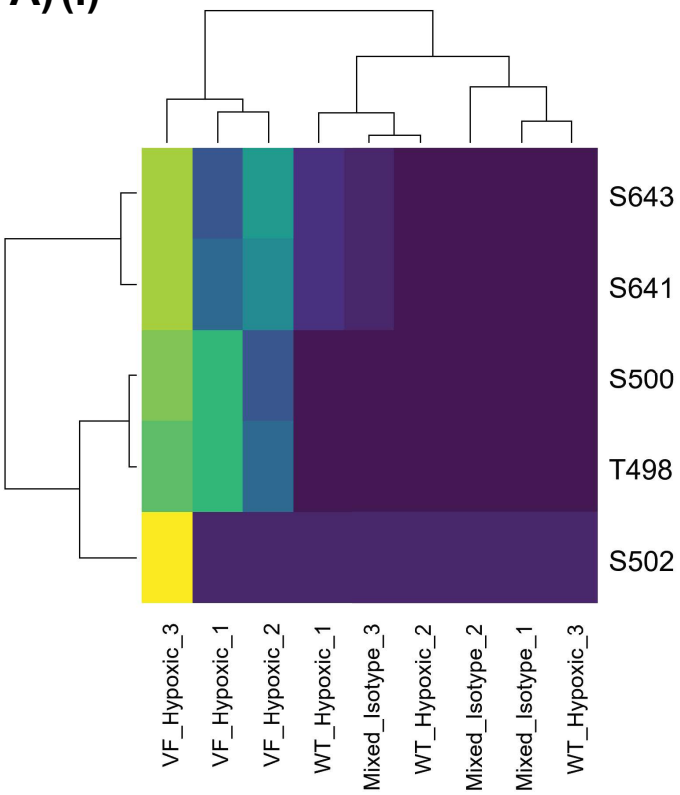


**(II)**

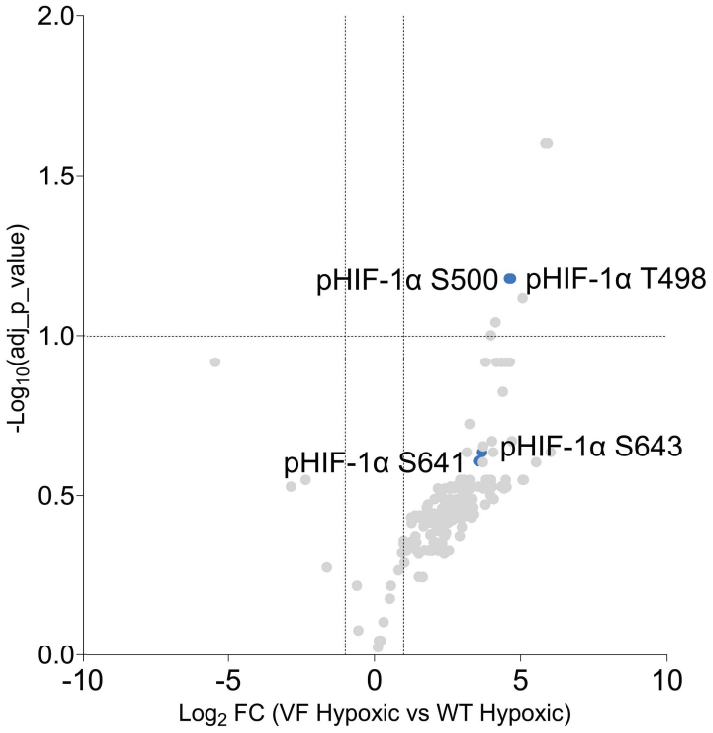


**B)**

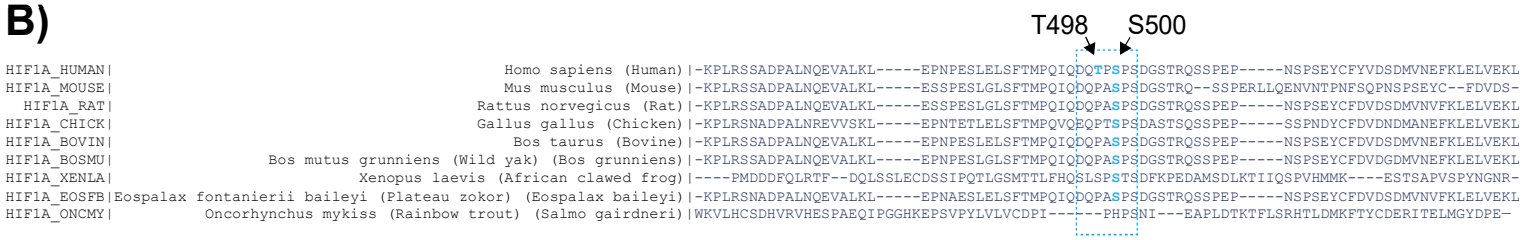


**C)**

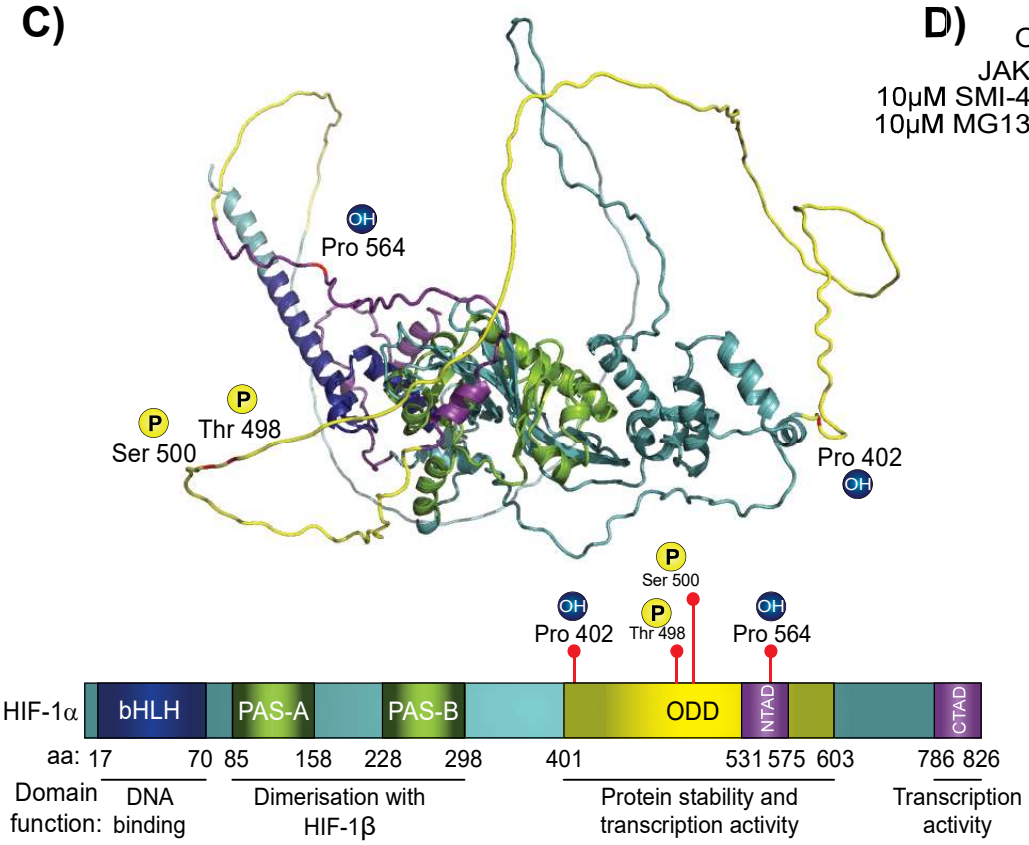


**D)**

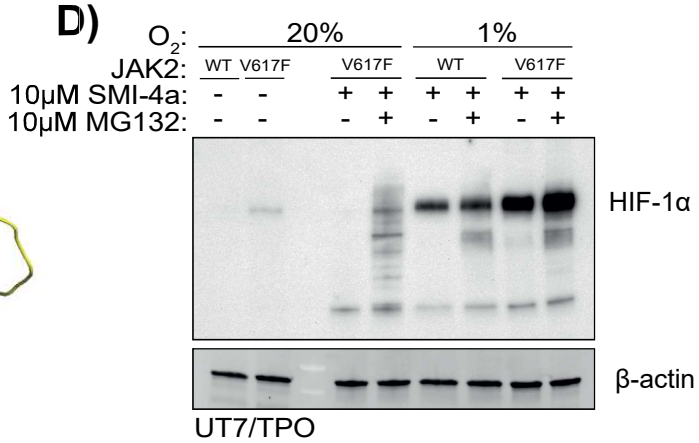

**Fig. 4**

**A) (I)** DOCIA procedure

| | 20% $O_2$ | 1% $O_2$ |
|---|---|---|
| JAK2$^{WT/WT}$ | WT_Nx | WT_Hx |
| JAK2$^{V617F/V617F}$ | VF_Nx | VF_Hx |

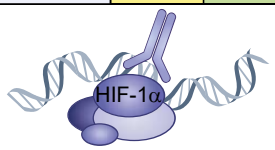


HIF-1α

**Chromatin Interactome**

RIME
LC-MS

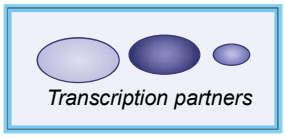


ChIPseq
NGS Illumina

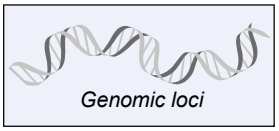


**(II)**

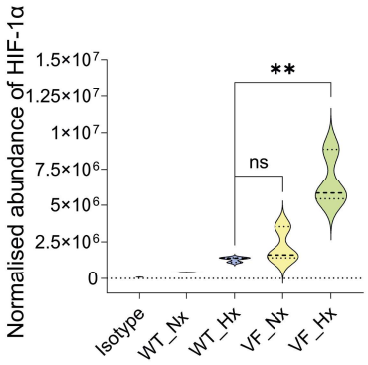


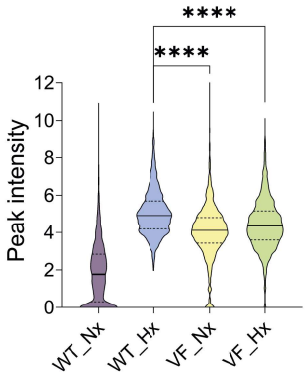


**B)**

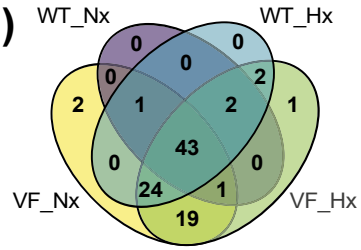


**C)**

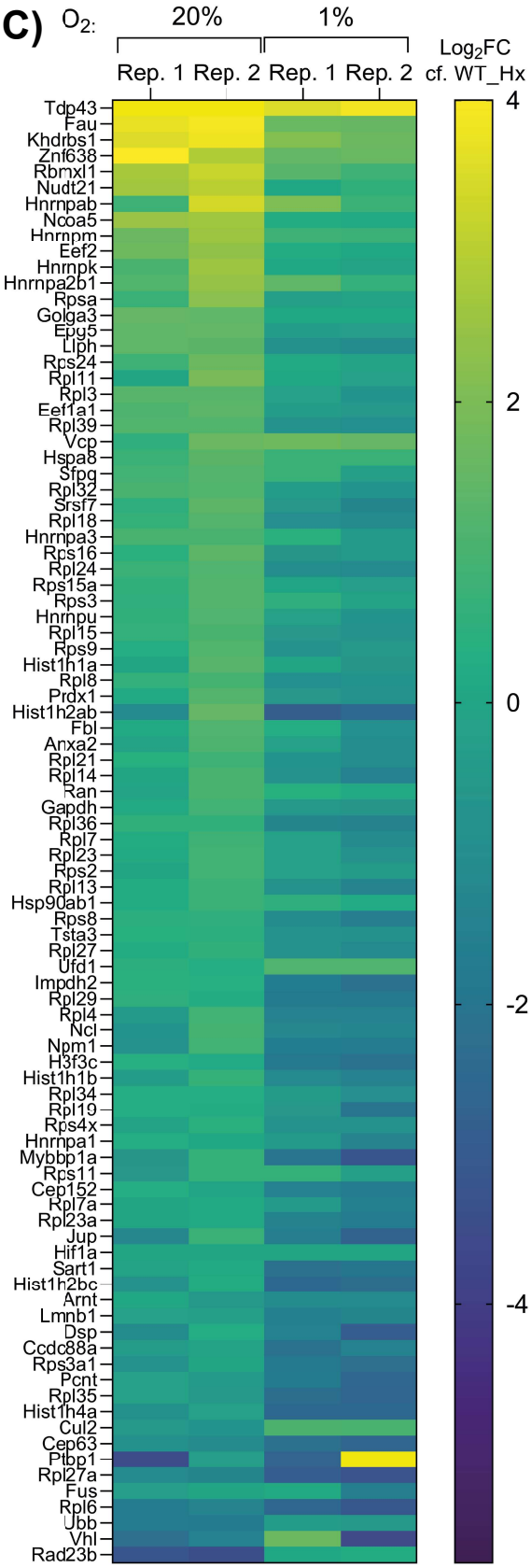


BaF3/hMPL JAK2V617F

**D)**

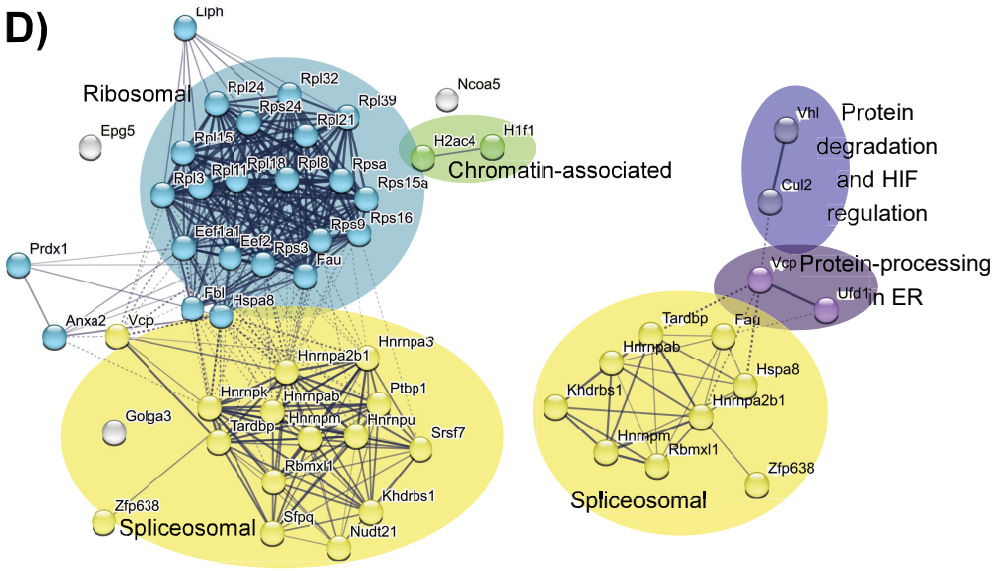


Enriched Partners: VF_Nx cf. WT_Hx

VF_Hx cf. WT_Hx

**E)** HIF-1α interactors at chromatin (RIME) vs. WT_Hx (1% $O_2$)

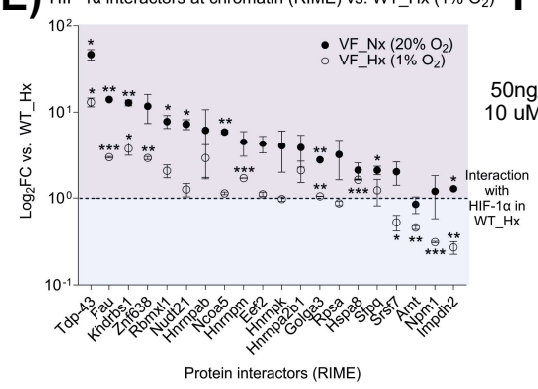


**F (I)**

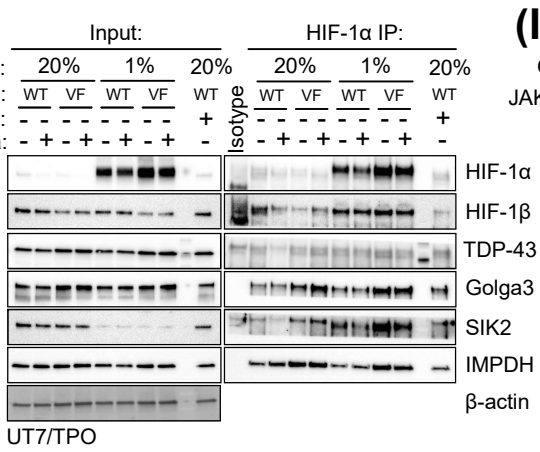


**(II)**

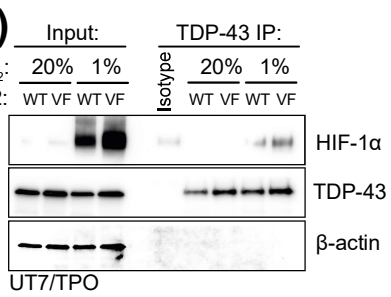

Fig. 5

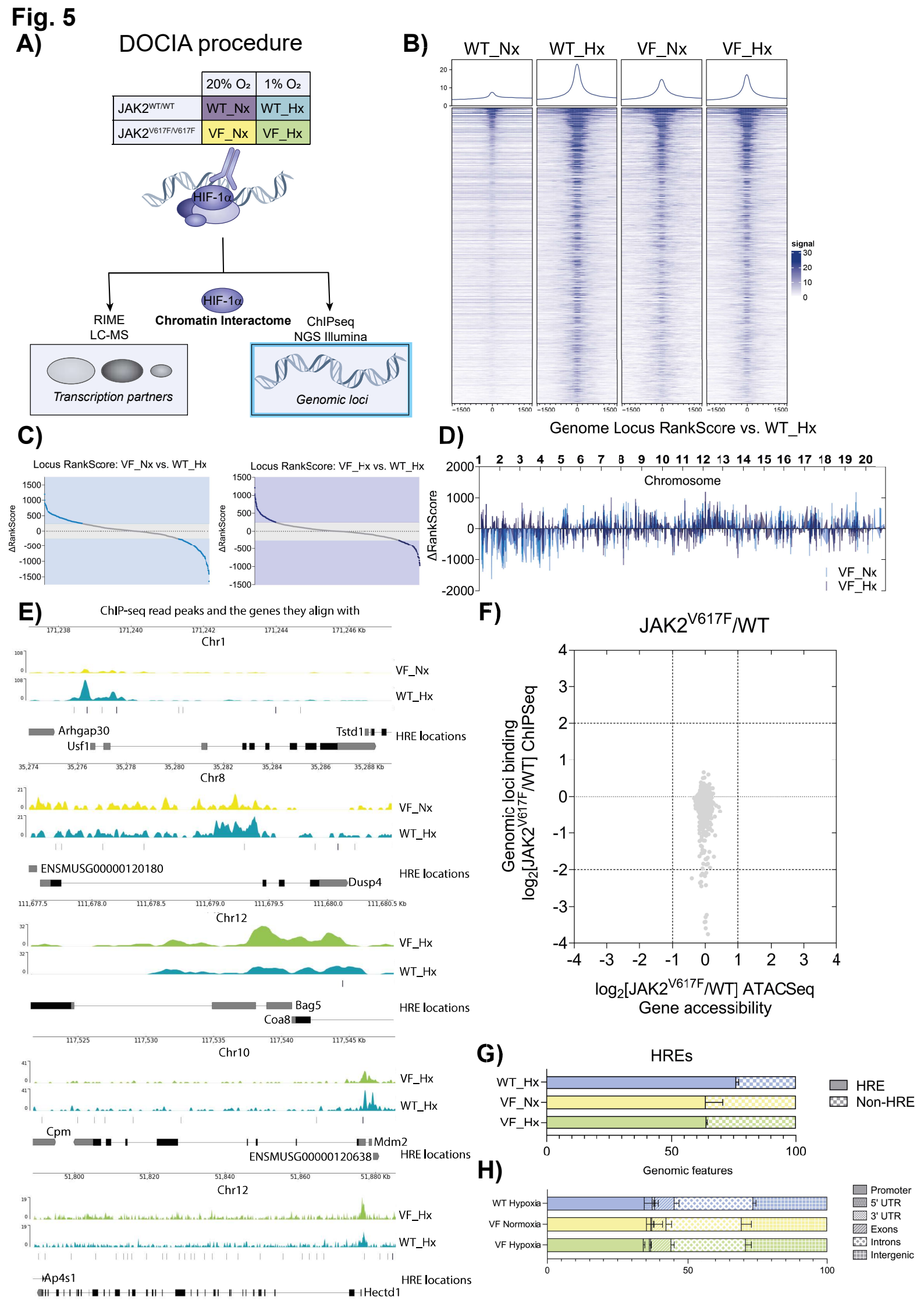
A)
DOCIA procedure
20% O₂
1% O₂
JAK2WT/WT
WT_Nx
WT_Hx
JAK2V617F/V617F
VF_Nx
VF_Hx
HIF-1α
RIME
LC-MS
Chromatin Interactome
ChIPseq
NGS Illumina
Transcription partners
Genomic loci
B)
WT_Nx
WT_Hx
VF_Nx
VF_Hx
signal
C)
Locus RankScore: VF_Nx vs. WT_Hx
Locus RankScore: VF_Hx vs. WT_Hx
ΔRankScore
D)
Genome Locus RankScore vs. WT_Hx
Chromosome
ΔRankScore
VF_Nx
VF_Hx
E)
ChIP-seq read peaks and the genes they align with
Chr1
VF_Nx
WT_Hx
Arhgap30
Usf1
Tstd1
HRE locations
Chr8
ENSMUSG00000120180
Dusp4
Chr12
Bag5
Coa8
Chr10
Cpm
Mdm2
ENSMUSG00000120638
Ap4s1
Hectd1
F)
JAK2V617F/WT
Genomic loci binding
log2[JAK2V617F/WT] ChIPSeq
log2[JAK2V617F/WT] ATACSeq
Gene accessibility
G)
HREs
HRE
Non-HRE
H)
Genomic features
WT Hypoxia
VF Normoxia
VF Hypoxia
Promoter
5' UTR
3' UTR
Exons
Introns
Intergenic

# Fig. 6

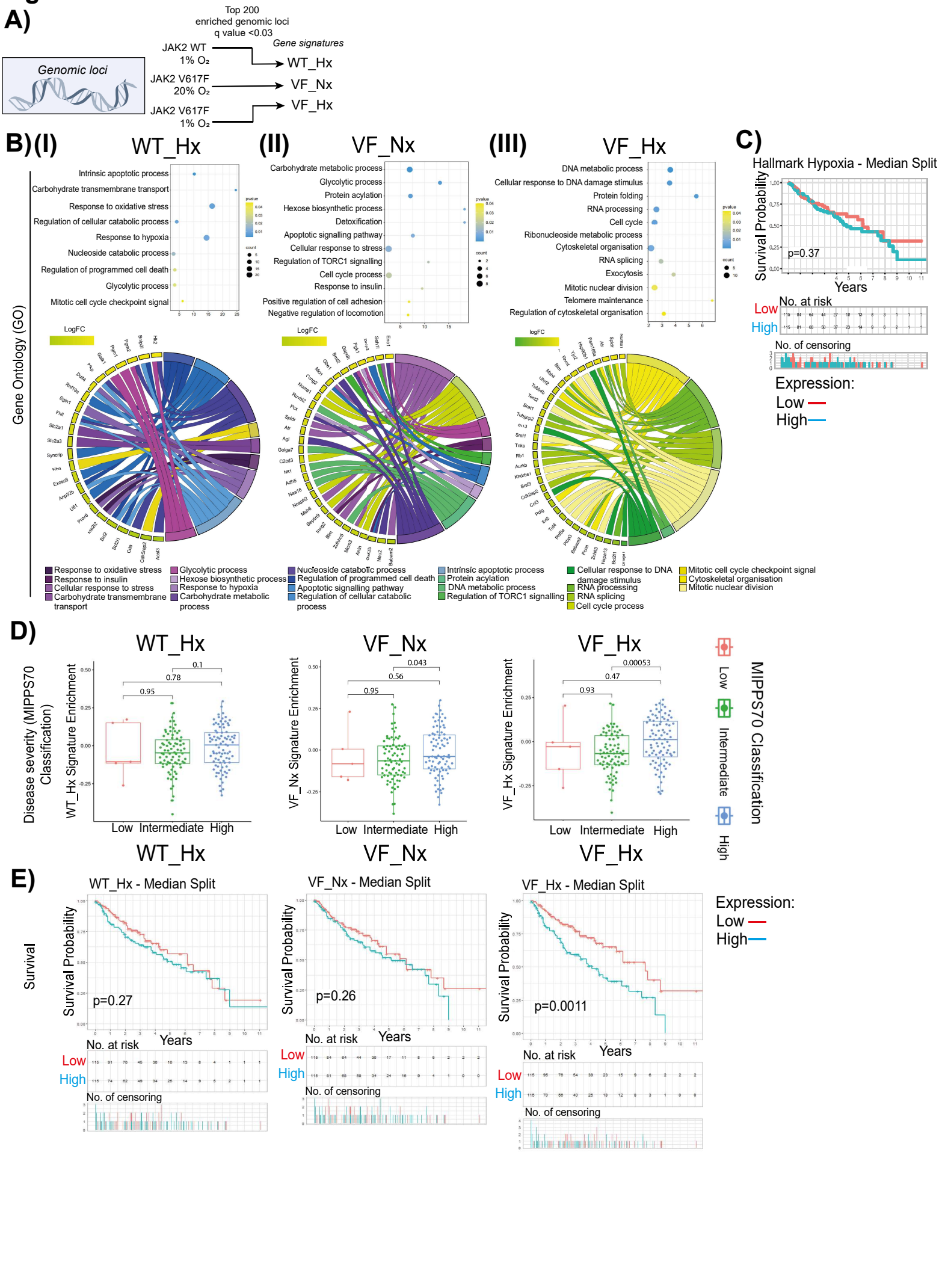
A)
Genomic loci
Top 200
enriched genomic loci
q value <0.03
Gene signatures
JAK2 WT
1% O₂
WT_Hx
JAK2 V617F
20% O₂
VF_Nx
JAK2 V617F
1% O₂
VF_Hx
B)(I)
WT_Hx
(II)
VF_Nx
(III)
VF_Hx
Gene Ontology (GO)
Intrinsic apoptotic process
Carbohydrate transmembrane transport
Response to oxidative stress
Regulation of cellular catabolic process
Response to hypoxia
Nucleoside catabolic process
Regulation of programmed cell death
Glycolytic process
Mitotic cell cycle checkpoint signal
Carbohydrate metabolic process
Glycolytic process
Protein acylation
Hexose biosynthetic process
Detoxification
Apoptotic signalling pathway
Cellular response to stress
Regulation of TORC1 signalling
Cell cycle process
Response to insulin
Positive regulation of cell adhesion
Negative regulation of locomotion
DNA metabolic process
Cellular response to DNA damage stimulus
Protein folding
RNA processing
Cell cycle
Ribonucleoside metabolic process
Cytoskeletal organisation
RNA splicing
Exocytosis
Mitotic nuclear division
Telomere maintenance
Regulation of cytoskeletal organisation
pvalue
count
LogFC
Response to oxidative stress
Response to insulin
Cellular response to stress
Carbohydrate transmembrane transport
Glycolytic process
Hexose biosynthetic process
Response to hypoxia
Carbohydrate metabolic process
Nucleoside catabolic process
Regulation of programmed cell death
Apoptotic signalling pathway
Regulation of cellular catabolic process
Intrinsic apoptotic process
Protein acylation
DNA metabolic process
Regulation of TORC1 signalling
Cellular response to DNA damage stimulus
RNA processing
RNA splicing
Cell cycle process
Mitotic cell cycle checkpoint signal
Cytoskeletal organisation
Mitotic nuclear division
C)
Hallmark Hypoxia - Median Split
Survival Probability
p=0.37
Years
No. at risk
Low
High
No. of censoring
Expression:
Low
High
D)
Disease severity (MIPPS70 Classification)
WT_Hx
WT_Hx Signature Enrichment
0.95
0.78
0.1
VF_Nx
VF_Nx Signature Enrichment
0.95
0.56
0.043
VF_Hx
VF_Hx Signature Enrichment
0.93
0.47
0.00053
Low
Intermediate
High
MIPPS70 Classification
E)
Survival
WT_Hx
WT_Hx - Median Split
Survival Probability
p=0.27
Years
No. at risk
Low
High
No. of censoring
VF_Nx
VF_Nx - Median Split
Survival Probability
p=0.26
Years
No. at risk
Low
High
No. of censoring
VF_Hx
VF_Hx - Median Split
Survival Probability
p=0.0011
Years
No. at risk
Low
High
No. of censoring
Expression:
Low
High

Fig. 7

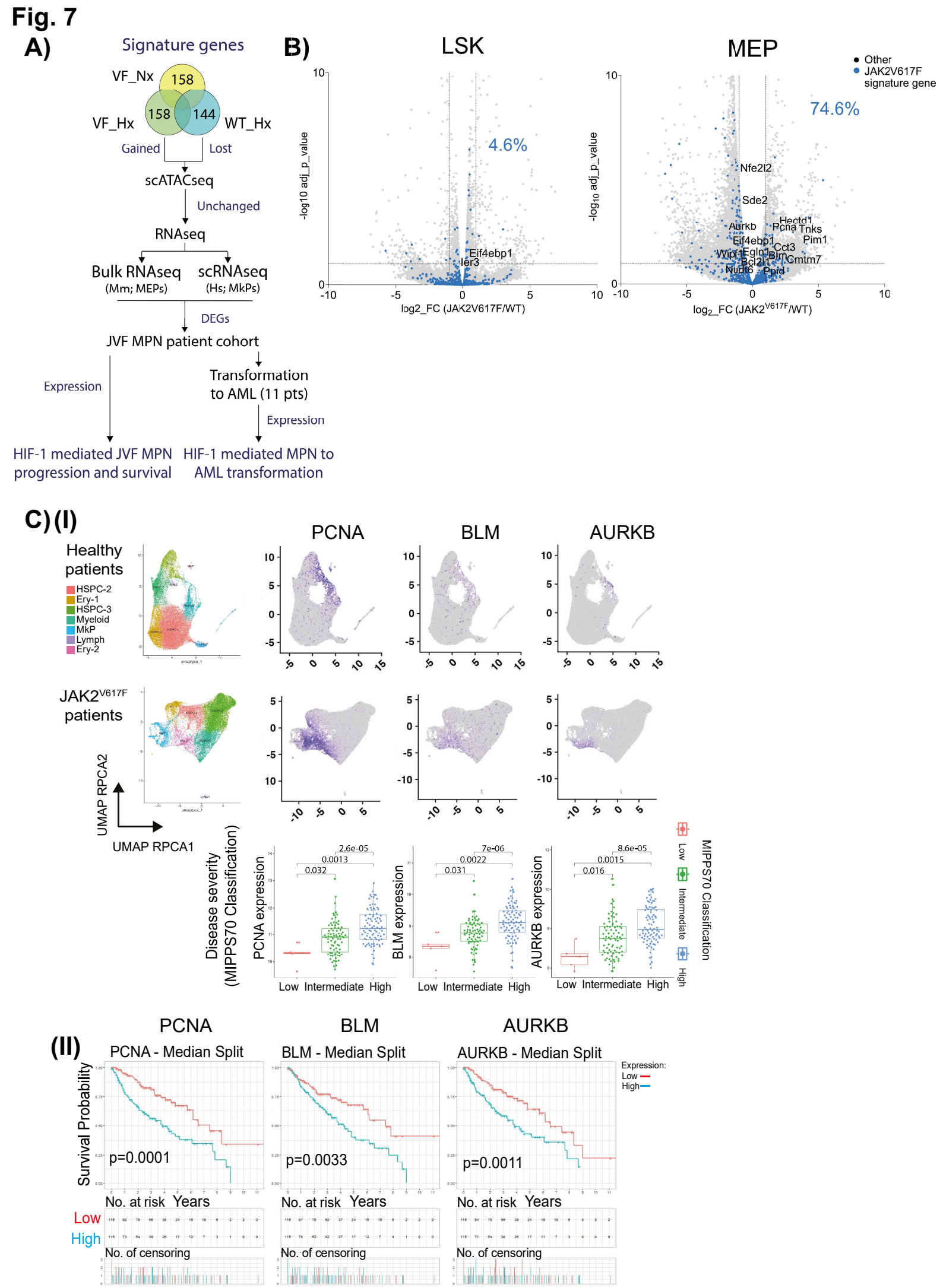
A)
Signature genes
VF_Nx
158
158
144
VF_Hx
WT_Hx
Gained
Lost
scATACseq
Unchanged
RNAseq
Bulk RNAseq
(Mm; MEPs)
scRNAseq
(Hs; MkPs)
DEGs
JVF MPN patient cohort
Expression
Transformation
to AML (11 pts)
Expression
HIF-1 mediated JVF MPN
progression and survival
HIF-1 mediated MPN to
AML transformation
B)
LSK
MEP
Other
JAK2V617F
signature gene
4.6%
74.6%
-log10 adj_p_value
log2_FC (JAK2V617F/WT)
Eif4ebp1
Ier3
Nfe2l2
Sde2
Aurkb
Hectd1
Pcna
Tnks
Pim1
Cct3
Cmtm7
Wipf1
Egln1
Blm
Bcl2l1
Nudt6
Ppid
C) (I)
Healthy
patients
HSPC-2
Ery-1
HSPC-3
Myeloid
MkP
Lymph
Ery-2
PCNA
BLM
AURKB
JAK2V617F
patients
UMAP RPCA2
UMAP RPCA1
Disease severity
(MIPPS70 Classification)
PCNA expression
BLM expression
AURKB expression
2.6e-05
0.0013
0.032
7e-06
0.0022
0.031
8.6e-05
0.0015
0.016
Low
Intermediate
High
MIPPS70 Classification
(II)
PCNA
BLM
AURKB
PCNA - Median Split
BLM - Median Split
AURKB - Median Split
Expression:
Low
High
Survival Probability
p=0.0001
p=0.0033
p=0.0011
No. at risk
Years
Low
High
No. of censoring

**Fig. 8**

**A)**

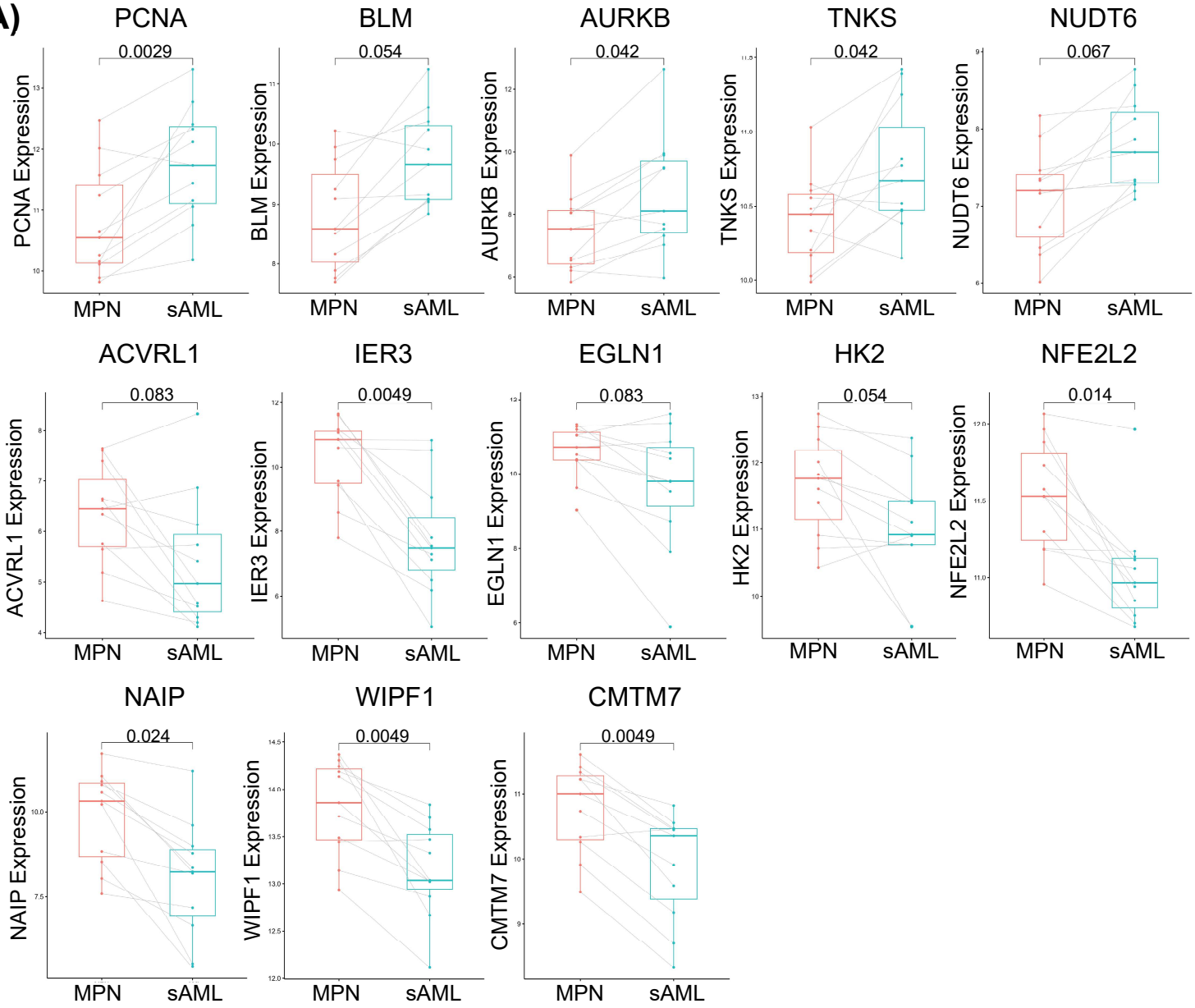
PCNA
0.0029
PCNA Expression
BLM
0.054
BLM Expression
AURKB
0.042
AURKB Expression
TNKS
0.042
TNKS Expression
NUDT6
0.067
NUDT6 Expression
ACVRL1
0.083
ACVRL1 Expression
IER3
0.0049
IER3 Expression
EGLN1
0.083
EGLN1 Expression
HK2
0.054
HK2 Expression
NFE2L2
0.014
NFE2L2 Expression
NAIP
0.024
NAIP Expression
WIPF1
0.0049
WIPF1 Expression
CMTM7
0.0049
CMTM7 Expression
MPN
sAML

**B)**

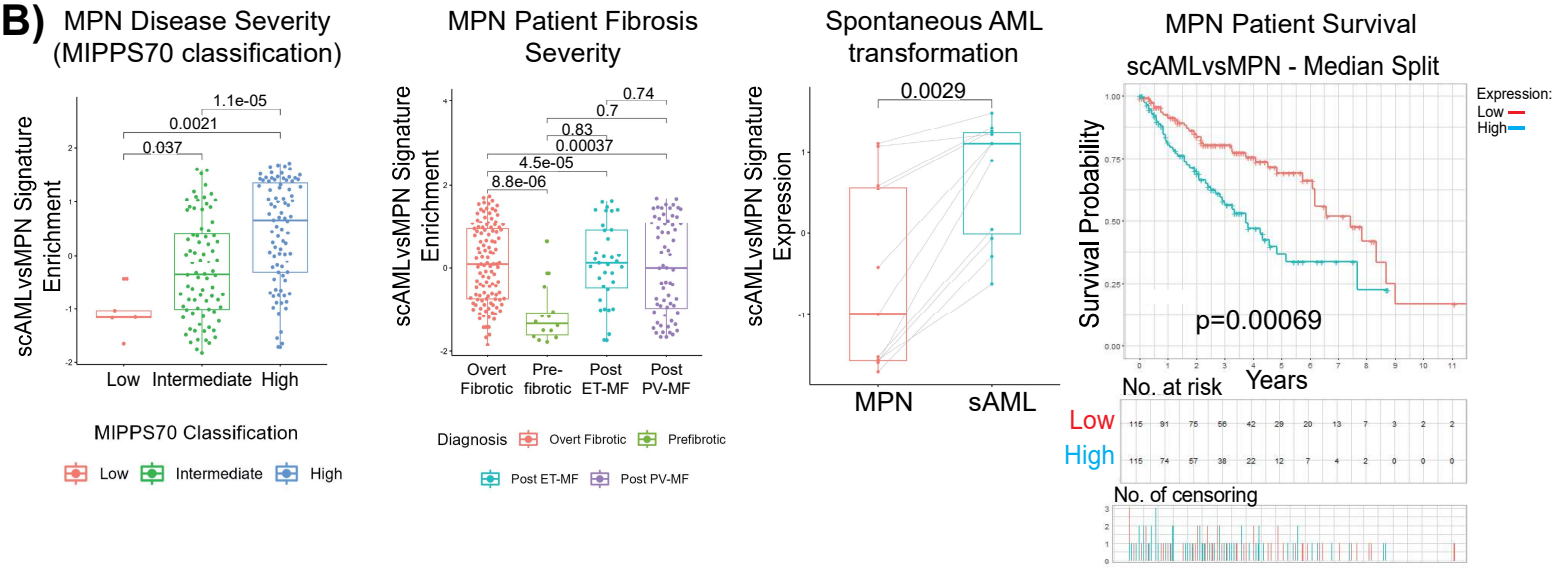
MPN Disease Severity (MIPPS70 classification)
scAMLvsMPN Signature Enrichment
1.1e-05
0.0021
0.037
Low
Intermediate
High
MIPPS70 Classification
Low
Intermediate
High
MPN Patient Fibrosis Severity
scAMLvsMPN Signature Enrichment
0.74
0.7
0.83
0.00037
4.5e-05
8.8e-06
Overt Fibrotic
Pre-fibrotic
Post ET-MF
Post PV-MF
Diagnosis
Overt Fibrotic
Prefibrotic
Post ET-MF
Post PV-MF
Spontaneous AML transformation
scAMLvsMPN Signature Expression
0.0029
MPN
sAML
MPN Patient Survival
scAMLvsMPN - Median Split
Expression:
Low
High
Survival Probability
p=0.00069
Years
No. at risk
Low
High
No. of censoring

# Fig. S1

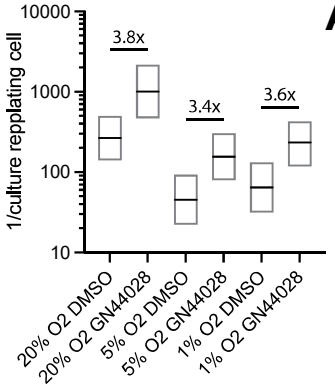


# Fig. S2

A)

| Sample Name | Subset Name | Count | Mean : Comp-FL1-H | SD : Comp-FL1-H | Mode : Comp-FL1-H |
|---|---|---|---|---|---|
| 01-Hom 4h 1% O2-D6.fcs | Live | 121088 | 47505 | 22840 | 36286 |
| 01-Het 4h 1% O2-D4.fcs | Live | 42195 | 48894 | 20804 | 42805 |
| 01-WT 4h 1% O2-D2.fcs | Live | 32855 | 46162 | 15640 | 52771 |
| 01-Mixed Isotype-B4.fcs | Live | 45774 | 28721 | 10183 | 28476 |

| Sample Name | Subset Name | Count | Mean : Comp-FL1-H | SD : Comp-FL1-H | Mode : Comp-FL1-H |
|---|---|---|---|---|---|
| 01-WT 4h 1% O2-D2.fcs | Live | 32855 | 46162 | 15640 | 52771 |
| 01-WT 0h-B6.fcs | Live | 49560 | 36641 | 12102 | 36688 |
| 01-Mixed Isotype-B4.fcs | Live | 45774 | 28721 | 10183 | 28476 |

| Sample Name | Subset Name | Count | Mean : Comp-FL1-H | SD : Comp-FL1-H | Mode : Comp-FL1-H |
|---|---|---|---|---|---|
| 01-Het 4h 1% O2-D4.fcs | Live | 42195 | 48894 | 20804 | 42805 |
| 01-Het 0h-B8.fcs | Live | 54658 | 32025 | 11389 | 27249 |
| 01-Mixed Isotype-B4.fcs | Live | 45774 | 28721 | 10183 | 28476 |

| Sample Name | Subset Name | Count | Mean : Comp-FL1-H | SD : Comp-FL1-H | Mode : Comp-FL1-H |
|---|---|---|---|---|---|
| 01-Hom 4h 1% O2-D6.fcs | Live | 121088 | 47505 | 22840 | 36286 |
| 01-Hom 0h-B10.fcs | Live | 86879 | 26601 | 9811 | 25227 |
| 01-Mixed Isotype-B4.fcs | Live | 45774 | 28721 | 10183 | 28476 |

B)

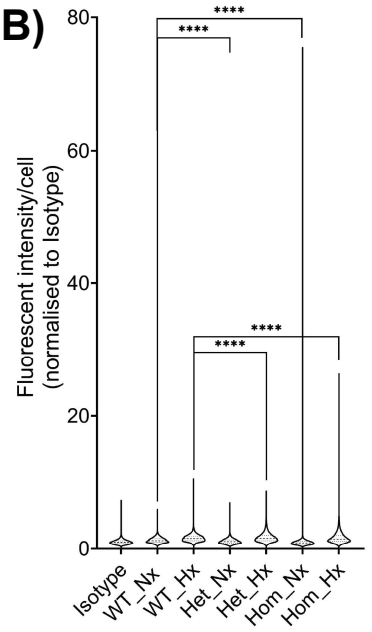


C)

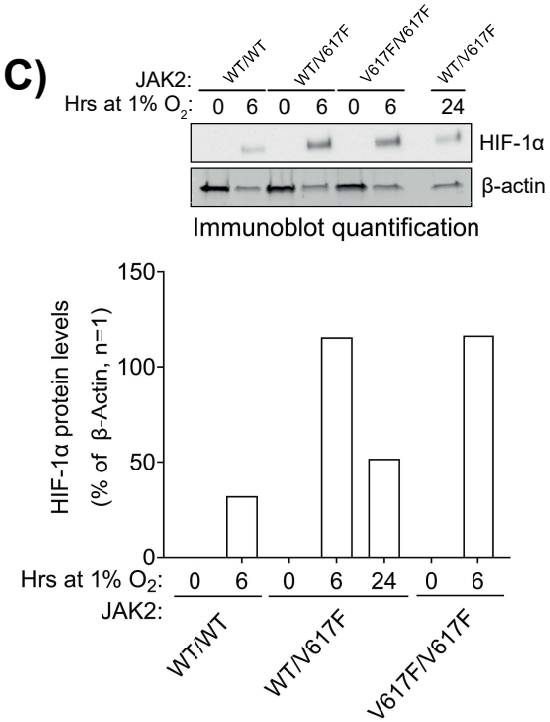


# Fig. S3

A) LSK

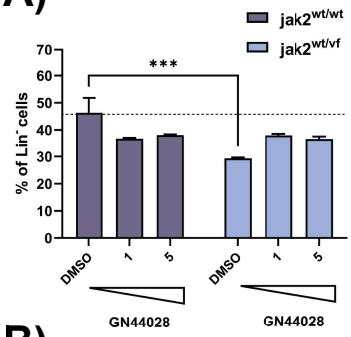


B) Progenitors

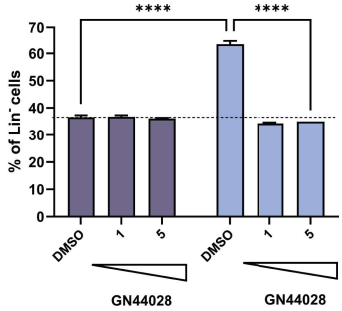


# Fig. S4

A)

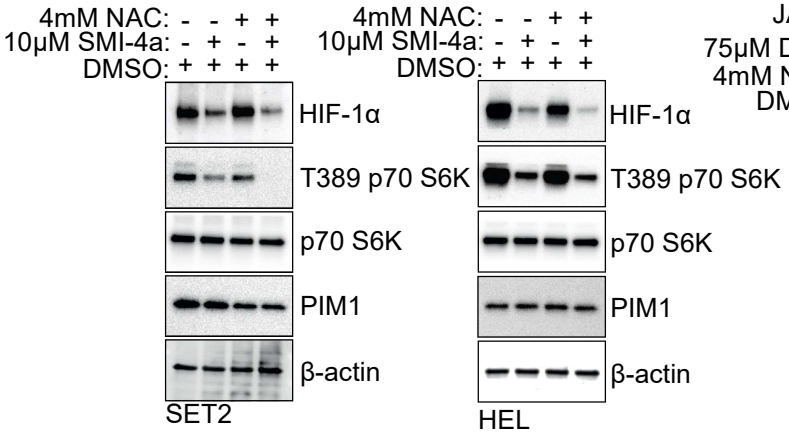


B)

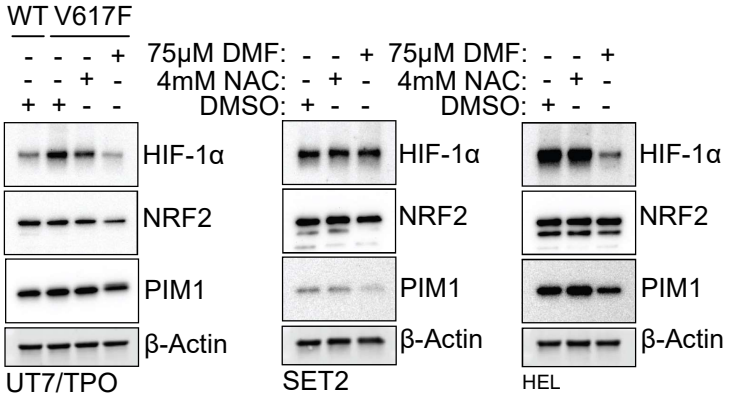

## Fig. S5

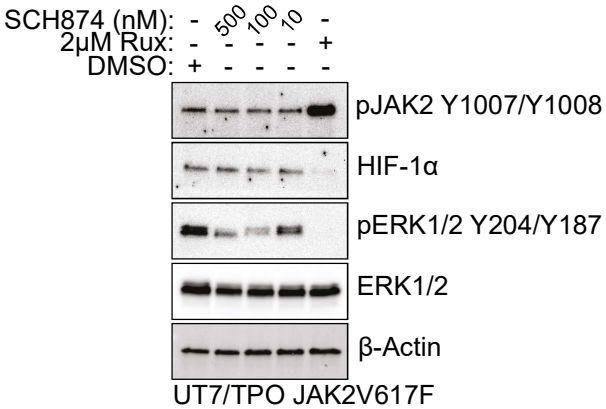


## Fig. S6

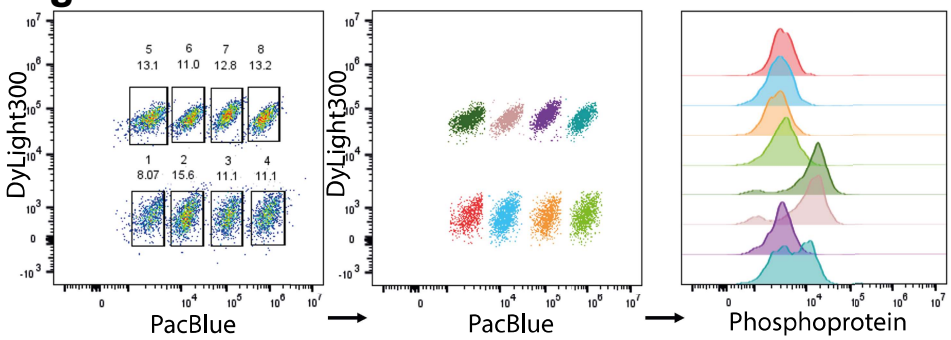


## Fig. S7

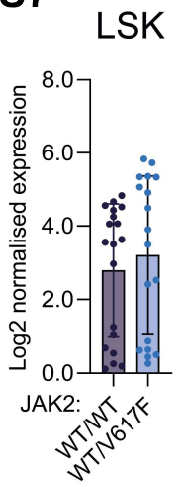


## Fig. S8

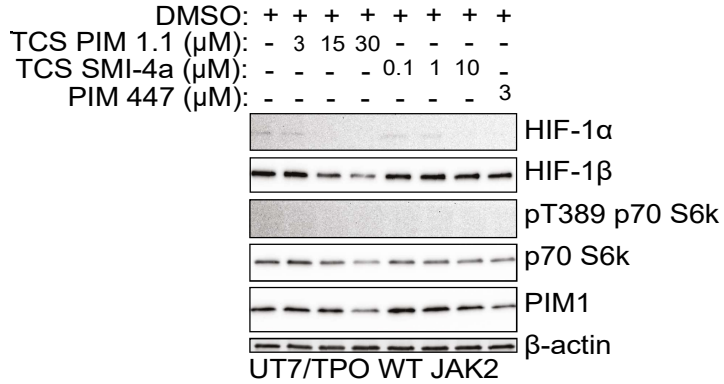


## Fig. S9

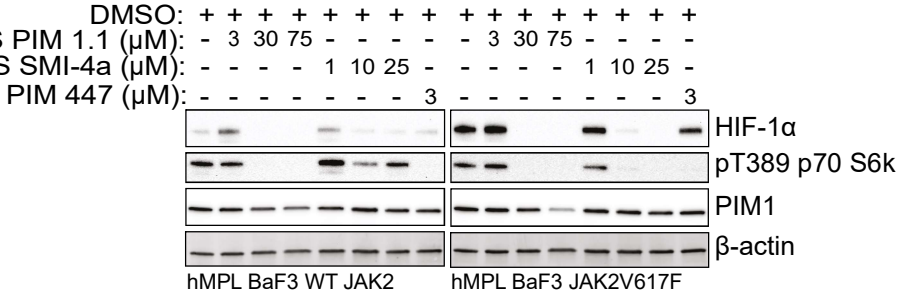


## Fig. S10

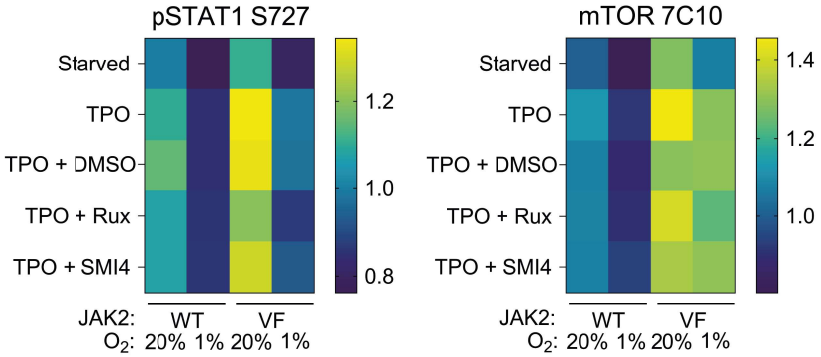

# Fig. S11

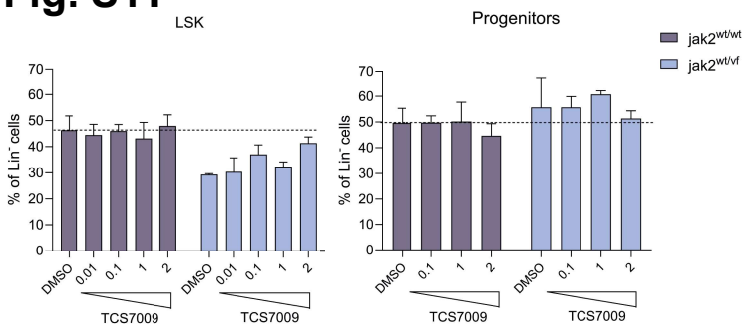


# Fig. S12

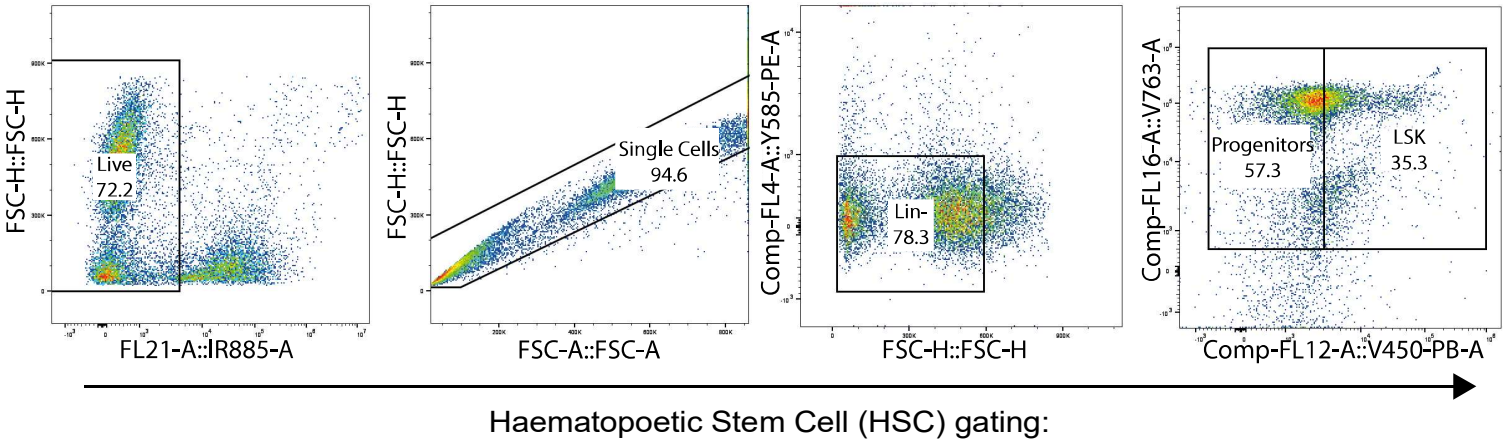


# Fig. S13

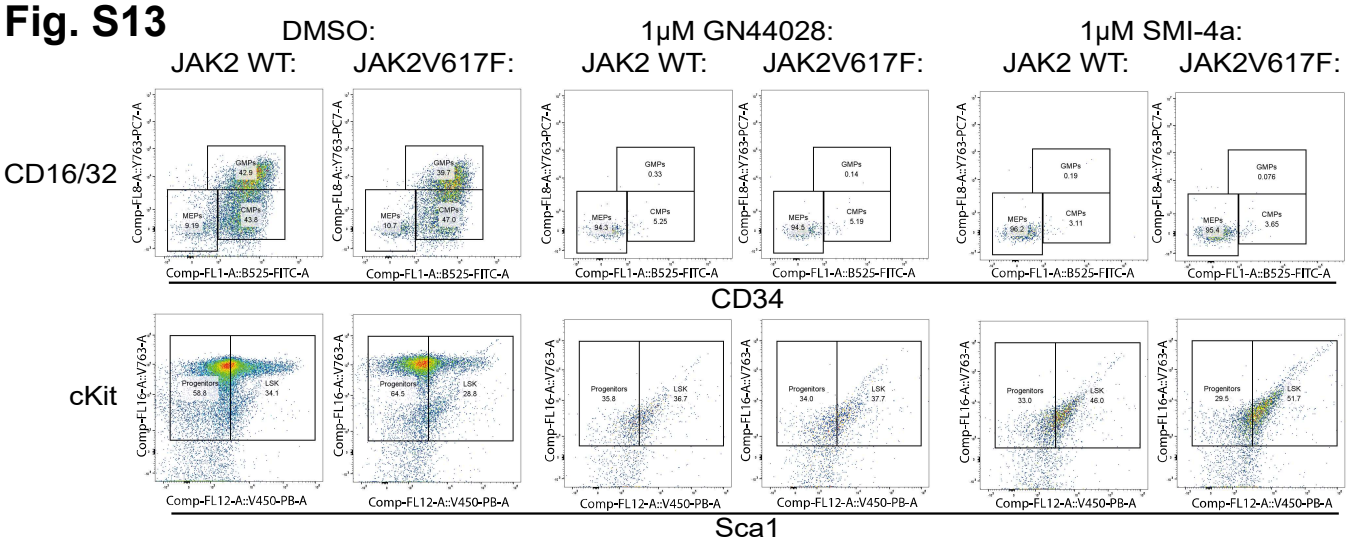


# Fig. S14

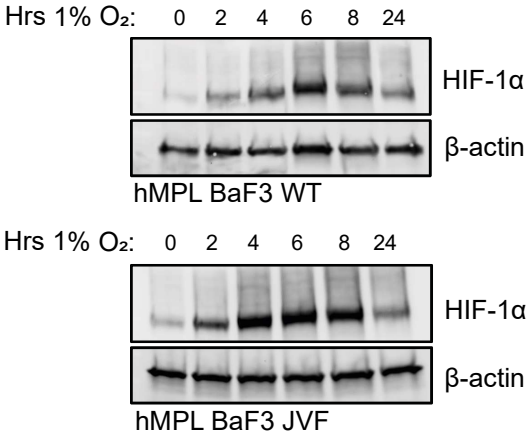

# Fig. S15

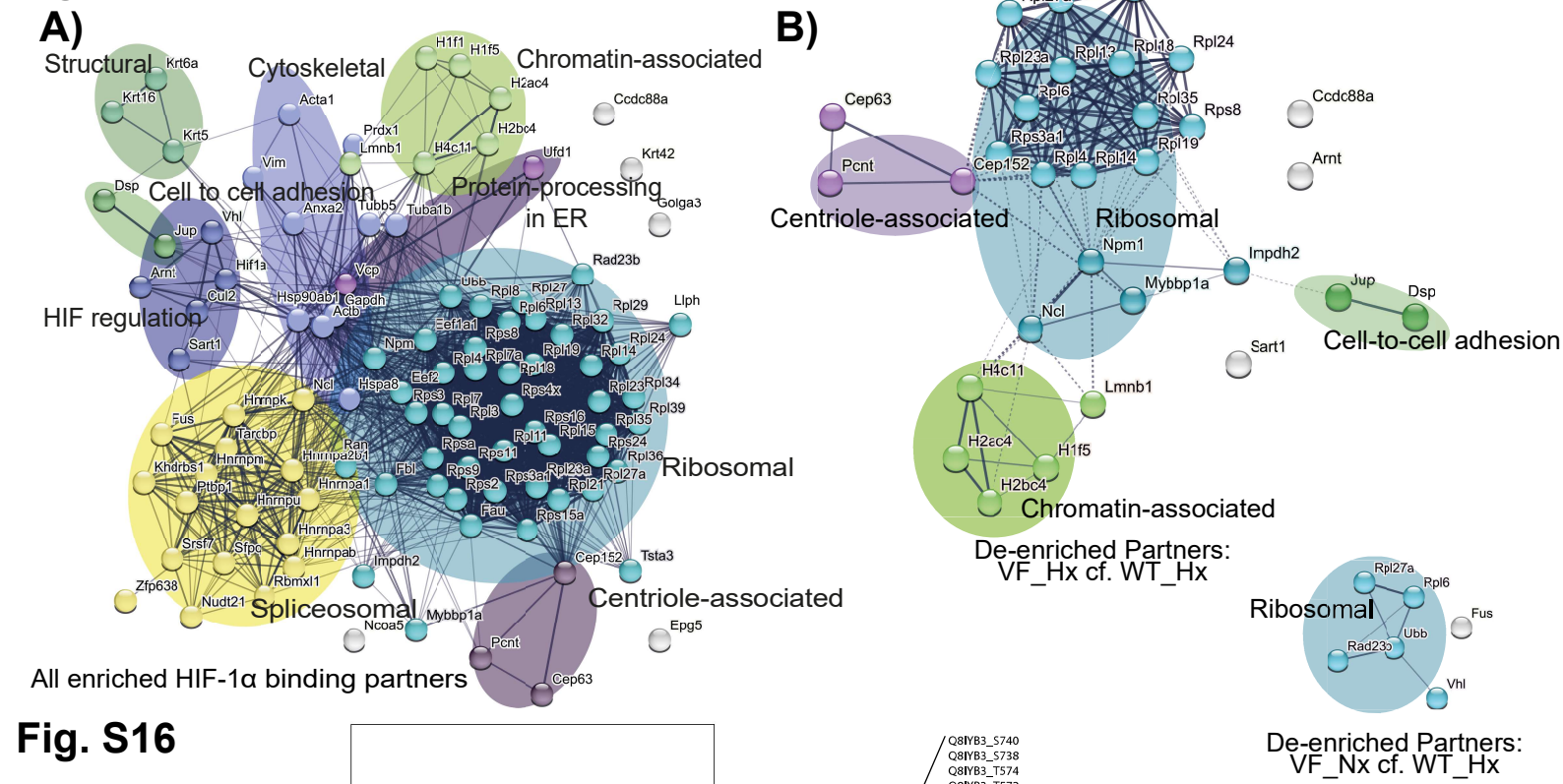


# Fig. S16

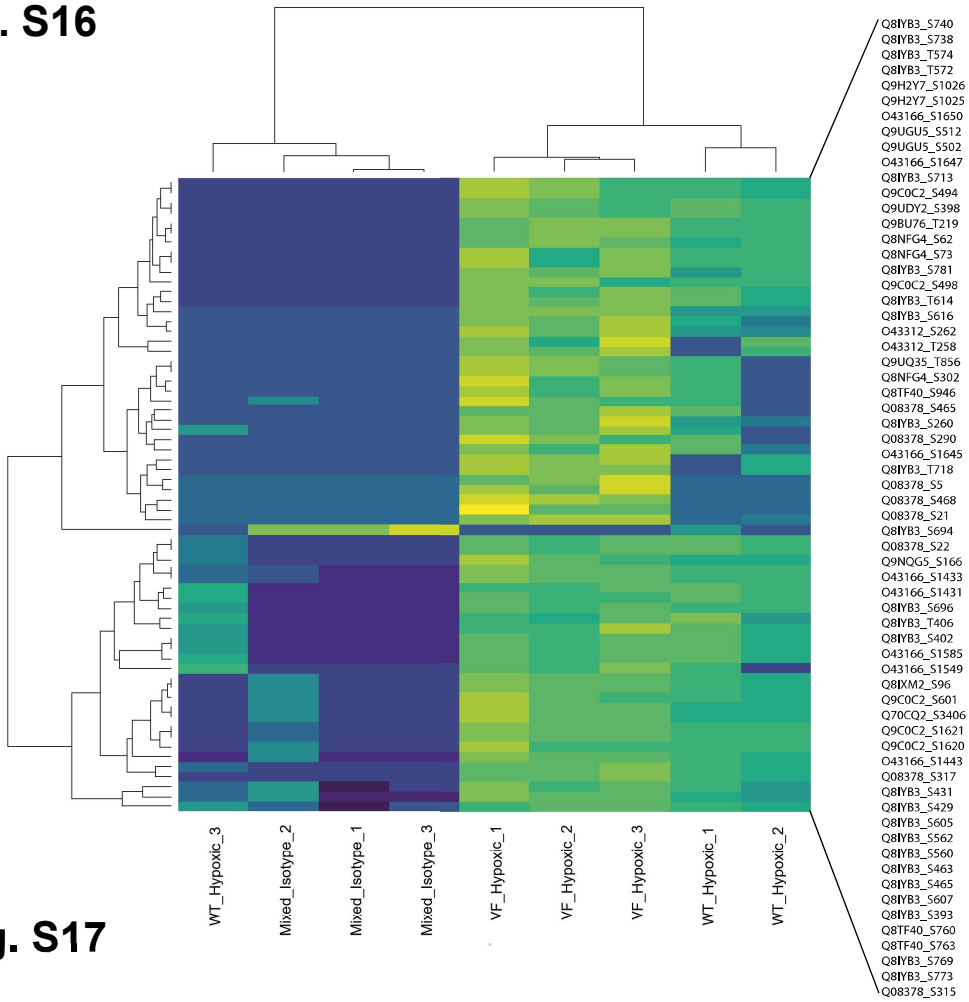


# Fig. S17

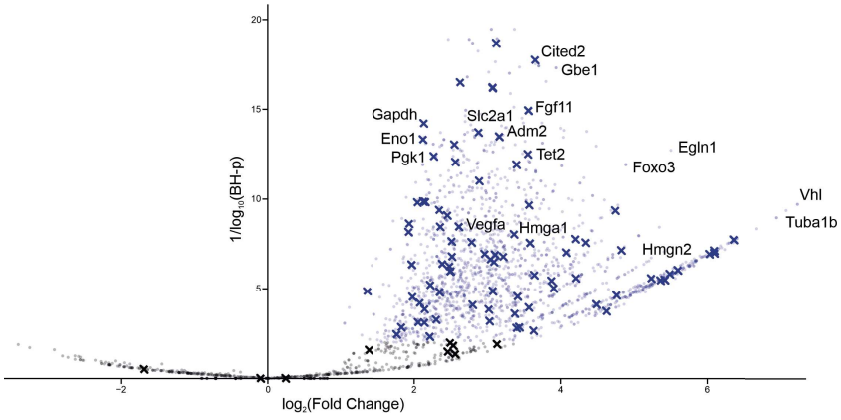

## Fig. S18

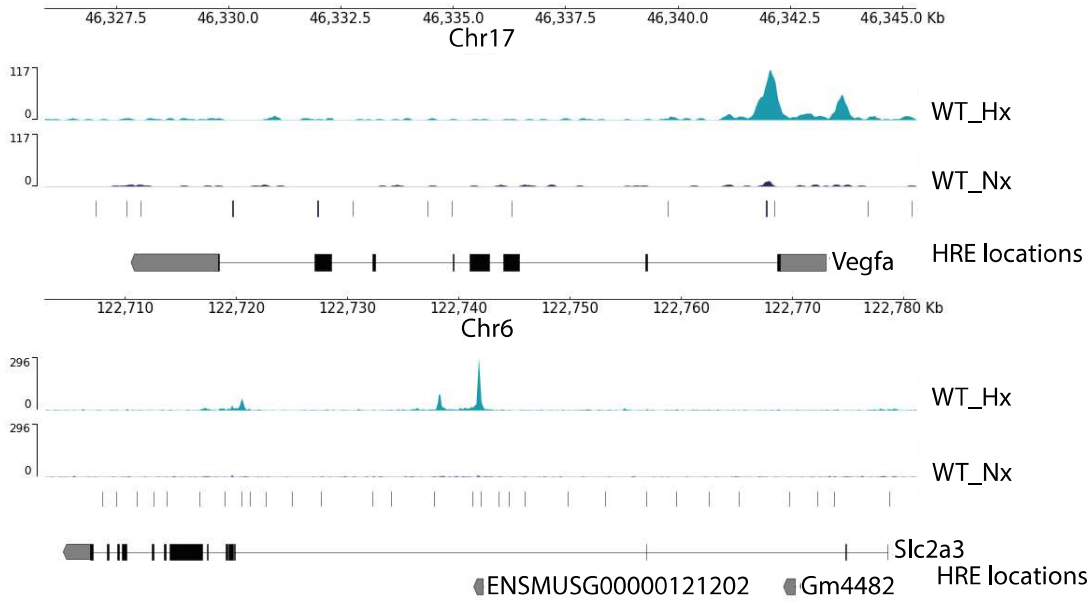


## Fig. S19

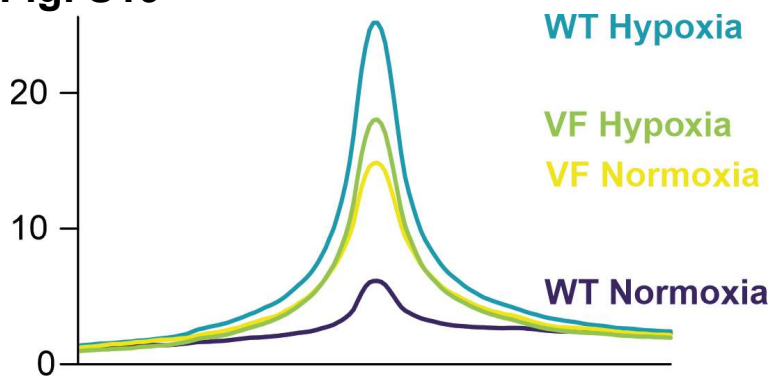


## Fig. S20

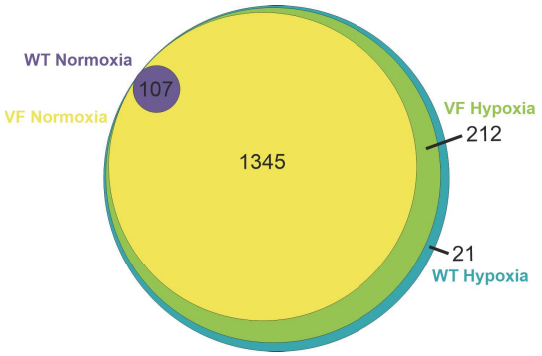


## Fig. S21

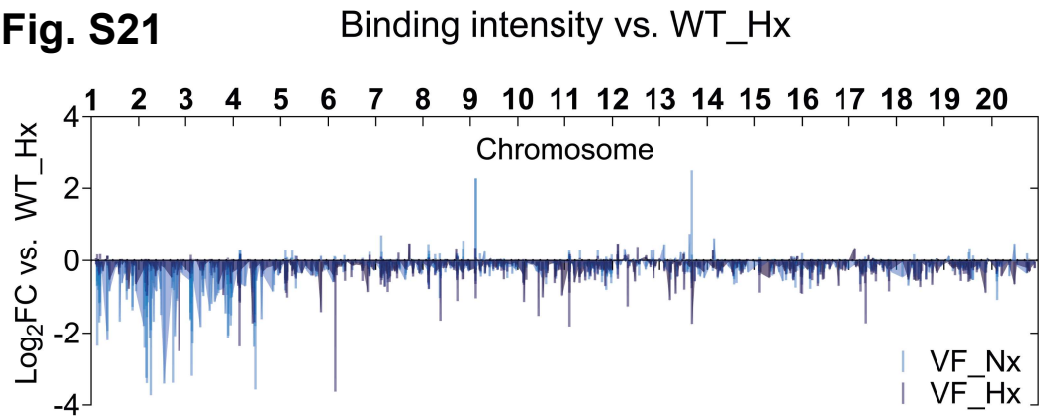


## Fig. S22

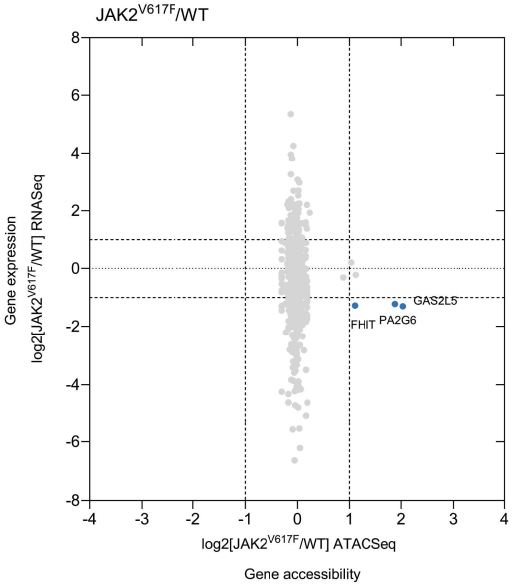


## Fig. S23

| Signature: | VF_Nx | VF_Hx |
|---|---|---|
| HIF-1 Metagene | RBPJ | RBPJ |
| | ENO1 | DDIT4 |
| | GBE1 | |
| | KDM4B | |
| | LDHA | |
| | MXI1 | |
| | PGAM1 | |
| | PGK1 | |
| | AK4 | |

## Fig. S24

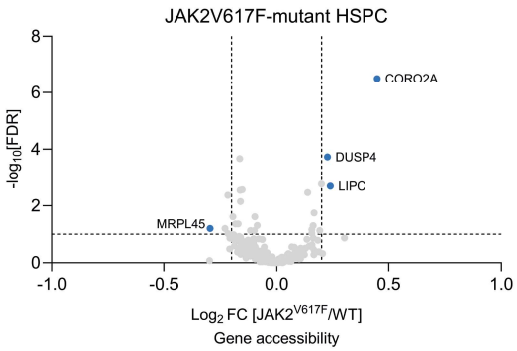

# Fig. S25

Key JAK2V617F gene signature genes

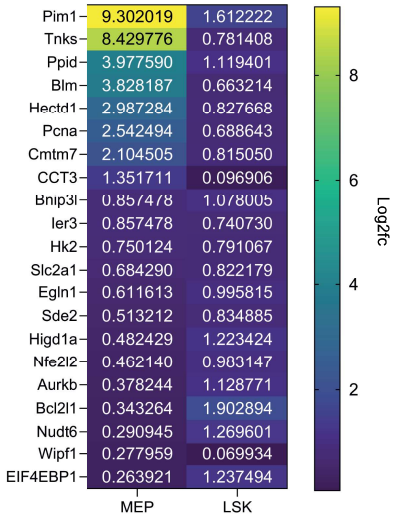


# Fig. S26

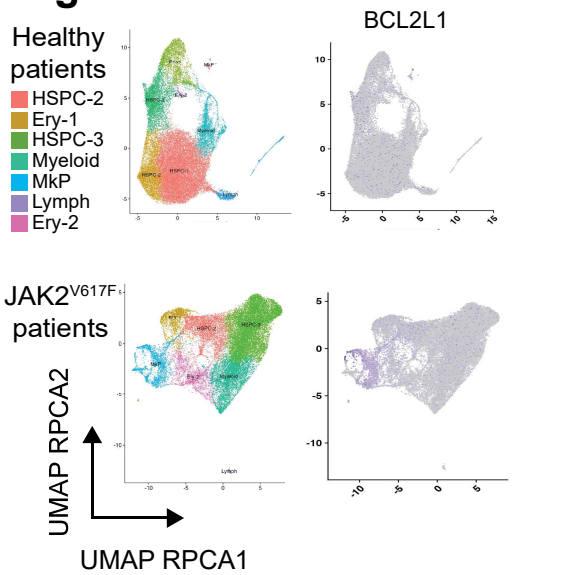


# Fig. S27

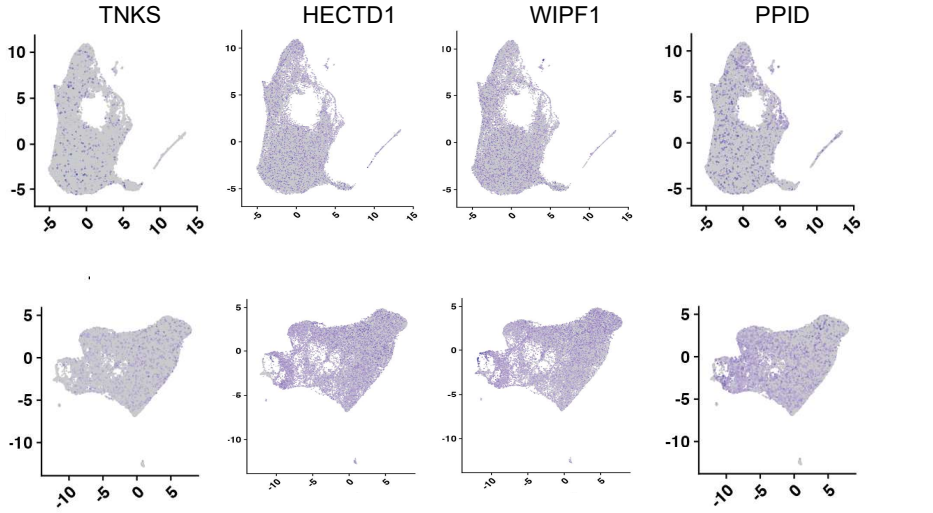


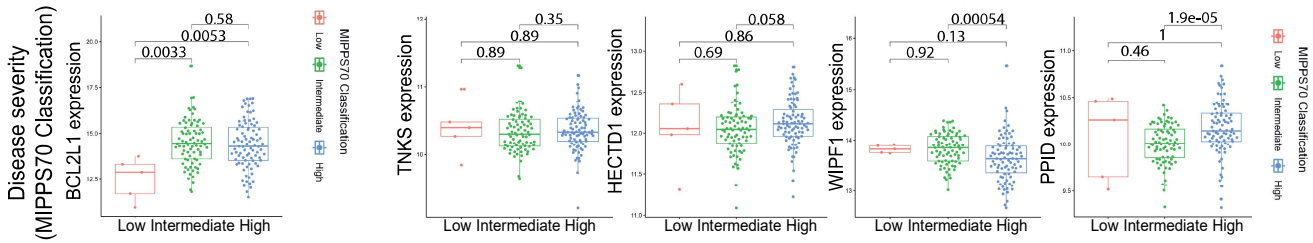


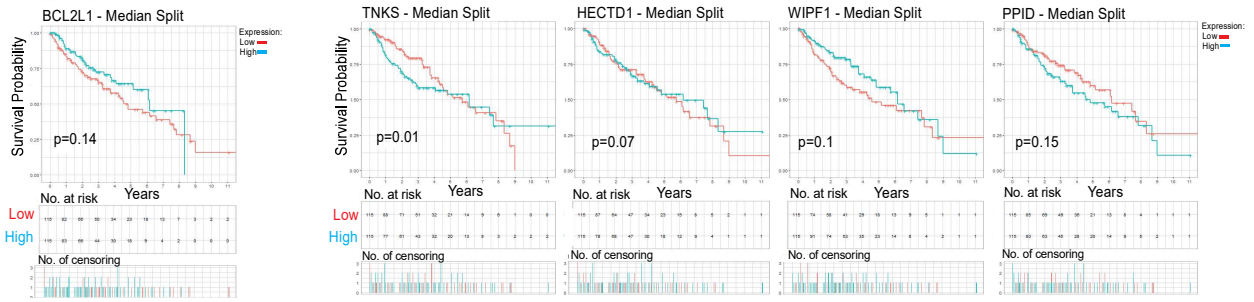

# Fig. S28

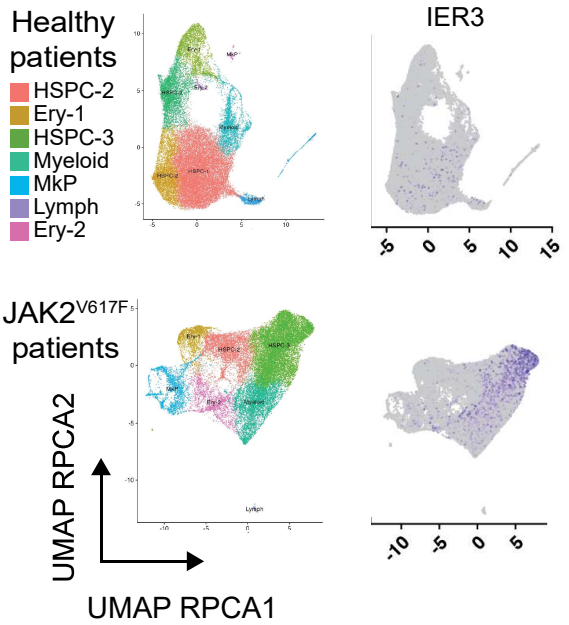


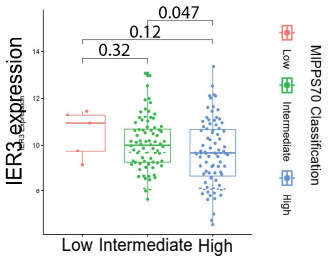


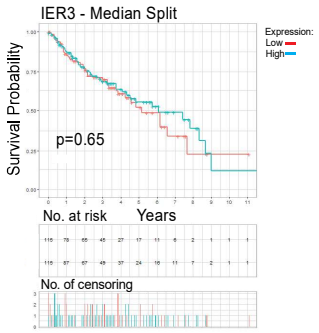


# Fig. S29

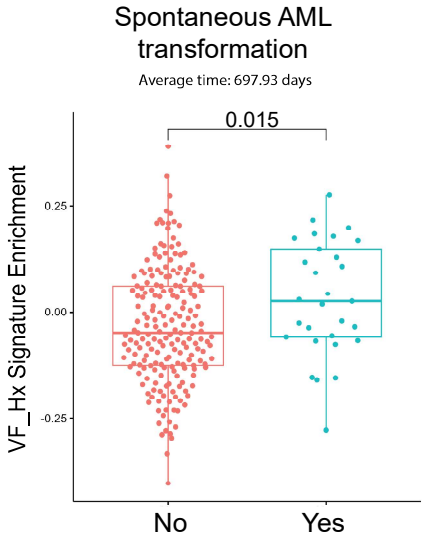

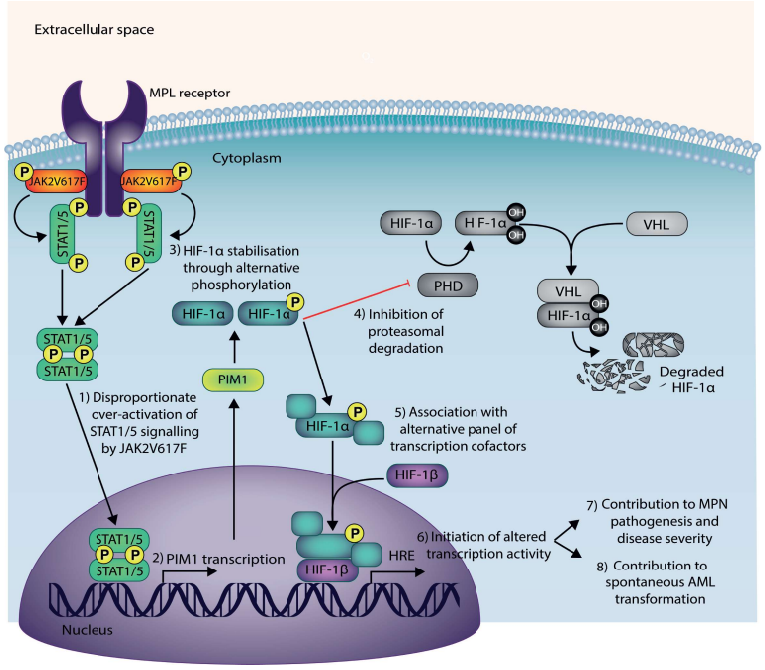
# Fig. S30